LABELLING AND LONGITUDINAL *IN VIVO* IMAGING OF RETINAL GANGLION CELLS

by

Corey A. Smith

Submitted in partial fulfilment of the requirements
for the degree of Doctor of Philosophy

at

Dalhousie University
Halifax, Nova Scotia
August 2017

Table of Contents

List of Tables

List of Figures

Abstract

The ability to detect and quantify retinal ganglion cell (RGC) loss is important for the diagnosis and monitoring of optic neuropathies, such as glaucoma. This thesis describes the development, assessment, and implementation of intravitreal injection labelling of RGCs for non-invasive and longitudinal *in vivo* imaging in mice. We tested the hypothesis that the neuronal tracer, cholera toxin subunit B (CTB), and adeno-associated viral (AAV) vectors with a green fluorescent protein (GFP) reporter gene are detectable labels for RGCs. Following CTB labelling, individual cells were detected by *in vivo* imaging with confocal scanning laser ophthalmoscopy after 10-15 days and were successfully imaged consecutively up to 100-days post-injection. With intravitreal CTB injection, approximately 53% of CTB+ cells were identified as RGCs, while >58% of all RGCs were successfully labelled. These findings showed that intravitreal injection administration of CTB is a reliable and effective label for RGCs in mice, by providing clear, sustained and strong labelling of cells in the ganglion cell layer. AAV2-GFP labelling in retinal cells was detected by *in vivo* imaging at 1-week post-injection. An increase in the number of cells expressing GFP occurred until approximately week 4 post-injection. Immunohistochemistry showed that 5-weeks post-injection, the mean (standard error) GFP+ cells that were positive for the RGC-specific RNA-binding protein with multiple splicing marker was 86 (4)% for the AAV2-DCX-GFP vector and 72 (3)% for the AAV2-CAG-GFP vector. Functional responses of the retina were assessed with electroretinography. The positive and negative scotopic threshold responses, which measure RGC activity, had similar amplitudes between AAV2 injected and uninjected eyes. Both CTB- and AAV-based methods of intravitreal injection labelling provided strong and sustained fluorescence labelling in RGCs. However, AAV2 vectors demonstrated higher specificity to RGCs that could be further improved with the cell type-specific *DCX* promoter. This work demonstrates a technique for labelling and imaging the presence of RGCs longitudinally, thereby providing a means to quantify changes in RGC density in experimental optic neuropathy, and after neuroprotective or neuroregenerative interventions.

List of Abbreviations Used

AAV	Adeno-associated virus
AAV2	Adeno-associated virus serotype 2
AMD	Age-related macular degeneration
CAG	Cytomegalovirus (CMV) early enhancer/chicken β actin promoter
CBA	Chicken β-actin
CFP	Cyan fluorescent protein
CSLO	Confocal scanning laser ophthalmoscopy
CTB	Cholera toxin subunit B
DCX	Doublecortin promoter
ERG	Electroretinogram
GABA	Gamma-aminobutyric acid
GCL	Ganglion cell layer
GFP	Green fluorescent protein
IEC	International Electrotechnical Commission
ILM	Inner limiting membrane
INL	Inner nuclear layer
IPL	Inner plexiform layer
nSTR	Negative scotopic threshold response
OCT	Optical coherence tomography
OD	Oculus dexter (right eye)
ONH	Optic nerve head
OS	Oculus sinister (left eye)
PBS	Phosphate-buffered saline
PFA	Paraformaldehyde
pSTR	Positive scotopic threshold response

RBPMS	RNA-binding protein with multiple splicing
RGC	Retinal ganglion cell
RNA	Ribonucleic acid
STR	Scotopic threshold response
Tat	Trans-activator of transcription of human immunodeficiency virus
Thy1	Thymocyte differentiation antigen 1
WPRE	Woodchuck hepatitis post-transcriptional regulatory element
YFP	Yellow fluorescent protein

Acknowledgements

The work accomplished in this thesis would not have been possible without the guidance and support of many.

First and foremost, I would like to thank Dr. Balwantray Chauhan for giving me the opportunity to be a part of his research group and join this exciting project, for inspiring and challenging me, and for sharing his research insight and passion. I appreciate the constructive criticism, providing me with excellent opportunities, and support both professionally and personally.

I owe special thanks to the members of the Retina and Optic Nerve Research Laboratory; especially Michele Hooper, Janette Nason, Kelly Stevens, Dr. Xu Wang, Dr. Spring Farrell, Andrea Nuschke and Julie Levesque. Each of you have provided important technical expertise and day-to-day support. The members of my supervisory committee, Dr. William Baldridge, Dr. Robert Brownstone and Dr. Alan Fine, have provided insightful suggestions that gave me the motivation to learn and overcome challenges. Thank you also to Jennifer Graves for always having an answer or solution to administrative questions.

I would like to acknowledge the financial support of the Atlantic Canada Opportunities Agency, Dalhousie University, Dalhousie Medical Research Foundation and Nova Scotia Health Research Foundation that was vital to the success of this work.

Thank you to my family for their pride as I continue my education. I am especially grateful for the love and patience of my wife, Katie.

CHAPTER 1 Introduction

The sense of vision enables humans to richly experience and interact with the world, however eye diseases compromise these vital activities of daily living. Age-associated vision loss is increasingly prevalent in our population due to the dramatic increase in the elderly in the population, increasing the economic, social and personal costs to individuals and society. Because light enters the eye and reaches the retina through transparent media for visual perception, these optical qualities can be used for imaging the retina. The retina is a highly organized tissue and segmental part of the central nervous system. In fact, the retina is the only part of the central nervous system that can be imaged optically and non-invasively, providing scientists with a unique medium for research and clinicians an opportunity to monitor eye diseases.

1.1. Anatomy of the Eye

The eye receives visual information from the environment in the form of light rays, which are converted into electrical signals that are transmitted along the visual pathway. Important anatomical features of the eye, for the purpose of this work, are shown in Figure 1.1. The cornea is the transparent and avascular tissue at the front of the eye that contributes to the largest proportion of light refraction. Together with the sclera, the visible white exterior coat, they act as a protective layer of the eye and help maintain the shape of the globe. The border zone or region where the cornea meets the sclera is called the limbus and is often used as an anatomical landmark during ophthalmic procedures or surgeries. The crystalline lens has two important optical properties, transparency and refraction. It further aids in focusing light onto the retina, most notably by changing the focal point through accommodation (Donaldson et al., 2017).

Accommodation is a change in the shape of the lens so that near objects can be focused on the retina. The vitreous body is a gel-like substance posterior to the lens that fills the vitreous chamber. Its functions are to provide support and physically retain the shape of the retina against the back of the eye, transmit and refract light onto the retina, and store and transport metabolites for the retina (Remington, 2012). The retina is the multi-layered neural tissue responsible for converting light energy into a neural signal. The signal then leaves the eye via the optic nerve and travels to centres in the brain for processing.

There are large differences in the anatomical dimensions and volume between the human eye and mouse eye. Figure 1.2 provides a schematic of the relative difference in the volume of each and key measurements. The most notable difference is that the mouse lens occupies approximately 75% of the eye (Gossman, 2004). This results in a significantly smaller relative vitreous volume compared to the human eye. These differences have important implications when administering substances into the vitreous, particularly the proximity to the retina when it is the target tissue.

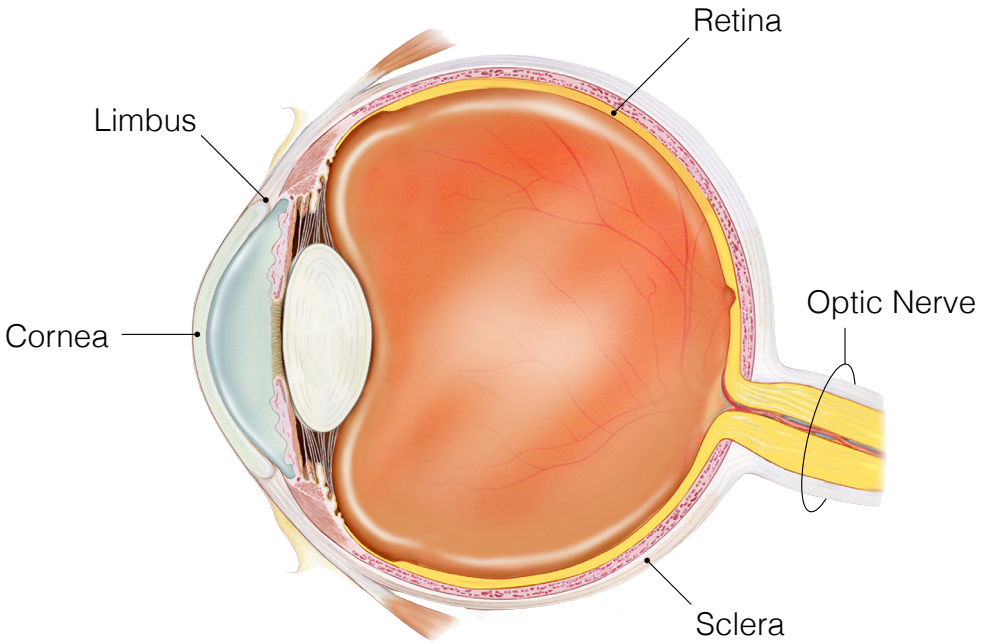

Figure 1.1 Anatomical structure of the human eye. A schematic sagittal cross-section of the human eye is shown. Major anatomical structures relevant to the work presented are labelled. Figure used with permission and adapted from National Eye Institute, National Institutes of Health.

	Human	Mouse
Length (a)	24 mm	3.37 mm
Diameter (b)	28 mm	3.32 mm
Vitreous Chamber Length (c)	16.78 mm	0.59 mm
Vitreous Volume	5.2 ml	5.3 ul

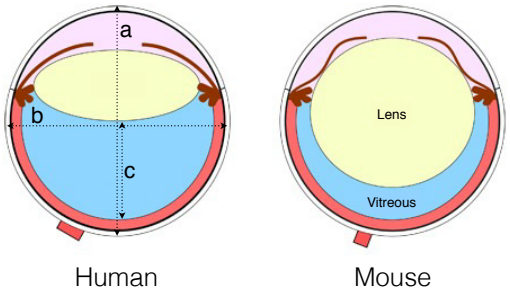

Figure 1.2 Comparison of human and mouse eye measurements. Values in the table compare gross differences in size and volume between human and mouse globes. Schematics are shown to demonstrate the relative difference in lens/vitreous volume ratio. Measures from Oyster (1999); figure used with permission (Creative Commons License) and adapted from Skeie et al. (2011).

1.2. Visual Processing in the Retina

The retina functions to detect light and initiate the initial steps of visual processing (Purves et al., 2001). There are five types of neurons in the retina: photoreceptors, bipolar cells, ganglion cells, horizontal cells, and amacrine cells. The retina is also organized into layers based on the location of cell somas and their processes (Figure 1.3). Light passes through most of the retinal layers until it reaches the light sensitive photoreceptors where a biochemical process is initiated. There are two types of photoreceptors, rods and cones, each containing a unique photopigment that is sensitive to a specific range of the visible spectrum. Rods are activated primarily in conditions with dim illumination, while cones are activated with bright and coloured stimuli. The absorption of light initiates the process of phototransduction; that is when photons are converted to graded signals of potential change. The somas of photoreceptors are located in the outer nuclear layer and photoreceptors synapse with bipolar cells in the outer plexiform layer. Bipolar cells respond to the release of glutamate with graded potentials. There are two types of bipolar cells: ON bipolar cells, that depolarize when the retina is stimulated by light, and OFF bipolar cells that are hyperpolarized in response to light. Bipolar cells synapse with retinal ganglion cells (RGCs) in the inner plexiform layer, which receive signals from both bipolar and amacrine cells, and transmit action potentials via the long RGC axon to visual centres in the brain. The innermost layer of the retina is the nerve fibre layer and is primarily comprised of RGC axons that traverse the retina to the optic nerve.

There are two other cells located in the inner nuclear layer (INL), horizontal cells and amacrine cells, both of which function to mediate lateral inhibition. Horizontal cells synapses with photoreceptors, bipolar cells and other horizontal

cells in the outer plexiform layer. Amacrine cells form synapses with bipolar cells, ganglion cells, and other amacrine cells in the inner plexiform layer.

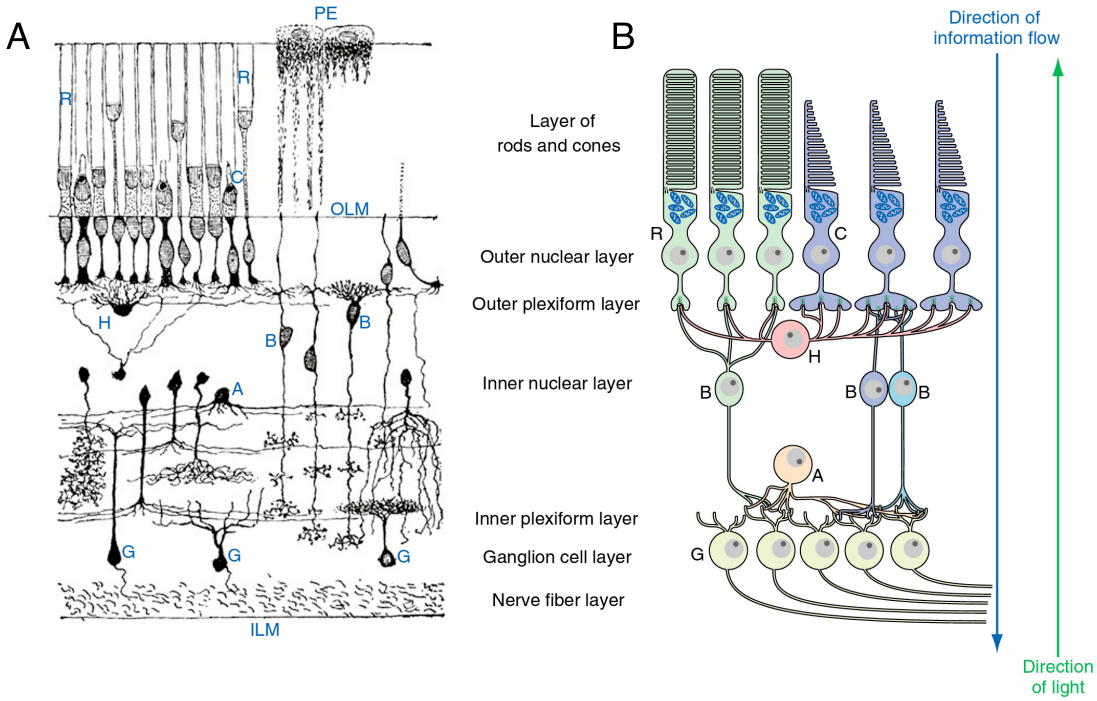

Figure 1.3 Retinal anatomy showing cell types and arrangement in layers. A) Drawing of Golgi-stained cells of the frog retina from Ramón y Cajal S. Histologie du système nerveux de l'homme & des vertébrés, vol 2, Paris, 1911). B) Schematic illustration of a generalized vertebrate retina showing retinal layers. A, amacrine cell; B, bipolar cell; C, cone; G, ganglion cell; H, horizontal cell; ILM, inner limiting membrane; OLM, outer limiting membrane; PE, pigment epithelium; R, rod. (Figure adapted from Vanderah et al. (2015), Nolte's The Human Brain, with permission from Elsevier)

1.3. Objectives and Hypothesis

The global objective of this work is to label RGCs with a clinically relevant technique for *in vivo,* non-invasive, and real-time imaging in wild-type mice. My hypothesis is that RGCs can be reliably imaged *in vivo* and longitudinally with fluorescent labels administered by intravitreal injection.

The specific objectives are:

1. To develop a method of labelling and detecting RGCs *in vivo* using a neuronal tracer and adeno-associated viral vectors (AAV).
2. To compare the rate of AAV transduction, *in vivo* image and signal quality, and specificity to RGCs between vectors with differing promoters.
3. To examine if AAV vectors affect the retinal structure and functional properties of RGCs.
4. To characterize the labelling changes visualized by *in vivo* fluorescence imaging as a result of RGC damage.

In **Chapter Two**, I begin by describing the background and motivation for this thesis. The chapter also contains the proof-of-principle work that I completed with cholera toxin subunit B (CTB) to demonstrate the ability to label and image retinal neurons *in vivo* and longitudinally. **Chapter Three** contains a study to test the efficacy and efficiency of labelling RGCs *in vivo* with adeno-associated viral vectors. **Chapter Four** provides an overall discussion for the entire thesis, in addition to discussing the implications of translating these methods to clinical application, limitations and future directions. In its entirety this work significantly adds to the development and understanding of methods for labelling and imaging RGCs *in vivo*.

CHAPTER 2 Imaging Retinal Ganglion Cells: Enabling Experimental Technology for Clinical Application

Co-Authorship Statement

The work in Chapter 2 is adapted from **Smith CA** and Chauhan BC. Imaging retinal ganglion cells: Enabling experimental technology for clinical application. *Progress in Retinal and Eye Research* 2015,44: 1-14.

CAS and BCC designed the research study, interpreted data and wrote the manuscript. CAS completed the literature review, conducted the experiments, acquired and analyzed data. BCC was the principal investigator and supervised the work.

2.1. Introduction

The leading causes of irreversible blindness include: age-related macular degeneration (AMD), glaucoma and diabetic retinopathy (Resnikoff et al., 2004). All three of these diseases affect the retina and specifically retinal neurons, leading to visual loss. The definition of open-angle glaucoma, the most common form of the neuropathy, is degeneration and loss of retinal ganglion cells (RGCs) and their axons with characteristic changes in the optic nerve head and the visual field (Kerrigan-Baumrind et al., 2000; Quigley and Green, 1979; Weinreb and Khaw, 2004). While diseases like AMD and retinitis pigmentosa are primarily associated with the loss of photoreceptors, studies of exudative AMD (Medeiros and Curcio, 2001) and retinitis pigmentosa (Humayun et al., 1999) have indicated that a significant cell loss in the ganglion cell layer (GCL) also occurs in these diseases. Therefore, RGC loss is an important characteristic of several significant eye diseases.

The eye possesses unique characteristics unlike any other tissue in the central nervous system in that non-invasive optical imaging of neural tissue *in vivo* is possible. By exploiting this property, a wide range of the electromagnetic spectrum can be utilized without introducing damaging radiation to the tissue. The transparency and physics of the ocular tissues allow light to pass directly through to the retina, creating an ideal scenario for the use of non-invasive imaging. Only minor manipulations to the eye, such as pupil dilation and corneal hydration, are required to achieve improved light transmission and optical quality. Development and advances of imaging devices has been growing at an overwhelming rate in recent years, in particular in the ophthalmic sector. An important goal of many devices is to provide longitudinal *in vivo* imaging of retinal tissue at a high resolution. The methods and means with which this can

be accomplished are constantly evolving, but many of the developments have not yet been translated for clinical use.

It has been estimated that approximately one-half of persons with glaucoma are unaware of their disease (Leske et al., 1994; Mitchell et al., 1996; Quigley, 1996; Tielsch et al., 1991; Wensor et al., 1998). Common clinical screening and detection methods for glaucoma include intraocular pressure measurement, perimetry and non-invasive imaging. However, the efficacy of these methods is not optimal since they do not represent direct measures of RGC properties. The current diagnosis that provides the best available evidence of glaucoma is based upon both structural changes obtained with optic nerve head and retinal nerve fibre layer imaging and functional changes, obtained with perimetry, that align with the clinical definition of glaucoma (Chong and Lee, 2012; Harwerth and Quigley, 2006). It is expected that a direct measure of RGC numbers would provide a more direct and accurate indication of ocular pathologies affecting RGCs and potentially allow for improved prognosis with more targeted and individualized therapeutic interventions.

This manuscript provides an overview of the current understanding and available technologies for imaging in glaucoma, specifically RGCs, in experimental and clinical environments. Direct imaging of RGCs can provide important opportunities to better understand glaucoma, however, it is not without challenges due to the various cell types in the GCL and cell labelling specificity. Unlike the use of the term 'specificity' in clinical diagnostic tests, specificity in the context of this thesis refers to cell labelling specificity, defined as the proportion of labelled cells that are of the desired population or cell-type. The potential for utilizing methods for the enhancement of ocular imaging by means

of cell labelling are highlighted with preliminary work that demonstrates the possibilities that exist in achieving retinal neuron labelling in a clinically relevant way. This review will discuss the clinical and engineering accuracy considerations of new technologies as well as the potential and challenges for translation of the work from the laboratory to the clinic.

2.2. Retinal Ganglion Cells

The retina is located in a relatively accessible portion of the central nervous system. As output neurons from the eye, RGCs are essential for signal transduction to the brain for visual processing. The human retina contains approximately 1.5 million RGCs (Massey, 2006) while the mouse retina contains approximately 60 000 (Jeon et al., 1998). The RGC somas are almost exclusively located in the GCL, however, a small minority of displaced RGCs are found in the inner nuclear layer (Drager and Olsen, 1981; Pang and Wu, 2011). On the other hand, the GCL does not only contain RGCs. It has been shown approximately 50% of GCL cells are displaced amacrine cells (Jeon et al., 1998) which are interneurons that aid in the signal transmission from inner retinal neurons to the RGCs. When analysis or imaging of a specific cell type, such as RGCs is desired, the heterogeneity of retinal layers presents a challenge. To overcome this challenge, methods of specific labelling or detection are required for cell specific identification and quantification.

2.2.1. Species Differences in Ganglion Cell Layer Composition and Retinal Projections

The composition of the GCL is largely the same among species, but there are small variations in the densities of cell types, soma size and projection targets. Studies have estimated that 41-49% of cells in the mouse GCL are RGCs (Farah and Easter, 2005; Jeon et al., 1998), while in the rat the figure is estimated to be

55% (Simon and Thanos, 1998). However, recent evidence indicates that the proportion of RGCs in the GCL of rodents is on average closer to 50% (Schlamp et al., 2013). In humans displaced amacrine cells account for 3% of the cells in the GCL of the central retina, but that number increases to almost 80% in the far periphery (Curcio and Allen, 1990). While in humans RGCs predominately project to the lateral geniculate nucleus (Levin et al., 2011), in rodents they predominately project to the superior colliculus which is the most common application site for retrograde tracers in rodent RGC labelling (Lund, 1965; Perry, 1981; Salinas-Navarro et al., 2009a). Other RGC projection sites in rodents include the suprachiasmatic nuclei, the accessory optic nuclei, the pretectal nuclei and the lateral geniculate nucleus (Rodieck, 1979), while in humans they include the suprachiasmatic nucleus of the hypothalamus, subcortical midbrain nuclei, accessory optic nuclei and pretectal nuclei (Calkins, 2012; Levin et al., 2011). Understanding the anatomical differences between animals and humans is an important consideration when developing a method with translational potential.

2.2.2. Retinal Ganglion Cells and Glaucoma

It has been shown that the GCL displays among the greatest neuronal loss in aging retinas (Lei et al., 2011) and that RGCs are arguably the most susceptible ocular neurons to aging (Weale, 2004). A defining characteristic of glaucoma is the death of RGCs and the degeneration of their axons, thereby leading to vision loss (Quigley, 2004). The optic nerve head (ONH) is the purported site of RGC axonal injury in glaucoma (Quigley, 1999). However, the progression of RGC death in glaucoma has also been proposed as compartmentalized damage, with distal-to-proximal degeneration (Calkins, 2012). Stressors would cause dysfunction of RGC transport and degeneration of the RGC dendrites, soma and axon. This idea provides evidence that RGC function and survival is dependent

on the entire cell. Suggested mechanisms of the damage have been vascular deficiencies, neurotoxicity, tissue remodelling and mechanical deformation (Burgoyne et al., 2005; Hernandez, 2000; Osborne et al., 2001; Tezel, 2008). However, how any specific mechanism precisely causes RGC death remains largely unknown. Hence, besides reduction of intraocular pressure, which has been shown to reduce the incidence of glaucoma and its progression (Collaborative Normal-Tension Glaucoma Study Group, 1998; Kass et al., 2002; Leske et al., 2003), additional neuroprotective approaches remain an objective and a challenge. Clinicians currently use structural measures, such as the width the neuroretinal rim area of the optic nerve head or thickness of the retinal nerve fiber layer, as surrogates for RGC quantification. However, there is currently no method of directly quantifying the number or density of RGCs in humans.

2.2.3. The Challenge of Identifying Retinal Ganglion Cells

The similarities between RGCs and amacrine cells make it difficult to determine the proportion of each within the GCL. Common structural and functional similarities are morphology, soma location, electrophysiology and light response (Cook and Werblin, 1994; Pang and Wu, 2011; Pang et al., 2002a, b; Taylor, 1996). The soma size in the two cell types differ in some species; however, this effect can be diminished when RGCs range in size according to their location in the retina (central vs. peripheral) (Kolb et al., 1992; Mitrofanis and Provis, 1990). Perhaps the most distinct difference between RGCs and amacrine cells is the presence of the RGC axon, which together with the axons of other RGCs forms the optic nerve. A continuing area of research is identifying labels or markers for RGCs, such as endogenous compounds, proteins or genes, which can then be used for identifying RGCs in intact retina. A reliable *in vivo* marker must be specific to only RGCs and must identify the majority of RGCs throughout the

retina. To date, there is little evidence that this has been accomplished with currently known markers, such as Thy1 (Feng et al., 2000), brain-derived homeobox/POU domain protein 3A (Brn3a) (Nadal-Nicolas et al., 2012) or γ - synuclein (Surgucheva et al., 2008). Recently, promising results have been published that demonstrated exclusive labelling of RGCs with an antibody against RNA-binding protein with multiple splicing (RBPMS) (Rodriguez et al., 2014). Ongoing work in our laboratory is investigating the application of RGC markers for longitudinal *in vivo* imaging in mice as a measure of RGC viability and damage.

2.2.4. Quantification of Retinal Ganglion Cells

Many RGC labelling methods and studies have focused on quantifying an absolute number of RGCs within the retina or an average density of RGCs in the GCL. However, there is substantial variation in the number of RGCs not only within species, but also across different strains of the same species (Williams et al., 1996). Such variability has been shown in mice, cats, monkeys and humans, in some cases revealing a more than two-fold difference between individuals (Curcio and Allen, 1990; Illing and Wässle, 1981; Spear et al., 1996). Small genetic or environmental differences appear to be in part responsible for this variation in RGC numbers (Williams et al., 1996).

With the large inter-subject variability in the number of RGCs, it is challenging to determine whether in a given subject the quantification represents normal variation or loss due to disease. Thus, quantification of RGCs at a single time point is an unreliable indicator of disease. Longitudinal changes in the number of labelled cells in each animal or patient is an important objective because the between-subject variability can be accounted for, however, it is important to note

that any aging effects will be compounded to those due to disease progression. Advances in microscopy and software techniques allow us to track the same eye longitudinally and monitor changes in labelled cells over time. Furthermore, if RGC density is utilized as a measure of disease progression, a given subject's density can be compared to reference values at one point in time, or over time to determine whether the observed changes exceed those due to normal aging. Some new ophthalmic imaging devices make these approaches increasingly possible with features to acquire images while adjusting for eye movements and image registration for imaging at repeated time points.

2.3. Retinal Imaging Modalities

Ophthalmic imaging continues to be an emerging field of medical technology that is growing at an unprecedented rate. While this presents opportunities for clinical use, the advances also provide practical challenges. Many clinicians are driven to provide innovative and advanced technological imaging modalities that provide superior diagnostics for their patients. The challenges associated with rapid improvements include the obsolescence of techniques, which makes it challenging to maintain consistent monitoring of chronic diseases, such as glaucoma. Imaging modalities often require a trade-off between resolution and penetration depth (Marschall et al., 2011), which is important in deciding which technology is best suited for the desired application (Figure 2.1). There has also been substantial research to improve the image quality of devices by applying adaptive optics. Adaptive optics compensates for aberrations in the optical path using active optical elements and has successfully used to image photoreceptors in monkeys and humans without the use of an exogenous label (Williams, 2011). This technology can monitor cells with improved lateral resolution and has demonstrated sufficient light penetration to discern all layers of the retina (Miller

et al., 2011) allowing for the possibility of measuring a true cell density. With improved imaging modalities, there is a need to build upon this technology with imaging techniques that can detect early changes in ocular tissue health.

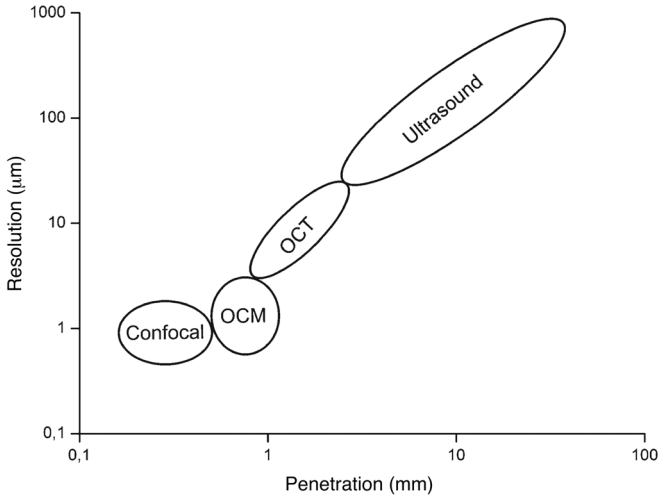

Figure 2.1 The relationship between spatial resolution and penetration depth when comparing imaging techniques. Optical coherence microscopy (OCM) utilizes the ability of deep tissue imaging from optical coherence tomography (OCT) and high spatial resolution of confocal microscopy. OCT and OCM close the gap between high-resolution optical microscopy techniques (e.g., confocal microscopy) and techniques with long penetration depth (e.g., ultrasound imaging). Figure adapted from Marschall et al., 2011, with permission of Springer.

2.3.1. Optical Coherence Tomography

Optical coherence tomography (OCT) uses echo time delay and the magnitude of backscattered light to obtain cross-sectional images in the form of B-scans. Cross-sectional images provide information about the thickness of the various retinal layers, but do not commonly provide the ability to image retinal neurons with single cell resolution. High resolution images produced by spectral-domain OCT have been shown to be useful to track longitudinal retinal structural changes in both experimental (Chauhan et al., 2012; Guo et al., 2010) and clinical glaucoma (Bussel et al., 2013; Schuman, 2008). Improved image quality has been made possible with advanced OCT technologies such as image registration for precise follow-up imaging and eye tracking systems to reduce motion artefacts and noise.

2.3.2. Confocal Scanning Laser Ophthalmoscopy

In confocal scanning laser ophthalmoscopy (CSLO), backscattered light from a laser light source and confocal optics is deviated by a beam splitter to a detector. The presence of a pinhole suppresses backscattered light outside of the focal plane, resulting in high axial resolution and the ability to generate tomographic images (Webb et al., 1987; Zinser et al., 1989). High resolution images acquired with CSLO have the ability to differentiate between small changes in retinal pathology, making it a useful tool for detecting the progression of glaucoma in patients (Chauhan, 1996). Several groups have utilized CSLO for *in vivo* imaging of RGCs in animal models of RGC degeneration by implementing either endogenous or exogenous cell labelling methods (Cordeiro et al., 2011; Higashide et al., 2006; Leung et al., 2008b).

2.4. Enhancing Ocular Imaging Using In Vivo Cell Labelling

Currently available imaging modalities provide important structural information about the retina, but there remains an untapped resource of functional information from retinal cells and neurons that could be shown by adapting existing imaging techniques. Many medical imaging modalities, such as magnetic resonance imaging (MRI), computed tomography (CT) and positron-emission tomography (PET), employ the use of contrast agents to either enhance detection of anatomical structures or visualize functional changes. The use of contrast agents has not been utilized in clinical ophthalmic imaging much beyond fluorescein or indocyanine green angiography despite the relatively ease of accessibility of administering them into the systemic circulation or directly in the eye. The introduction of contrast agents or labelling dyes could provide a new dimension to ocular imaging of the retina. However, to date, they are largely only used in experimental animal studies for understanding neuronal projection, cell-to-cell interactions and cellular degeneration.

Since the layers of the retina contain non-neurons and supporting tissue, there is a need to distinguish the neurons of interest, in this case RGCs, from the rest of the retina. The potential advantage of utilizing labelling dyes and contrast agents is for differentiation of specific cells types in the GCL. Fluorescence is one mechanism for providing *in vivo* visualization of specific cells and has been used extensively for visualizing a specific population of retinal neurons experimentally. To the best of our knowledge, *in vivo* fluorescence visualization of retinal neurons in humans has only been achieved using apoptotic markers (Cordeiro et al., 2017).

2.5. Experimental Studies

2.5.1. Retrograde Tracers

To label RGCs, investigators have introduced tracers via the superior colliculus (Figure 2.2A) (Higashide et al., 2006; Sabel et al., 1997; Vidal-Sanz et al., 1987), lateral geniculate body (Gray et al., 2006) or optic nerve (Köbbert et al., 2000) in animal models. Several types of neuronal tracers have been used, most commonly fluorescent dyes, which are distributed primarily by active transport within the neurons (Köbbert et al., 2000). The proportion of RGCs labelled in rodents by transport via the superior colliculus has been shown to be greater than 96%, compared to that of labelling via the transected optic nerve stump, which is assumed to be 100% (Salinas-Navarro et al., 2009a; Salinas-Navarro et al., 2009b).

Retrograde labelling has been well established for identifying and quantifying RGCs, but requires invasive surgery. A further concern about this technique for RGC specific labelling is the possibility that other cell types, such as microglia and macrophages, are frequently labelled due to phagocytosis of RGCs after injury (Bodeutsch and Thanos, 2000; Wang et al., 2010), creating a challenge for longitudinal studies and acquiring data specifically for RGC density. Retrograde labelling is a possible approach for longitudinal *in vivo* labelling and histological analysis of RGCs in experimental animal studies, but its invasiveness and potential lack of specificity to RGCs following injury does not provide potential for clinical translation.

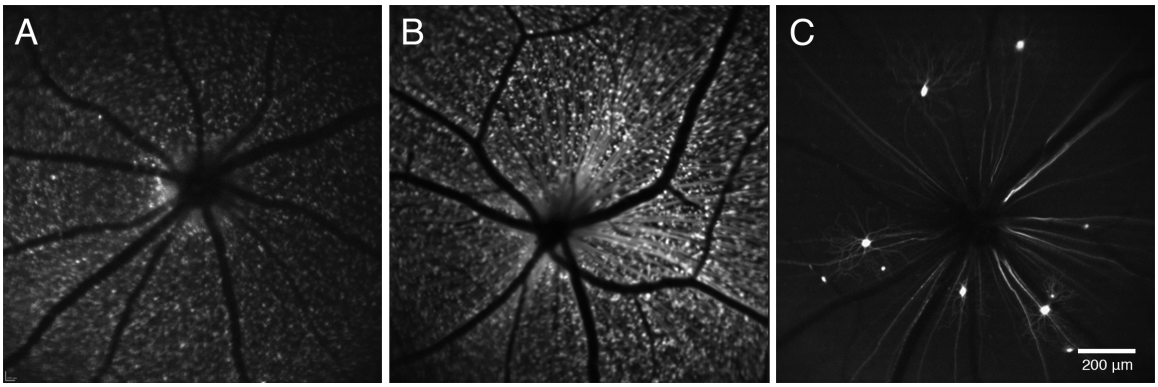

Figure 2.2 ***In vivo*** **confocal scanning laser ophthalmoscopy images of mouse retina.** Fluorescent images in animals A) with retrograde superior colliculus RGC labelling of cholera toxin subunit B, a non toxic neuronal tracer, conjugated to Alexa Fluor® 488, B) expressing cyan fluorescent protein (CFP) under the Thy1 promoter and C) expressing yellow fluorescent protein (YFP) under the Thy1 promoter.

2.5.2. Electroporation

The application of voltage across the specimen (e.g. eye) provides rapid and effective transfection of labelling agents or DNA vectors into the cells (Dezawa et al., 2002; Garcia-Frigola et al., 2007; Nickerson et al., 2012). If the target cells are within the GCL the dye is commonly administered into the vitreous, whereas if the cells of interest are in the outer nuclear layer the dye is administered via a subretinal injection (scleral side). This rapid transfection allows for immediate imaging and assessment of retinal cells including RGCs. Approximately 41.5% of RGCs are transfected in the electroporated area of the retina when compared to co-localization of retrograde labelling in the same animals (Dezawa et al., 2002).

The greatest disadvantage of this method is that the loading of dye is not specific to a particular cell type (Yu et al., 2009) and is technically challenging when performed in the eye. Damaging tissue within the eye is of obvious concern during electroporation, especially if the intent is to perform *in vivo* imaging. Transfection of dyes by electroporation also has limitations of poor labelling efficiency in some cell types and in larger animal models (Matsuda and Cepko, 2004). The advantage of electroporation is that it reduces the challenge of introducing a polar dye to cross the cell membrane, which it does in a fast and efficient manner in animal studies.

2.5.3. Transgenic Animals

Transgenic animals have been generated for expression of fluorophores under the control of specific RNA promoters. For example, the Thy1-CFP mouse strain expresses cyan fluorescent protein (CFP) under the modified Thy1 gene promoter (Feng et al., 2000). This technique has the capability of non-invasive labelling, but is limited to animal models due to the unlikely acceptance of

genetically altering human genes for purpose of cell labelling. CFP expression occurs in approximately 90% of RGCs in mouse retinas (Figure 2.2B). However, Thy1-CFP is not exclusively expressed in RGCs as approximately 20% of CFP-positive cells were displaced amacrine cells (Wang et al., 2010). Furthermore, after optic nerve transection, CFP labelling was taken up by microglia, presumably due to phagocytosis of RGC fragments (Wang et al., 2010). Most recently Thy1-CFP mice have been used to demonstrate the ability to detect structural changes of RGC density (Leung et al., 2008a; Leung et al., 2009) and retinal thickness post-transection of the optic nerve in longitudinal studies (Chauhan et al., 2012).

Another relevant transgenic mouse is the Thy1-YFP that expresses yellow fluorescent protein (YFP) under the same Thy1 gene promoter (Feng et al., 2000). These mice express fluorescence in fewer RGCs (Figure 2.2C), despite using the same regulatory elements, and have been shown to be a valuable tool in studying individual RGCs in longitudinal studies. Parameters such as cell body size, axon diameter, dendritic field size, branching complexity, number of terminal branches and total dendritic length can all be measured in these mice to characterize the morphology of RGCs (Kalesnykas et al., 2012; Leung et al., 2011; Oglesby et al., 2012). While these transgenic models are not clinically relevant, they are useful for experimental studies and in developing new imaging technologies.

2.5.4. Opportunities and Limitations

Experimental approaches for *in vivo* retinal cell labelling, via retrograde transport of fluorescent dyes, electroporation and transgenic animals, are very useful in providing cell labelling in animal models and in some cases demonstrate cell

specificity. All experimental approaches described here, especially retrograde labelling (Thanos et al., 2002) and transgenic animals (Chauhan et al., 2012; Leung et al., 2011), are a valuable resource that can be used in longitudinal studies of retinal degeneration. A major limitation of these approaches is that they cannot be translated to human applications. The challenge now is to translate the successes of experimental animal studies into clinical practice to aid in assessing the progression of diseases such as glaucoma.

2.6. Clinically Applicable Methods

A Canadian study indicated that between 2005 and 2007, the rate of intravitreal injections increased 8-fold, from 3.5 to 25.9 injections per 100 000 patients per month (Campbell et al., 2010). The trend of increased intravitreal injection usage is not limited to North America (Keenan et al., 2012) and the average number of injections per patient has remained constant for several years (Lebel et al., 2013). The increase has been attributed to the development of drugs for posterior segment diseases, specifically AMD. Intravitreal injection is a mildly invasive method of introducing drugs or tracers into the eye and while there is potential for systemic uptake, it is an effective route with a relatively low rate of complication (Jager et al., 2004; Jonas et al., 2008). Patient pain intensity is reported as low to mild during intravitreal injection procedures (Rifkin and Schaal, 2012) and was shown to be reduced with smaller needle gauge (Rodrigues et al., 2011) and subsequent injections (Rifkin and Schaal, 2012).

While many new methods are under development for retinal drug delivery in humans, intravitreal injection is currently the primary choice for administering drugs to the posterior segment of the eye (Eljarrat-Binstock et al., 2010). The injected drug is expected to reach the target site, commonly the retina, by means

of diffusion and convection. A challenge of intravitreal injections is the large diffusion distance from the injection site through the vitreous to the retina. In terms of drug delivery, the desirable effect of the drug is to be present at the target site at a therapeutic level of concentration for a sufficient time period without reaching levels of toxicity (Kwak and D'Amico, 1992; Rosenfeld et al., 2005).

Recent clinical trials have shown promising results by administering agents via viral vectors in the treatment of Leber's congenital amaurosis (Bainbridge et al., 2008; Jacobson et al., 2012; Maguire et al., 2008). These agents are most often administered by either intravitreal or subretinal injection of the vector. With the advancement of such treatments, it is anticipated that improved direct administration methods will be developed for human use. Furthermore, the safety and concerns of introducing agents into the eye for diagnostic and treatment purposes will likely be diminished. Extensive research is currently devoted to developing sustained-release or biodegradable implants (Kuno and Fujii, 2010; Saati et al., 2010), controlled-delivery (Wells et al., 2011) and nano/microparticles (Jeun et al., 2011; Ryu et al., 2011) for the posterior segment (Eljarrat-Binstock et al., 2010); however, these methods still require initial administration by means of intravitreal injection. Alternative methods, such as transcleral administration via iontophoresis are also currently being investigated (Myles et al., 2005).

The introduction of an agent into the vitreous puts it in close proximity to the GCL. When administering a small volume of compound in a relatively large region, parameters of volume, concentration and toxicity are vitally important. However, this route of delivery opens a host of possibilities for the type of tracer

that can be introduced for labelling the neurons of the retina. Intravitreal injection delivery of cell penetrating peptides (Barnett et al., 2009; Johnson et al., 2007), viral vectors (Folliot et al., 2003; Yin et al., 2011), proteins (Barnett et al., 2006) and now neuronal tracers (Figure 2.3) all carrying fluorescent labels are possible approaches to visualizing RGCs. Work has been completed that introduced agents to show apoptosis of RGCs (Barnett et al., 2009; Cordeiro et al., 2011), but no biomarkers have been utilized via intravitreal injection that labelled healthy RGCs. Labelling apoptotic cells does not provide the desired degree of specificity to RGCs, nor does it provide an indication of how many RGCs still remain. An *in vivo* biomarker for healthy RGCs would be a useful indicator to the overall health of the RGC population in a live animal or patient.

2.7. Cholera Toxin Subunit B Labelling of Retinal Ganglion Cells

The purpose of this study was to assess RGC labelling after administering a neuronal tracer via intravitreal injection for *in vivo* non-invasive and real-time imaging in wild type mice. The presence of a neuronal label in RGCs has not shown a diminished functional response, providing no evidence that labelling interferes with the normal function of RGCs (Germain et al., 2013). Cholera toxin subunit B (CTB), conjugated to a fluorescent label, was chosen for RGC soma detection for the following reasons: 1) CTB is available conjugated to a bright and stable fluorophore that is compatible with the laser and filters of our imaging system, 2) immunohistochemical protocols can be completed on the tissue following application of CTB as a tracer (Angelucci et al., 1996) and 3) CTB has been shown not to remain in axons for extended time periods, but does persist in cell somas making it useful for estimating cell density (Köbbert et al., 2000). Furthermore, CTB has been shown to be non-toxic to cells (Aman et al., 2001) and has been administered systemically to patients (Sanchez and Holmgren, 2011).

Both anterograde and retrograde transport of CTB has been shown to occur along RGC axons (Abbott et al., 2013; Mikkelsen, 1992). As a means of determining CTB specificity to RGCs, RBPMS was used as an immunohistochemical marker which is selectively expressed by RGCs (Piri et al., 2006) with high specificity in several mammalian species (Kwong et al., 2010; Rodriguez et al., 2014). It was hypothesized that uptake of CTB by RGCs serves as a detectable tracer for longitudinal *in vivo* imaging of viable RGCs.

2.8. Methods

2.8.1. Animals

Animal procedures complied with the Canadian Council of Animal Care standards and animal ethics approval was obtained from the University Committee on Laboratory Animals at Dalhousie University. Adult male C57BL/6 mice, 18-20 g in weight (JAX™ Mice Stock Number: 000664, Charles River Laboratories, Saint-Constant, QC, Canada), were used. Mice were housed in a 12-hour light-dark cycle environment and provided food and water *ad libitum*. A total of 16 mice were used: group 1 for establishing CTB labelling time points for *in vivo* imaging (n = 6), group 2 for retrograde labelling (n = 2) and group 3 for RBPMS immunohistochemistry (n = 8).

2.8.2. In Vivo Imaging

For *in vivo* imaging, mice were anesthetized with initial induction of 3-4% isoflurane (vol) (Baxter Corporation, Mississauga, ON, Canada) with 1.5 L/min oxygen flow and maintained at 1.5-3% isoflurane with 0.8 L/min oxygen flow via a nose cone.

Prior to imaging, the pupil of the left eye was dilated with topical mydriatics: one drop each of 1% tropicamide (Alcon Canada Inc., Mississauga, ON, Canada) and 2.5% phenylephrine hydrochloride (Alcon Canada). A small amount of ophthalmic liquid gel (Tear-Gel, Novartis Pharmaceuticals Canada, Inc., Mississauga, ON, Canada) and a plano (0 D) polymethyl methacrylate contact lens (Cantor and Nissel, Brackley, UK) was placed on the cornea to maintain corneal hydration. *In vivo* CSLO imaging (Spectralis Multiline, Heidelberg Engineering GmbH, Heidelberg, Germany) was performed for each animal with an auxiliary +25 diopter lens attached to the camera objective.

Baseline images focussed at the level of the nerve fiber layer were first acquired with infrared (820 nm) illumination. The camera focus was adjusted to obtain the optimal fluorescence images (488 nm excitation, 500 - 550 nm emission bandpass filter) at the GCL layer. Each image was averaged 16 times using automatic real-time eye tracking software. The imaging protocol was repeated at multiple time points post-injection with the image tracking software to ensure that the same retinal areas were imaged.

2.8.3. Intravitreal Injection and Retrograde Labelling of Retinal Ganglion Cells

Labelling of RGCs was achieved by an intravitreal injection performed approximately 0.5 mm posterior to the superotemporal limbus at a depth of approximately 1 mm in the left eye only. A prototype injection device was designed, manufactured and tested with the objective of completing an efficient and reproducible intravitreal injection in mice (Appendix C). However, manual freehand injections were found to be more effective compared to the prototype, which required further development. A 30G needle was used to puncture the sclera for the injection and a 10 μl syringe with a 33G needle (Hamilton

Company, Reno, NV, USA) was used to administer 1 μl of 0.5% concentration CTB (recombinant) conjugated to Alexa Fluor® 488 (Molecular Probes Inc., Eugene, OR, USA) (CTB-488) mid-vitreous. The same anaesthesia protocol described above was used.

As a means of comparing and validating the intravitreal injection labelling, some retinas were retrograde labelled via the superior colliculus by CTB conjugated to Alexa Fluor® 594 (Molecular Probes) (CTB-594) and then later labelled by intravitreal injection of CTB-488. Once anesthetized, the mouse was placed in a stereotaxic frame and the skull exposed and kept dry. One hole was made on the right side at 2.92 mm posterior to bregma and 0.5 mm lateral to the midline using a drill. Two (2) microlitres of 0.5% CTB-594 was injected at a depth of 2 mm from the brain surface into the superior colliculus on the right side over a duration of 1 minute.

2.8.4. Tissue Preparation and Immunohistochemistry

Fifteen days post-intravitreal injection, animals were sacrificed with an overdose of sodium pentobarbital by intraperitoneal injection. The cornea and lens were removed and the eye cups fixed in 4% paraformaldehyde for 2-3 hours. The eyes were then hemisected and half the retina flat-mounted while the other half was transferred to 30% sucrose prior to being cryo-sectioned at 14 μm thickness. All chemicals, reagents and solutions were obtained from Sigma-Aldrich (Oakville, ON, Canada) unless otherwise stated, and were prepared fresh in phosphate-buffered saline (PBS) from stock solution.

2.8.5. Retinal Flatmounts

Retinas were washed in 1X phosphate-buffered saline (PBS) for 10 minutes and incubated in blocking buffer (10% normal goat serum, 0.5% Triton X-100) overnight at 4°C. Retinas were incubated for 6 days at 4°C in primary antibody against RNA binding protein with multiple splicing (RBPMS, 1:1000 guinea pig anti-RBPMS, gift from Dr. Nicholas Brecha; Rodriguez et al., 2014). Retinas were then washed in PBS and incubated overnight at 4°C in Cy3 (1:500 Cy3-conjugated goat anti-guinea pig, Jackson Immuno Research Laboratories Inc., West Grove, PA, USA). A nuclear counterstain, TO-PRO-3 Iodide (Molecular Probes), was used confirm that quantification of CTB-488 positive staining was cellular. Retinas were rinsed in PBS, incubated in 0.1% Triton X-100 and PBS for 10 minutes, incubated in TO-PRO-3 Iodide stain for 15 minutes and rinsed in PBS. Slides were mounted with anti-fade fluorescent mounting medium and coverslipped.

2.8.6. Retinal Sections

Immunohistochemical amacrine cell labelling was performed in retinal sections with primary antibodies for amacrine cells, including choline acetyltranferase (ChAT) and gamma-aminobutyric acid (GABA).

For ChAT immunohistochemistry, sections were incubated in 0.4% Triton X-100 in PBS at room temperature for 30 minutes, rinsed in PBS, incubated in blocking buffer (3% normal donkey serum, 2% bovine serum albumin (BSA), 0.1% Triton X-100) for 1 hour at room temperature and incubated overnight at room temperature in primary antibody against ChAT (1:100 goat anti-ChAT, Millipore, Billerica, MA, USA). Sections were then rinsed in PBS and incubated in Alexa Fluor® 633 (1:200 Alexa Fluor® 633 conjugated donkey anti-goat IgG) for 2 hours. For GABA immunohistochemistry, sections were washed in PBS, incubated in

blocking buffer (3% normal donkey serum, 0.1% Triton X-100) for 1 hour at room temperature and incubated overnight at room temperature in primary antibody against GABA (1:2000 rabbit anti-GABA, Sigma-Aldrich). Sections were then rinsed in PBS and incubated in Cy5 (1:200 Cy5-conjugated donkey anti-rabbit, Jackson Immuno Research) for 2 hours. All slides were mounted with anti-fade fluorescent mounting medium and coverslipped.

2.8.7. Cell Sampling and Statistical Analyses

Flat mounts and sections were imaged with confocal microscopy (Nikon C1, Nikon Canada Inc., Toronto, ON, Canada) equipped with narrow-band fluorescent filters centred for excitation wavelengths of 488, 594 and 633 nm. Fluorescence images were captured with Nikon EZ-C1 software with 1024 x 1024 pixel frame size and pixel dwell of 5 μs. Z-stacks had a range that included the thickness of the GCL in flat mounts or the thickness of the tissue in sections and were acquired in 2-4 μm steps.

Images were acquired with a 40x objective with a frame area of approximately 0.1 mm^2. In flat mounted half retinas, a total of nine images were acquired to quantify labelling in the GCL, three images from each of three regions, namely, central, mid-peripheral and peripheral, with respect to the optic nerve head. In each sampled field, the number of cells labelled by (1) CTB-488, (2) RBPMS, and (3) RBPMS with CTB-488 were quantified independently with graphics editing software (Adobe Photoshop CS6, Adobe Systems Inc.). Retinal sections were used for qualitative analysis of co-localization between (1) CTB-488 and retrograde labelled cells (CTB-594) and (2) CTB-488 and immunohistochemical amacrine cell (ChAT and GABA) co-localization.

Cell counts were expressed as median densities and the Kruskal-Wallis test used for comparing all groups. The Mann-Whitney test was used for comparisons between RBPMS cell counts and cell counts previously reported in C57BL/6 mice using retrograde labelling (Salinas-Navarro et al., 2009a). This analysis was performed to determine whether RBPMS labelled a similar proportion of cells in the GCL compared to retrograde labelling. The Wilcoxon signed-rank test was used for comparison between intravitreal injection CTB-488 and RBPMS cell counts. Statistical tests were two-tailed and statistical significance was assumed when $p < 0.05$.

2.9. Results

Mice that received intravitreal injections of CTB-488 had strong fluorescence labelling in the GCL. Individual cells were detected by *in vivo* CSLO imaging after 10-15 days and successfully imaged consecutively up to 100 days post-injection (Figure 2.3). Furthermore, animals were imaged post-injection with minimal to no apparent signs of retinal damage as a result of the intravitreal injection. There were no cases of the needle damaging the lens, which would result in an inflammatory response causing opacification, compromising the ability to complete CSLO imaging. These results demonstrate the ability to image, *in vivo*, individual cells repeatedly over time after a single injection.

Retinal sections imaged by confocal microscopy confirmed the *in vivo* findings of strong labelling of intravitreal injection CTB-488 in the GCL and dimmer labelling in the inner nuclear layer (INL) (Figure 2.4A). CTB-594 provided strong labelling in the GCL and a few displaced RGCs in the INL (Figure 2.4B). There was a high degree of co-localization of the intravitreal injection labelling with

retrograde labelling and all CTB-488 labelling appeared to be associated within cells when compared to a nuclear stain (Figure 2.4C).

RBPMS co-localized with CTB-488 positive cells in the GCL, indicating most of the CTB-488 labelling is that of RGCs (Figure 2.5). RBPMS immunohistochemical labelling was used as a comparison to intravitreal injection labelling because it represents a more complete population of RGCs, not only those projecting to the superior colliculus. Amacrine cell markers co-localized with a few CTB-488 positive cells in the GCL and INL, indicating some of the CTB positive cells are amacrine cells (Figure 2.6). However, CTB-488 administered by intravitreal injection does appear to label more RGCs than amacrine cells.

Fifteen days post-injection, the median (interquartile range) density of intravitreal injection CTB-488 labelled cells was 3110 (2980, 3240) cells/mm^2 and RBPMS labelled cells was 2560 (2500, 2740) cells/mm^2 in the same animals. The distributions of RGC densities for the two labelling methods are shown in Figure 2.7. The difference between CTB-488 and RBPMS cell counts was 19.4%, with the number of CTB-488 labelled cells significantly higher than those labelled with RBPMS ($p < 0.05$), an expected finding since CTB-488 was shown to be labelling some amacrine cells in the GCL. In previous work by Salinas-Navarro *et al.* (2009a), the mean (standard deviation) density of RGCs retrogradely labelled at the superior colliculus in C57BL/6 mice was 2821 (281) cells/mm^2. The Kruskal Wallis test revealed a significant effect of labelling methods on RGC density ($H = 12.6$, $p < 0.05$). However, the average RGC density of RBPMS labelling in the GCL, 2560 (2500, 2740) cells/mm^2, was non-significantly lower than that reported for retrograde labelling, 2821 (281) cells/mm^2, ($p = 0.062$). This result was expected as a small minority of RGCs project to targets other than the superior

colliculus. Table 2.1 shows that over 58% of RBPMS positive cells were labelled with CTB-488 fifteen days after intravitreal injection. At the same time, the number of CTB-488 positive cells that were labelled with RBPMS was approximately 53%.

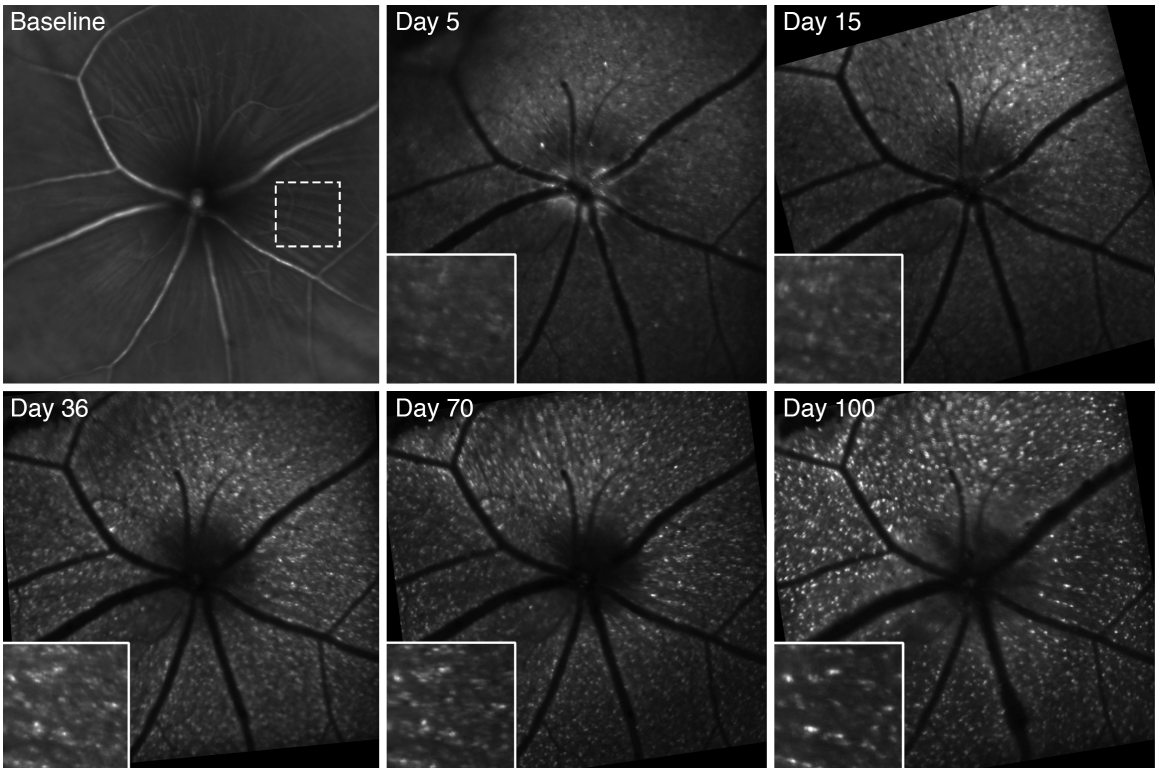

Figure 2.3 Longitudinal confocal scanning laser ophthalmoscopy images of a mouse retina fluorescently labelled with cholera toxin subunit B (CTB). Images are from the same animal and acquired *in vivo* sequentially up to 100 days following intravitreal injection of CTB-Alexa Fluor® 488. Baseline image was acquired using infrared mode (820 nm) and all other images using 488 nm excitation laser. Inset images are higher magnification of the region outlined in the baseline image.

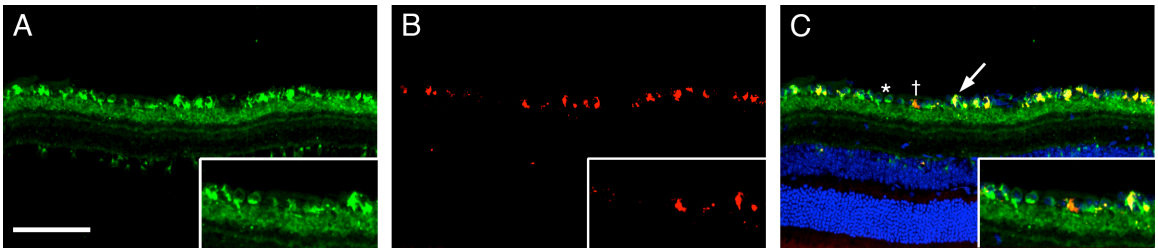

Figure 2.4 Intravitreal injection and retrograde labelling of mouse retina. Confocal microscopy of a 14 μm section of mouse retina following **A)** labelling via intravitreal injection of CTB-Alexa Fluor® 488 (green), **B)** retrograde labelling via superior colliculus injection of CTB-Alexa Fluor® 594 (red) and **C)** merge image with nucleic stain TO-PRO Iodide (blue). Most of cells in the GCL are co-labelled indicating intravitreal injection labelling by CTB-Alexa Fluor® 488 labels most RGCs (see Table 2.1). The arrow indicates a double labelled cell, the dagger (†) a cell labelled by retrograde labelling only and the asterisk (*) a CTB-488 only labelled cell. Scale = 100 μm.

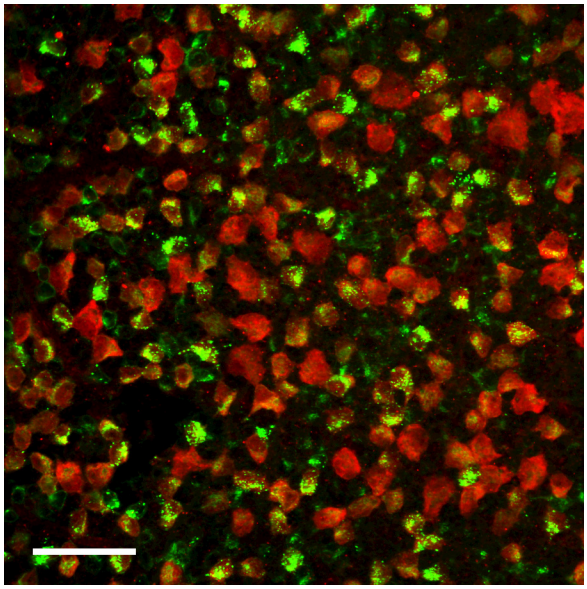

Figure 2.5 Co-localization of cells labelled with CTB and RBPMS in mouse retina. Confocal microscopy of flat mounted retina 15 days post- injection of CTB-Alexa Fluor® 488 (green) and immunohistochemical labelling of RGCs by RBPMS (red). Scale bar = 50 μm.

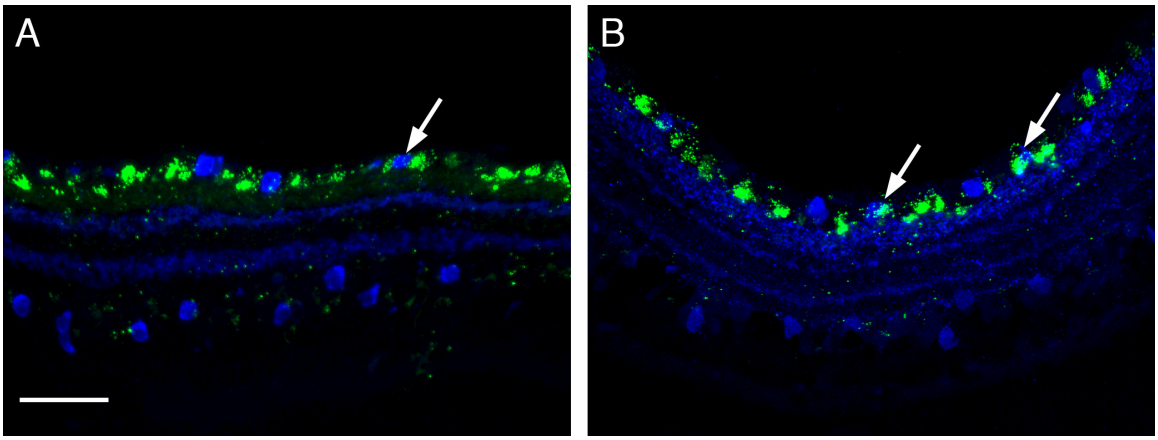

Figure 2.6 Co-localization of cells labelled with CTB and amacrine cells in mouse retina. Confocal microscopy of a 14 μm section of mouse retina following intravitreal injection of CTB-Alexa Fluor® 488 (green) and immunohistochemical labelling of amacrine cells by **A)** ChAT (blue) or **B)** GABA (blue). Arrows indicate co-localization that demonstrates some amacrine cells are being labelled by CTB-Alexa Fluor® 488. Scale bar = 50 μm

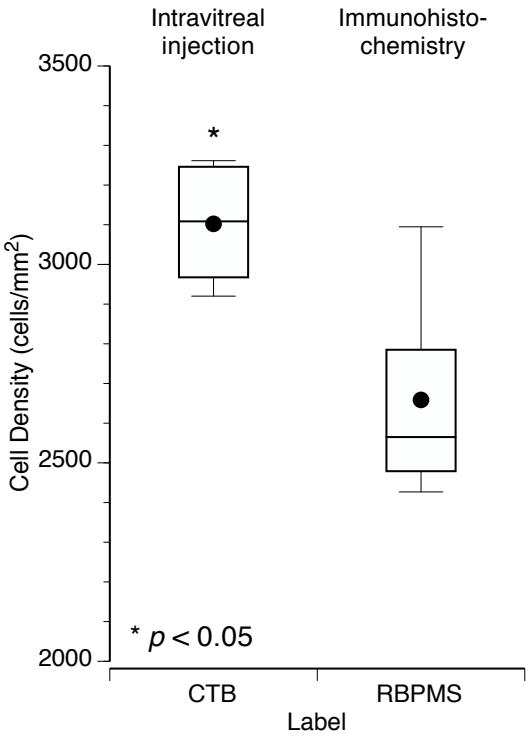

Figure 2.7 Cell densities for cholera toxin subunit B (CTB) and RBPMS labelled retinal cells in the ganglion cell layer. Box plots showing RGC densities in retinal flat mounts as a function of labelling method at 15 days post-injection of CTB-Alexa Fluor® 488. Dot indicates mean; horizontal line inside box indicates median; box boundaries indicate 25th and 75th percentiles; and tails indicate 10th and 90th percentiles.

Table 2.1 Comparison between intravitreal injection labelling with CTB immunolabelling with RBPMS. RBPMS+ cells that are CTB+ shows the proportion of RGCs labelled by CTB and CTB+ cells that are RBPMS+ shows the specificity of CTB to RGCs. Values are expressed as mean (standard deviation).

Region	RBPMS+ cells that are CTB+ (%)	CTB+ cells that are RBPMS+ (%)
Central	58 (10)	53 (5)
Mid-peripheral	62 (11)	54 (7)
Peripheral	70 (9)	53 (8)

2.10. Discussion

Our findings have demonstrated that an intravitreal injection of CTB-488 is a reliable and effective labelling method for adult retinal neurons, particularly RGCs, in mice. It was shown that more than half of CTB-488 labelled cells in the GCL are RGCs. Intravitreal injection administration of the neuronal tracer provides an efficient and minimally invasive method of delivery to RGCs. The administered bolus is effectively transported, presumably due to diffusion (Xu et al., 2000) as was seen by CTB-488 labelling in the GCL in both central and peripheral regions of the retina. The tracer is then naturally cleared from the vitreous without interfering with *in vivo* CSLO imaging.

2.10.1. Longitudinal In Vivo Imaging of RGCs is Achieved with CTB Labelling

The results have shown that following an intravitreal injection of CTB-488, cell labelling in the GCL can be detected by *in vivo* CSLO imaging for several weeks (Figure 2.3). Precise CSLO alignment (Chauhan et al., 2012) and image acquisition software allows for repeated imaging of precisely the same region and cell population in the retina. Stable fluorescence in the GCL *in vivo* from CTB-488 administered by intravitreal injection was confirmed with histology to be correlated with RGCs (Figure 2.4). Combining these findings and methods has established the framework for longitudinally monitoring changes in RGC labelling in wild-type animals.

The mechanism by which CTB remains in the soma of RGCs is not known, however CTB binds to monosialoganglioside receptors, GM1, on the surface of neurons (Gonatas et al., 1983) and localized to rodent RGCs and possibly some amacrine cells (Schwarz and Futerman, 1996). The high level of GM1 in the inner retina of rodents likely explains the strong uptake of CTB in the GCL observed in

our study. Labelling of RGCs with CTB has been primarily restricted to RGC axonal labelling and the regions in which they project in the visual pathway (Abbott et al., 2013; Fite and Janusonis, 2002; Hattar et al., 2006; Murphy et al., 2007). In these applications, molecular motor proteins are primarily responsible for active axonal transport, specifically kinesin for anterograde and dynein for retrograde (Gross et al., 2007; Hirokawa and Takemura, 2005). RGC density measurements with CTB have not been used as often (Lambert et al., 2011) and until now utilized to image RGC somas *ex vivo* only.

2.10.2. Intravitreal Injection Labelling with CTB Provides an Approximation of RGC Density

The number of cells that were actively labelled with CTB-488 was shown to be significantly higher than those labelled with RBPMS, however this difference was in part explained by amacrine cell labelling that co-localized with CTB-488 labelled cells in the GCL. While CTB-488 is not fully specific to RGCs, it labelled most RGCs (Table 2.1). This population of CTB-488 positive cells detected by *in vivo* imaging provides an approximation of the RGC density in the individual animals studied. It was observed that the population of RGCs labelled remained consistent (Figure 2.3) throughout the duration of the study, which is important prior to implementing injury models that mimic clinical diseases affecting RGCs.

Previous investigators have shown that despite the majority of RGCs in mice projecting to the superior colliculus, there remains a population that project to the lateral geniculate nuclei, superchiasmatic nuclei, pretectal nuclei and the accessory optic nuclei (Hattar et al., 2006; Rodieck, 1979; Salinas-Navarro et al., 2009a). This would result in not all RGCs being reliably labelled via the superior colliculus in retrograde labelling (Galindo-Romero et al., 2011) and could account

for some of the intravitreal injection labelled cells that are not retrograde labelled. Therefore, the use of an immunohistochemical method of labelling RGCs was chosen with the aim of not preferentially labelling RGCs that project to the superior colliculus. Immunohistochemistry also provided more consistent results than retrograde labelling as retrograde labelling via the superior colliculus proved technically challenging when utilizing CTB as the tracer in mice.

2.10.3. Limitations

Our findings demonstrated labelling in both RGCs and amacrine cells indicating that CTB-488 is not specific to RGCs. While it was confounding to find labelling in the INL, the labelling was excluded from acquired *in vivo* GCL images by ensuring the focal depth of the CSLO excludes the INL. Despite CTB-488 labelling both RGCs and amacrine cells, experimental glaucoma models of elevated intraocular pressure and optic nerve transection show no significant changes in amacrine cell density despite RGC loss (Kielczewski et al., 2005; Vidal-Sanz et al., 2011). Therefore, if an intravitreal injection of CTB-488 were to be used to measure RGC loss following injury, the percentage loss would not directly represent actual RGC loss. However, the rate of RGC loss could be approximated with knowledge of the amacrine cell population that is labelled.

2.11. Opportunities for Translation

This work has provided evidence that an intravitreal injection of CTB-488 is a reliable and efficient label for RGCs in mice. These findings are the proof-of-principle work for developing techniques of minimally invasive *in vivo* single cell resolution RGC imaging in wild-type animals. For basic science techniques to be translated to human studies, there are a variety of pre-clinical steps first

required, such as those presented in this paper. From these steps, important and relevant findings are discovered for further experimental study. This new information, like the work described here, advance the opportunities for clinical translation while also allowing for more robust animal studies to be performed when investigating degenerative disease.

2.11.1. Ex Vivo Evaluation

The ability to confirm specific labelling of RGCs first requires *ex vivo* analysis of labelled retinal tissue. Extensive and specific labelling of RGCs has been largely confined to *ex vivo* studies using immunohistochemistry. Methods to specifically label RGCs have used POU-domain transcription factors (e.g. Brn3a) (Xiang et al., 1995), a modified Tat-peptide (Barnett et al., 2006), γ-synuclein (Surgucheva et al., 2008) and RNA binding protein (Kwong et al., 2010; Rodriguez et al., 2014). Studies have also used double labelling as a means to validate efficiency and specificity of newly developed labelling methods (Cong et al., 2005; Pang and Wu, 2011). Rigorous analysis of labelling is possible through *ex vivo* methods and provides details of expression and specificity that is not easily achieved with *in vivo* work.

2.11.2. In Vivo Translation with Animal Models

The first step to clinical translation of imaging modalities requires the use of animal models for *in vivo* evaluation of safety, efficacy and efficiency of developed technologies and methods. This process helps identify the objectives and challenges associated with use in a clinical environment that may not otherwise be a concern in the laboratory. It also ensures developed devices, labelling methods, algorithms and accuracy are maintained during *in vivo* evaluation. Optimization of experimental methods is required to ensure

minimally invasive, or ideally non-invasive, procedures can achieve the desired results. The imaging procedure duration, system settings and required manipulations are all factors responsible for the success of an imaging session and are better understood using animal models. Establishing imaging techniques and methods in animal models that are in real-time creates opportunities for clinical relevance and translation.

2.12. Pre-clinical and Clinical Applications

Although methods of labelling RGCs have existed for decades, the application has yet to be translated to the clinic. The translation from biomedical research to clinical practice includes different stages (Figure 2.8), but is not easily or quickly achieved due to a variety of challenges along the continuum (Sung et al., 2003). Basic research has provided insight into the progression of glaucoma, determining that the death of RGCs is a defining characteristic of the disease. This knowledge has provided a basis for monitoring disease progression in animals and opened up the possibility of utilizing it for diagnosis and prevention in humans. The next step is to translate this work into human clinical trials. One such study will reportedly be occurring in the near future for *in vivo* imaging of cells undergoing apoptosis in the eye (Galvao et al., 2013). Broader implications could be made if a clinical trial could be devised to image RGCs in healthy and diseased states in human patients. Successful outcomes from clinical trials will then proceed to clinical practice to aid in improved health outcomes and quality of life for patients.

Figure 2.8 Clinical research continuum from experimental animal models to improved human health. The continuum of biomedical and health research requires considerable progress, especially at the two translation steps, in order to achieve human benefit from experimental studies. Figure adapted from Sung et al., 2003, with permission from the American Medical Association.

2.13. Accuracy Considerations

Accuracy constraints, and therefore the success of interventions, are strikingly different when compared between the clinical perspective and the engineering perspective. A few questions need to be addressed by the respective fields to successfully achieve the common goal of improved therapeutic outcome: What is the tolerable clinical error for detecting the ocular pathology? How accurate is the imaging system? What variation could be introduced by the operator/physician? Longitudinal studies often provide answers to these questions and allow for meaningful decisions to be made by clinicians when making assessments and diagnoses (Nema and Nema, 2013). However, the rapid pace of technological advances in ophthalmic imaging devices makes it difficult for longitudinal studies to be produced.

2.13.1. Clinical Accuracy Constraints

Clinical accuracy may be defined as the ability to distinguish between two different states or the progressive changes towards a pathological classification. The accuracy constraints defined in the clinic may also be patient specific, as baseline values are likely to differ (e.g. intraocular pressure or RGC density). Therefore, defining such tolerances is problematic as they can be disease, procedure or patient specific. It has been shown that disease severity affects the ability to detect glaucoma when using visual field testing (Sample, 2000) or OCT imaging (Leite et al., 2010). The implication of such findings is that the diagnostic accuracy results obtained in some studies may only be true for patients with moderate or severe disease states of RGC loss. The parameters of imaging devices must be rigorously tested to determine the diagnostic accuracy for not only moderate to severe disease states, but also for the use of screening and early detection.

Imaging modalities can introduce artefacts and lead to misdiagnosis if the advantages and limitations of the instruments are not fully understood. In OCT imaging of the retinal layers common artefacts include defocusing, depolarization and decentration; all of which can largely influence segmentation algorithms, thereby compromising accurate detection of retinal boundaries (Somfai et al., 2007). Similar artefacts, such as shadowing and scattering, exist with CSLO and fluorescence imaging that can cause misrepresentation of acquired images (Charbel Issa et al., 2012; van Oterendorp et al., 2011). It is important to understand the types of artefacts that can exist from each imaging device and utilize methods to minimize their effect. Steps were taken to minimize such artefacts in our own experiments by maintaining a darkened room, pupil dilation, corneal hydration, and centred placement of the contact lens and camera position for maximal light penetration.

2.13.2. Engineering Accuracy Constraints

One approach to clinically relevant research is to first clearly define the requirements needed to achieve a desired outcome in the clinic, which in this case could be defining the spatial resolution required of an imaging system to detect changes in retinal layers or the number of functional retinal neurons. This is a necessary step for determining if currently available hardware is capable of the required spatial resolution where the cells of interest are located. As indicated earlier, in optical imaging, an increased spatial resolution requires a trade-off in penetration depth. The limitations of the imaging device, such as penetration depth, spatial resolution and field of view, need to be identified to determine precisely when the clinical performance will be affected. Equally important, scientists, engineers and device manufacturers must implement

device parameters that provide a fair balance of subjectivity and objectivity for the clinician to make an educated diagnosis. Normative databases are used to provide information on the characteristics of a "normal" subject, however there are significant variations in the normal population, among devices and changes with age that could introduce false-positive and false negative results (Chong and Lee, 2012).

2.14. Conclusions and Future Directions

Assessing RGC injury and death with surrogate methods in glaucoma provide important indications for clinical management. However, clinical practice is moving toward earlier diagnosis and higher specificity in monitoring disease progression, requiring enhanced detection mechanisms and imaging modalities. An imaging system that assesses both direct structural and functional changes to RGCs would appreciably change clinical diagnoses. With a firm understanding of the risk factors associated with diseases, such as glaucoma, being developed (Chauhan et al., 2008; Ernest et al., 2013; Gordon et al., 2002), high-risk patients could be screened for early or pre-clinical signs of disease in an attempt to make appropriate early interventions and reduce the impact of disease on quality of life. Treatment could be initiated if signs of ocular disease are found early, leading to delayed onset of symptoms and an improved quality of life.

While significant strides have been made in clinical ophthalmic imaging with improved resolution and efficiency, there remains a gap between advances in the laboratory and the clinic. There are now opportunities to translate and implement experimental methods being used for animals to human application. Basic science is capable of addressing the need to close the gap. If measures of biological, chemical or physical changes can be made in real-time *in vivo* imaging

in basic science, they would provide the blueprint for highly useful methods in clinical practice.

Further experimental work, described in the next chapter, utilizes an alternate method for improved specificity, adeno-associated viral vectors, administered via intravitreal injection for RGC labelling. *In vivo* labelling and imaging studies with this method of labelling will be carried out in mice to determine what cell populations are being labelled and the longitudinal efficacy of the labelling method. It is important to confirm if cells other than RGCs are being labelled and if it is dependent on the time after injection. Introducing a disease model of RGC loss is also an important step in the progress of this work to fully understand how these labelling methods may be useful in studying clinical diseases.

CHAPTER 3 *In Vivo* Imaging of Adeno-Associated Viral Vector Labelled Retinal Ganglion Cells in Mice

Co-Authorship Statement

The work in Chapter 3 is being prepared for submission in: **Smith CA** and Chauhan BC. *In vivo* imaging of adeno-associated viral vector labelled retinal ganglion cells in mice. *In preparation*.

CAS and BCC designed the research study, interpreted data and wrote the manuscript. CAS completed the literature review, conducted the experiments, acquired and analyzed data. BCC was the principal investigator and supervised the work.

3.1. Introduction

The retina has served as a successful model for numerous significant advances in neuroscience. Retinal ganglion cells (RGCs) are the output neurons of the retina whose axons provide the essential pathway for visual signals to reach the brain. A hallmark of glaucoma, one of the most common causes of irreversible visual disability and blindness, is progressive loss of RGC somas and axons. There are currently no methods of directly imaging living RGCs in humans to assess disease severity, instead measures of optic nerve head neuroretinal rim, retinal nerve fiber layer and ganglion cell layer thickness with modern imaging techniques, such as optical coherence tomography, are used as surrogates of how many RGCs axons and somas are present. However, the sensitivity and specificity of these surrogate measures of RGC degeneration, and ultimately death, is poorly understood (Raza and Hood, 2015; Tatham et al., 2013). It is also important to consider a proportion of RGC loss may not be due to disease, but rather normal ageing (Vianna et al., 2015). The ability to image RGC axons or somas directly would allow earlier and accurate detection of diseases such as glaucoma and with serial imaging, a more accurate rate of RGC loss as an indicator of disease progression.

Advances in adaptive optics imaging have allowed *in vivo* imaging of photoreceptors, the most abundant neuron in the retina, in monkeys and humans (Liang et al., 1997; Rossi et al., 2011). Unlike photoreceptors, which contain pigment, RGCs are transparent and therefore less amenable to imaging without the introduction of contrast material. As shown in Chapter 2, because the ganglion cell layer contains other cell types, particularly, displaced amacrine cells (Curcio and Allen, 1990), the specificity of imaging RGCs in the ganglion cell layer is problematic without a RGC-specific indicator (Rossi et al., 2017). An

indicator that is highly specific, reproducible and which allows RGC quantification would represent a significant advance in the assessment of glaucomatous damage.

Ideally, a clinically applicable method of labelling and imaging RGCs should be minimally invasive, have single cell resolution and have persistence such that longitudinal changes in RGC counts can be monitored (Balendra et al., 2015). One such method utilizes apoptotic indicators, annexin V (Cordeiro et al., 2004) or effector caspases (Barnett et al., 2009; Qiu et al., 2014), to measure cell death in the retina of rodents and humans (Cordeiro et al., 2017) in conjunction with *in vivo* fluorescence imaging. The specificity of this approach for RGCs is not known and could lead to a high number of false positives when other retinal neurons are labelled. Furthermore, this approach provides evidence of cells undergoing cell death at a single time point, making it difficult to ascertain how many RGC are lost and how many remain, thereby making it challenging to document disease progression. Other investigators used genetically encoded calcium indicators for repeated *in vivo* functional imaging of foveal RGCs in macaque (Yin et al., 2012; Yin et al., 2014). This method required implementation of adaptive optics to obtain sufficient fluorescence intensity in a small region of the retina, but represents important progress as it measures not only the presence of RGCs, but their functional responses via fluorescence intensity to light stimuli.

Adeno-associated viral (AAV) vectors have been used in clinical trials for retinal diseases with successful safety and transduction outcomes (Pierce and Bennett, 2015). AAV vectors can be customized to improve cell-type specificity and rate of labelling. Such approaches include manipulation of the capsid (i.e., wild-type or engineered), genome (i.e., promoters and reporter gene, such as a fluorophore,

e.g., green fluorescence protein (GFP)) and route of delivery (i.e., intravitreal or subretinal). Most recently, research has addressed the limited capacity for DNA, approximately 4.7 kilobases, in AAV vector mediated transduction. Small gene promoters of human DNA ("MiniPromoters") were developed to drive gene expression in neural tissue (de Leeuw et al., 2014; Portales-Casamar et al., 2010). One of these MiniPromoters is for the gene *DCX* that encodes for the protein doublecortin; previously shown to be expressed in developing and mature retinal neurons. Specifically, there is evidence the protein is present in RGCs as well as amacrine, bipolar and horizontal cells (Sanchez-Farias and Candal, 2015; Wakabayashi et al., 2008). When the MiniPromoter developed for *DCX* was used in an AAV vector, it primarily targeted the RGCs in mice (de Leeuw et al., 2014). However, the efficiency, specificity and persistence of these promoters when incorporated into an AAV vector are not known. These tools provide an opportunity for *in vivo* labelling of RGCs with improved specificity.

In this study we demonstrate the feasibility of AAV delivery via intravitreal injection as a means for *in vivo* RGC labelling in mice. This method was used to test if AAV vectors provide specific fluorescence labelling for longitudinal *in vivo* imaging. Confocal scanning laser ophthalmoscope (CSLO) imaging was used for *in vivo* detection of fluorescence labelling, while OCT imaging and electroretinography (ERG) was used to detect any structural or functional changes to the retina, respectively. It is expected the results could provide a minimally invasive method for efficient and robust RGC labelling with longitudinal imaging, offering the ability to detect changes in RGCs and track progression of diseases such as glaucoma.

3.2. Methods

3.2.1. Adeno-Associated Viral Vector

Two different AAV2 serotype recombinant vector constructs were employed. The first utilized the cytomegalovirus early enhancer/chicken β actin (CAG) promoter to drive the expression and synthesis of the reporter, enhanced GFP packaged in recombinant AAV2 wildtype capsid (AAV2-CAG-GFP, Vector Biolabs, Malvern, PA, USA). The second utilized a tissue or cell specific promoter from the *DCX* gene to drive the expression and synthesis of the reporter humanized GFP packaged in recombinant AAV2 capsid with quadruple tyrosine residues mutated to phenylalanine (AAV2-DCX-GFP, provided by Dr. William Hauswirth, Retinal Gene Therapy Group, University of Florida, Gainesville, FL, USA). Mutations of surface-exposed tyrosine to phenylalanine have been shown to enhance transduction efficiency by eliminating the hydroxyl group associated with phosphorylation and consequently ubiquitination and degradation of the vectors (Petrs-Silva et al., 2011; Petrs-Silva et al., 2009; Zhong et al., 2008).

3.2.2. Animals

Adult female C57BL/6 mice (JAX™ Mice Stock Number: 000664, Charles River Laboratories, Saint-Constant, QC, Canada) were used. Mice were housed in a 12-hour light-dark cycle and provided food and water *ad libitum*. Mice were divided into the following groups: group 1 for AAV2-CAG-GFP labelling (n = 6), group 2 for AAV2-DCX-GFP labelling (n = 7), group 3 for ERGs and group 4 for optic nerve transection following intravitreal injection of AAV2-CAG-GFP or AAV-DCX-GFP (n = 2).

3.2.3. Intravitreal Injection

Mice were anaesthetized with a mixture of ketamine (100 mg/kg body weight) and xylazine (10 mg/kg body weight). The left eye was dilated topically with one

drop of 1% tropicamide (Alcon Canada Inc., Mississauga, ON, Canada) and continuously rehydrated with lubricant eye drops. Under an operating microscope, a scleral puncture approximately 0.5 mm from the limbus was made with a 30G hypodermic needle. A 33G needle (Hamilton Company, Reno, NV, USA) was then inserted into the puncture and 1.5 μl of the vector injected slowly into the vitreous cavity with at titer of least 1×10^{12} vg μl^{-1} for the *CAG* promoter and 3.94×10^{12} vg μl^{-1} for the *DCX* promoter. After the injection antibacterial drops and ophthalmic gel (Novartis Pharmaceuticals Canada Inc.) were applied.

3.2.4. In Vivo Imaging

In vivo imaging was performed with a confocal scanning laser ophthalmoscope (CSLO) and spectral domain optical coherence tomography (OCT) device specially modified for use in mice (Spectralis Multiline, Heidelberg Engineering GmbH, Heidelberg, Germany) (Chauhan et al., 2012). CSLO imaging was performed to visualize the GFP-positive cells after intravitreal injection while OCT imaging was used to derive B-scans of the retina to quantify inner retinal thickness (see below). All laser sources were Class 1 according to International Electrotechnical Commission (IEC) (IEC, 2014).

The left pupil was dilated (one drop of 1% tropicamide and one drop of 2.5% phenylephrine hydrochloride, Alcon Canada) and the mouse anaesthetized with inhalant isoflurane, induction of 3-4% volume (Baxter Corporation, Mississauga, ON, Canada) with 1.5 L/min oxygen flow and maintained at 1.5-3% volume with 0.8 L/min oxygen flow, via a nose cone attached to a portable inhalation system. The mouse was placed on a heating pad for the duration of imaging. Ophthalmic gel and a custom-made polymethyl methacrylate plano contact lens (Cantor and Nissel Limited, Brackley, UK) were used to maintain corneal hydration and

improve image quality. Baseline images focused at the level of the nerve fiber layer were first acquired with infrared (820 nm) illumination. Fluorescence images were then acquired in CSLO mode with a 488 nm excitation laser and bandpass filter of 505 – 545 nm. Each image was averaged a minimum of 20 times with automatic real-time eye tracking software to increase the signal-noise ratio. The imaging protocol was repeated at several time points post-injection (Figure 3.1) with the image tracking software to ensure that the same retinal areas were imaged in each session.

The same animal protocol and imaging set-up was used for OCT imaging to quantify inner retinal thickness. The principles of OCT for retinal imaging have been described elsewhere (Wojtkowski et al., 2005); briefly, the technique employs the principle of low coherence interferometry to generate high-resolution cross-sectional images of the retina. A raster pattern of 19 equally spaced horizontal B-scans, each 30 degrees wide, centred on the optic nerve head was used (Figure 3.2A). The scanning speed was 40 000 A-scans per second and each B-scan comprised of 1536 A-scans. Each B-scan was averaged 20 times.

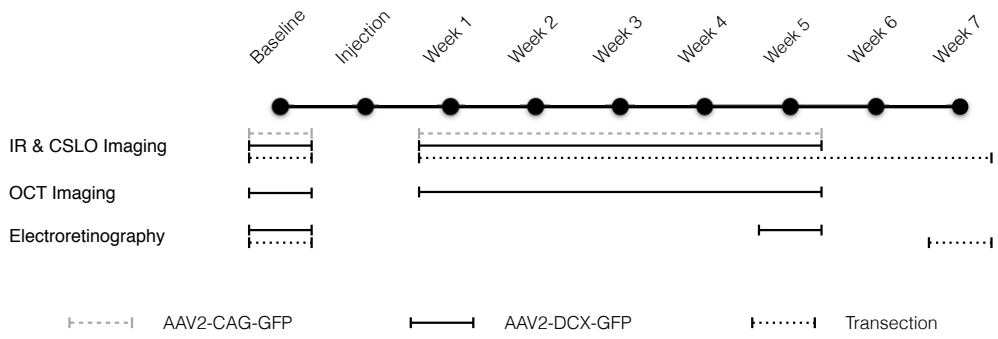

Figure 3.1 Timeline for *in vivo* procedures performed on each group of animals. Imaging and electroretinography procedures were performed repeatedly on animals within the same group as shown the timeline. All animals were sacrificed at week 5, except those in the optic nerve transection group that were sacrificed at week 7 (14 days post-transection).

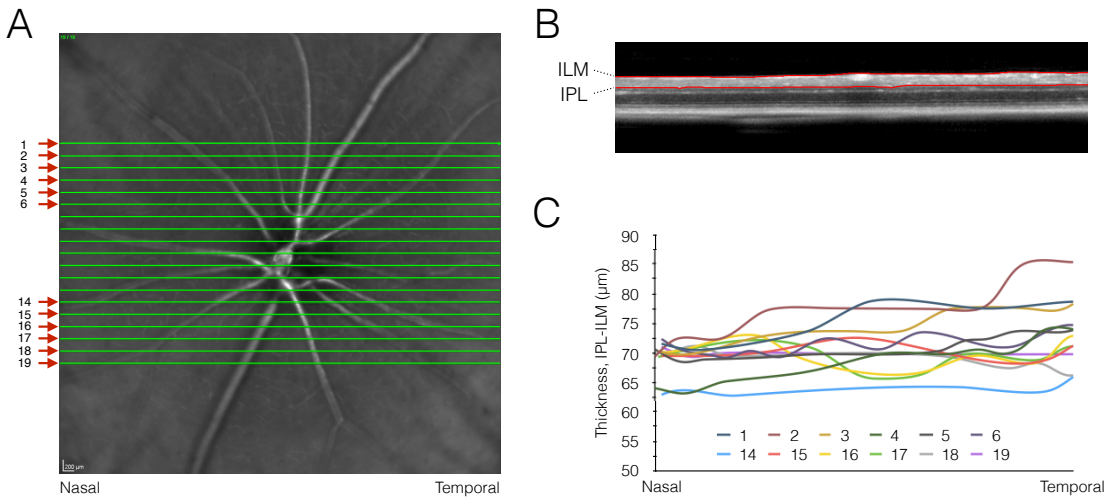

Figure 3.2 OCT imaging and analysis procedures. OCT imaging was completed longitudinally in each animal. **A)** Infrared image of a mouse retina centred on the optic nerve head with a raster scanning pattern shown. Six B-scans from the top and bottom (total of 12), marked by red arrows were segmented. **B)** Segmentation of the retina is shown by the red lines defining the inner limiting membrane (ILM) and inner plexiform layer (IPL). **C)** Thicknesses of the IPL-ILM region are plotted for each of the B-scans marked by red arrows in (A). An average thickness is computed for each animal at each time point.

3.2.5. Electroretinography

Full field ERG analysis was performed prior to intravitreal injection and at week 5 post-injection to determine if the AAV-mediated GFP labelling driven by the *DCX* promoter had detrimental effects on retinal function (Figure 3.1). To demonstrate the ability of our ERG protocol to detect changes in retinal function, specifically that of the RGCs, a subset of animals received an optic nerve transection (Figure 3.12). Mice were dark-adapted overnight (≥ 12 hrs) before being anesthetized with an intraperitoneal injection of ketamine (100 mg/kg) and xylazine (10 mg/kg). Pupils were dilated with one drop each of 1% tropicamide and 2.5% phenylephrine hydrochloride (Alcon Canada Inc., Mississauga, ON, Canada). Body temperature was maintained between 35 and 37°C with a heating pad and monitored with a rectal probe. A platinum subdermal electrode (Grass Instruments, Quincy, MA, USA) was placed in the base of the nose for reference. A microfiber electrode (DTL Plus Electrode™, Diagnosys, Littleton, MA, USA) was placed on the corneal surface of each eye with ophthalmic liquid gel (Tear-Gel, Novartis Pharmaceuticals Canada, Inc., Mississauga, ON, Canada) applied to maintain hydration and conductivity. Impedances of the corneal and ground electrodes were measured at 30 Hz and the ERG protocol was commenced only if impedance values were < 150 ohms.

Signal amplification and recording setup are detailed elsewhere (Smith et al., 2014), however briefly, flash stimuli were delivered with a Ganzfeld stimulator (LKC Technologies, Gaitherburg, MD, USA) and attenuated by neutral density filters (Kodak Wratten, Rochester, NY, USA). After a ten-minute stabilization period, ERG responses were recorded in the following order of flash intensity: -3.2, -3.8, -4.4, - 4.8, -6.0, -6.8 and 1 log cd s m^{-2}. For flash intensities between 1.0 and -4.4 log cd s m^{-2}, between 2 to 10 responses were averaged, while for the two

lowest intensities, 10 to 14 responses were averaged. Each response was obtained with a 4.5 second interval between flashes.

3.2.6. Optic Nerve Transection

Animals that underwent optic nerve transection were injected with AAV vector 5-weeks prior. Mice were anaesthetized using inhalant isoflurane as described for *in vivo* imaging. Under and operating microscope, the globe of the left eye was rotated downwards and held in place with a 9-0 conjunctival suture. To expose the optic nerve, an incision was made in the skin near the supraorbital ridge then the intraorbital subcutaneous tissues were dissected. The optic nerve dura was cut longitudinally and the optic nerve transected completely approximately 0.5 mm from the globe. The ophthalmic artery, located underneath the transected nerve, was kept intact. The incision was closed and the fundus examined to confirm no ischemic damage.

3.2.7. Immunohistochemistry

To estimate the cell density and specificity of GFP labelling in the whole retina, immunohistochemistry was performed on retinal flat-mounts. Five weeks post-intravitreal injection animals were sacrificed with an overdose of sodium pentobarbital by intraperitoneal injection. The cornea and lens were removed and the eye-cups fixed in 4% paraformaldehyde for 2-3 hours. Retinas were washed in 1x phosphate-buffered saline (PBS) for 10 min and incubated in blocking buffer (10% normal donkey serum, 0.3% Triton X-100) overnight at 4°C. Retinas were incubated for 6 days at 4°C in primary antibodies against RNA binding protein with multiple splicing (Kwong et al., 2010; Kwong et al., 2011; Rodriguez et al., 2014) (RBPMS, 1:1000 guinea pig anti-RBPMS, gift from Dr. Nicholas Brecha) and choline acetyltransferase (ChAT, 1:100 goat anti-ChAT,

Millipore, Billerica, MA, USA) to identify RGCs and cholinergic amacrine cells, respectively. Retinas were then washed in PBS and incubated overnight at 4°C in Alexa Fluor 488 (1:400 Alexa Fluor® 488 conjugated rabbit anti-GFP, Molecular Probes, Eugene, OR, USA), Cy3 (1:1000, Cy3 conjugated donkey anti-guinea pig (Jackson Immuno Research Laboratories Inc., West Grove, PA, USA) and Alexa Fluor® 633 (1:1000 Alexa Fluor® 633 conjugated donkey anti-goat, Molecular Probes). Retinas were rinsed in PBS, mounted with anti-fade fluorescent mounting medium (Vectashield®, Vector Labs, Burlingame, CA) and coverslipped.

3.2.8. Image Data Analysis

Image processing, analysis and cell quantification algorithm implementation of CSLO acquired images were performed with a customized analysis tool in MATLAB software (Appendix B). Measures of signal intensity and image quality for *in vivo* fluorescence images were calculated (signal-to-background ratio, signal-to-noise ratio, and contrast-to-noise ratio) at week 5 post-injection. This was completed to determine if the GFP variants (enhanced vs. humanized) affected the signal intensity or image quality. For cell quantification a Gaussian filter (σ=3, h = 19) was used to remove noise and a minima transform (h = 10) implemented to extract markers for each labelled cell. If a labelled region was greater than 200 pixels, it was assumed to be a cluster of cells and an eroding function applied as a method of segmentation. Connected components in the binary image were automatically counted and markers were superimposed on the original CSLO image to indicate their position. The final cell quantification was performed after manual correction of the automated algorithm to include cells not correctly identified, or to exclude objects incorrectly identified as cells. The total number of labelled cells divided by the retinal area, excluding the optic

nerve region, was used to calculate cell density. A percentage of labelled retinal area in the 30° *in vivo* images was measured at week 5 post-injection by tracing and calculating the region with prominent labelling then divided by the total image area.

OCT layer segmentation was performed with the device segmentation algorithm (Heidelberg Eye Explorer, Heidelberg Engineering) after which each B-scan was checked for segmentation errors and manually corrected when required (Figure 3.2B). The retinal nerve fibre and ganglion cell layers in mice are very thin, especially beyond the peripapillary region, and therefore cannot be reliably identified in OCT images. The signal interface between the inner plexiform layer and inner nuclear layer is easily identifiable and therefore used for segmentation. Inner retinal thickness was measured from the vitreous-retina surface to the inner plexiform layer (Figure 3.2C).

Micrographs of retinal flat-mounts were imaged with a Zeiss Axio Imager M2 microscope (Carl Zeiss AG, Oberkochen, Germany) and a 20x Plan-Apochromat objective (Carl Zeiss). Fluorescence images of the ganglion cell layer were captured with the ZEN software (Carl Zeiss) sampling the central, mid-peripheral, and peripheral retinal regions, with respect to the optic nerve head. In each sampled region, the number of cells labelled by (1) GFP, (2) RBPMS, and (3) RBPMS with GFP were quantified independently in graphics editing software (Adobe Photoshop CS6, Adobe Systems Incorporated, San Jose, CA, USA).

3.2.9. ERG Data Analysis

ERG waveforms were analyzed with a custom toolbox for Matlab (Mathworks, Natick, MA, USA) and filtered with a low-pass eighth-order Butterworth filter at

50 Hz prior to measuring amplitudes. Analysis of the scotopic threshold response (STR) included amplitude measurement of the positive component (pSTR), from the baseline to the initial peak, and the negative component (nSTR), from baseline to the local minimum after the pSTR (Figure 3.3). Both the pSTR and nSTR signals have been shown to reliably measure RGC function in mice (Alarcon-Martinez et al., 2010; Smith et al., 2014). For photoreceptor response, the a-wave amplitude was measured from the baseline to the maximum negative trough, while the b-wave was measured from the a-wave trough to the maximum positive peak. For comparison between experimental and control eyes, the relative amplitude (experimental /control eye) was calculated.

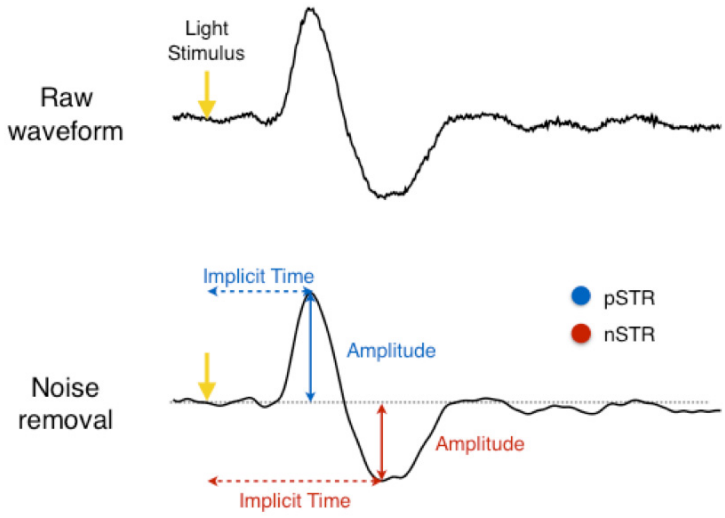

Figure 3.3 Method for measuring STR components of the ERG response
Example raw waveform of ERG recording obtained from corneal ERG to low stimulus strength. Noise removal was completed with Butterworth filter. pSTR components are shown in blue and nSTR components are shown in red with the amplitude (vertical solid lines) and implicit time (horizontal dashed lines). The yellow arrow indicates the time of the light stimulus.

3.2.10. Statistics

Statistical analyses were performed in the open-source R platform (version 3.1.3, R Core Team, http://www.R-project.org) and Prism (version 7 for Mac, GraphPad Software, La Jolla, CA, USA). Unless otherwise indicated, all results are expressed as mean (95% confidence interval) and statistical significance was assumed when $p < 0.05$. For *in vivo* cell densities second-order polynomial regression was used for each vector and the Holm-Sidak's multiple comparisons test was used to test significance between vectors at each time point. Two-way analysis of variance (experimental/control vs. ERG stimulus strength) was applied to test the significance of the ERG data.

3.2.11. Study Approval

Animal procedures complied with the Canadian Council of Animal Care standards and animal ethics approval was obtained from the University Committee on Laboratory Animals at Dalhousie University.

3.3. Results

Following intravitreal injection of the AAV vector, GFP labelling was detectable by *in vivo* CSLO fluorescence imaging in 17 mice (81%) at week 1 post-injection. The four (19%) animals that did not show any GFP labelling at week 1 did have labelling by week 2. Examples of the images acquired weekly are shown in two different animals labelled by vectors containing the *CAG* (Figure 3.4) and *DCX* (Figure 3.5) promoters. Cells that were labelled in the early weeks post-injection continued to express the GFP until at least week 5. However, GFP labelling in the majority of cells was not evident until 2 - 4 weeks post-injection (Figures 3.4 and 3.5). The *in vivo* mean (95% confidence interval) central retina cell density for the AAV2-CAG vector was 97 (50) cells/mm^2 at week-1 and 534 (201) cells/mm^2 at

week-4. For the AAV2-DCX vector, cell density was 29 (40) cells/mm^2 at week-1 and 288 (105) cells/mm^2 at week-4. That is 77 (6)% of cells ultimately labelled with GFP at week 5, became GFP positive between weeks 1 and 5 in the AAV2-CAG injected animals and 85 (5)% of cells in the AAV2-DCX injected animals. The density of GFP labelled cells for both vectors follow a similar trend over time and fit with second-order polynomial models of $R^2 = 0.43$ for AAV2-CAG and $R^2 = 0.38$ for AAV2-DCX (Figure 3.6). The AAV2-CAG vector labelled significantly more cells than the AAV2-DCX vector ($p < 0.05$), however, this difference was not apparent until week 3. At all subsequent time points, the percent difference of labelled cells between the AAV2-CAG and AAV2-DCX vectors was an average of 65 (10)% (Figure 3.6). The trend of increasingly more labelled cells over time occurred until approximately week 4 post-injection, at which time neither vector had significantly more cells labelled than the previous week consecutively for two time points. The proportion of retina labelled in the *in vivo* images with the AAV2-CAG vector was 97 (7)% whereas the AAV2-DCX was 53 (30)%.

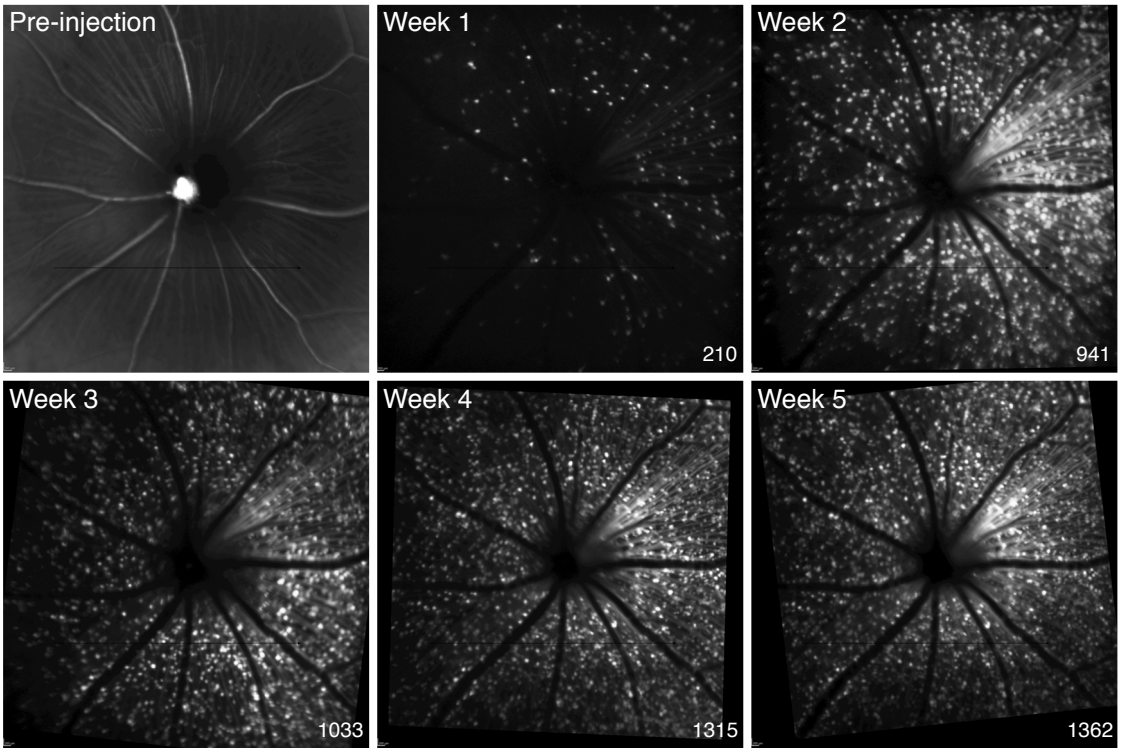

Figure 3.4 Longitudinal *in vivo* CSLO images of a mouse retina post-injection of AAV2-CAG-GFP vector. Images are from the same animal and acquired sequentially up to 5-weeks following intravitreal injection. Pre-injection image was acquired using infrared mode (820 nm) and all other images using 488 nm excitation laser. Cell counts are given for each fluorescence image (bottom right corner).

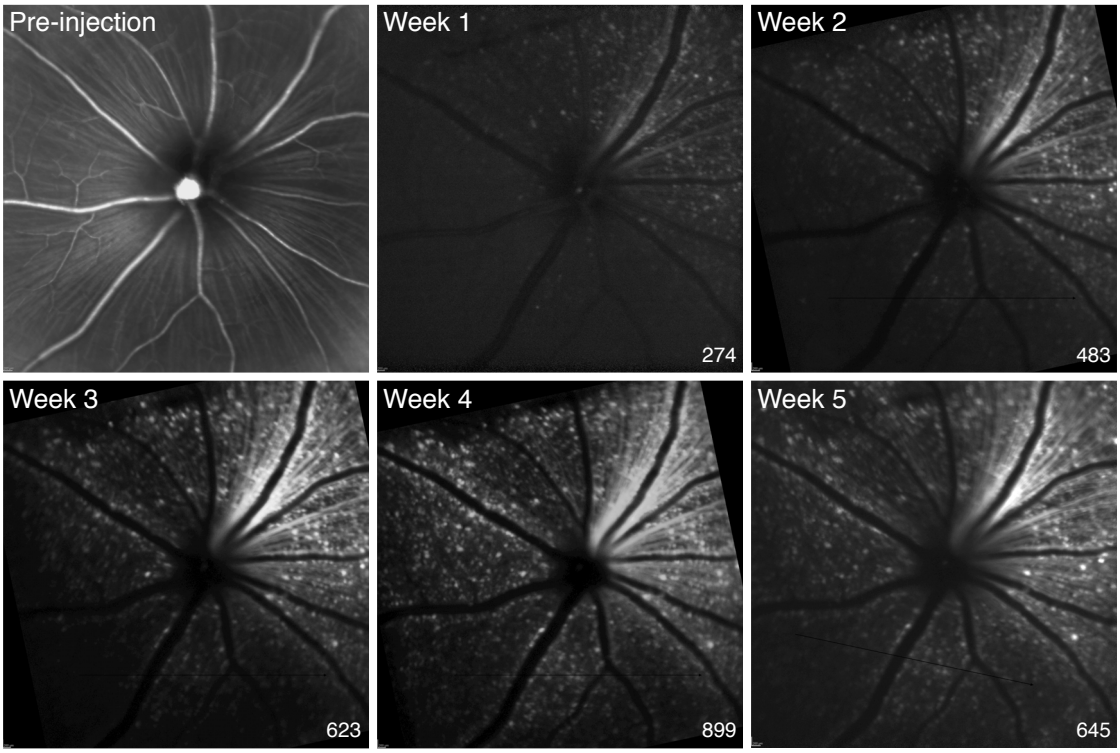

Figure 3.5 Longitudinal *in vivo* CSLO images of a mouse retina post-injection of AAV2-DCX-GFP vector. Images were acquired in the same manner as described in Figure 1. GFP expression driven by the DCX promoter is also detectable with real-time fluorescence imaging (488 nm excitation). Cell counts are given for each fluorescence image (bottom right corner).

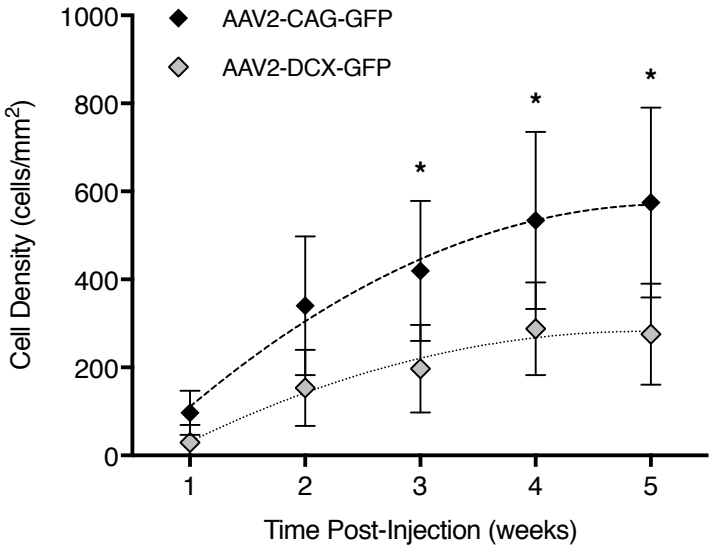

Figure 3.6 Comparison of *in vivo* GFP expression in the ganglion cell layer between vectors after intravitreal injection. Cell densities were calculated from 30-degree field of view (approximately 1.36 mm) centred at the optic nerve head for AAV2-CAG and AAV2-DCX vectors. Trendlines show the second-order polynomial regression results calculated for each group. Error bars represent 95% confidence interval; * $p < 0.05$; n = 6.

Both the AAV2-CAG and AAV2-DCX vectors had a high signal-to-background ratio (Table 3.1) and difference in means equal to 0.67 (0.90). The measures of image quality were also comparable between the two vectors for signal-to-noise ratio and contrast-to-noise ratio with percent differences of 9.7% and 3.3%, respectively. There was no statistically significant difference between the vectors for any of the measures (Table 3.1).

Figure 3.7 shows example micrographs with labelling from intravitreal injections (panels A-B) and immunohistochemical markers (panels C-F). The co-localization of GFP positive cells in the ganglion cell layer with RBPMS are shown in the merged micrographs in addition to the distribution of cholinergic amacrine cells (Figure 3.7E and F). The cell densities of GFP labelled cells, 723 (287) cells/mm^2 for AAV2-CAG and 715 (177) cells/mm^2 for AAV2-DCX, revealed the AAV labelling via intravitreal injection was not significantly different between the two vectors (Figure 3.8A, $p = 0.97$). Based on immunohistochemical labelling, RGC densities of 2671 (256) cells/mm^2 for AAV2-CAG and 2817 (379) cells/mm^2 for AAV2-DCX were not significantly different ($p = 0.55$). Co-localization showed the specificity of GFP labelling to RGCs to be very high at week 5 post-injection for both vectors (Figure 3.8B) with the proportion of GFP positive cells that were RGCs as 72 (3)% for the AAV2-CAG vector and 86 (4)% for the AAV2-DCX vector. There was significantly higher specificity of RGC labelling with the AAV2-DCX vector ($p < 0.05$) and it was independent of the region of retina (central vs. peripheral). However, the proportion of RGCs labelled by each vector (RBPMS+ that are GFP+) was 20 (9)% for AAV2-CAG and 35 (7)% for AAV2-DCX and not significantly different between vectors ($p = 0.38$). For the AAV2-DCX group, a paired t-test showed that there was a significant difference between the *in vivo* and *ex vivo* densities 242 (111) cells/mm^2 and 716 (177) cells/mm^2,

respectively; $p < 0.05$). Linear regression revealed $R^2 = 0.01$ for *in vivo* vs. *ex vivo* GFP densities and $R^2 = 0.16$ for *in vivo* GFP density and *ex vivo* RBPMS density.

At baseline, prior to the intravitreal injection, there was no significant difference of the amplitude or implicit time between control and experimental eyes (Figure 3.9). Week 5 post-injection there was no significant decrease in the positive (p = 0.44) and negative (p = 0.84) STR amplitudes or implicit times (pSTR, p = 0.31 and nSTR, p = 0.33) between the control and experimental eyes following intravitreal injections with the AAV2-DCX vector, indicating the RGC contribution to the ERG was unaffected (Figure 3.10 and Figure 3.11). The mean relative pSTR amplitude was 0.86 (0.04) and nSTR amplitude was 1.12 (0.06) across all signal strengths. Furthermore, the amplitudes of the a- and b- waves were not significantly different between the two eyes (p = 0.87 and p = 0.70, respectively (Figure 3.11). The ERG response in the animals that received an optic nerve transection demonstrated significantly reduced pSTR and nSTR amplitudes, with the pSTR amplitude in the transected eye 47 (9)% that of control eye, while the nSTR amplitude was 83 (14)% that of the control eye (Figure 3.12).

Inner retinal thickness, the region of the retina between the ILM and IPL, was used to include the ganglion cell layer and retinal nerve fibre layer (Figure 3.13A). The range of mean thicknesses in all animals across all time points was 65 – 72 μm. The mean proportional change in ILM-IPL thickness compared to pre-injection was 1.025 (0.007) and no significant change (p = 0.51) in the thickness between time points was shown up to five weeks after an intravitreal injection of an AAV vector (Figure 3.13B).

Table 3.1 Comparison between the AAV vectors of signal intensity and image quality measures. Signal-to-background ratio measured the intensity ratio between the signal and background, signal-to-noise ratio and contrast-to-noise ratio represents the image quality at 5-weeks post-injection. Ratios are expressed as mean (95% CI). No statistically significant difference was found for any measure.

	Signal-to-Background		**Signal-to-Noise**		**Contrast-to-Noise**	
	Ratio	***p***	**Ratio**	***p***	**Ratio**	***p***
AAV2-CAG	2.97 (0.66)	0.08	6.84 (1.35)	0.49	4.35 (0.49)	0.85
AAV2-DCX	2.30 (0.33)		7.54 (1.30)		4.21 (1.09)	

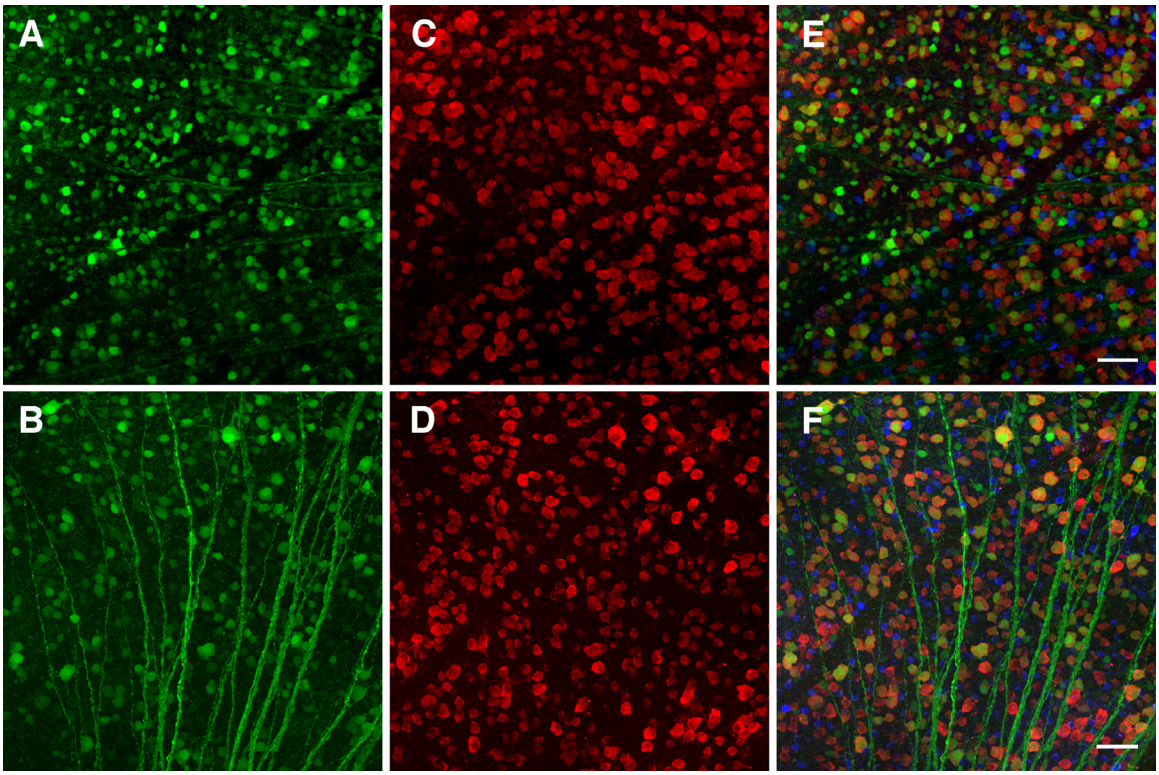

Figure 3.7 Flat-mounted mouse retina following intravitreal injection. **A-B)** show GFP labelling via intravitreal injection of AAV2-GFP vector (*green*), **C-D)** immunohistochemical labelling of RGCs with RNA binding protein with multiple splicing (RBPMS) (*red*) and **E-F)** merged image with choline acetyltranferase (ChAT) (*blue*). Panels **A,C,E** are from an animal that received an injection of the AAV2-CAG-GFP vector and panels **B,D,F** are from an animal that received an injection of the AAV2-DCX-GFP vector. Scale bars = 50 μm.

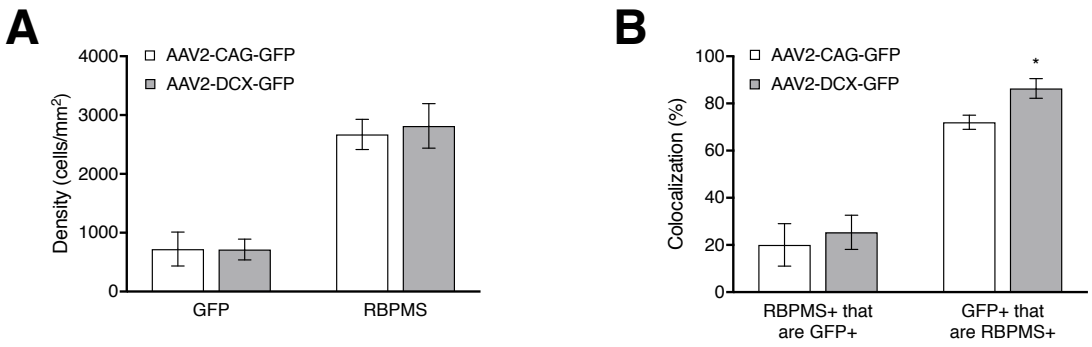

Figure 3.8 Quantification of cellular labelling in flatmount retinas compared between the AAV2 vectors. A) Density of GFP positive cells from an AAV intravitreal injection and RBPMS positive cells from immunohistochemical labelling. **B)** RBPMS+ cells that are GFP+ indicates the proportion of RGCs labelled by GFP and GFP+ cells that are RBPMS+ indicates the specificity of the AAV vector to RGCs. Mean (95% confidence interval) values are reported; * $p < 0.05$; n = 6.

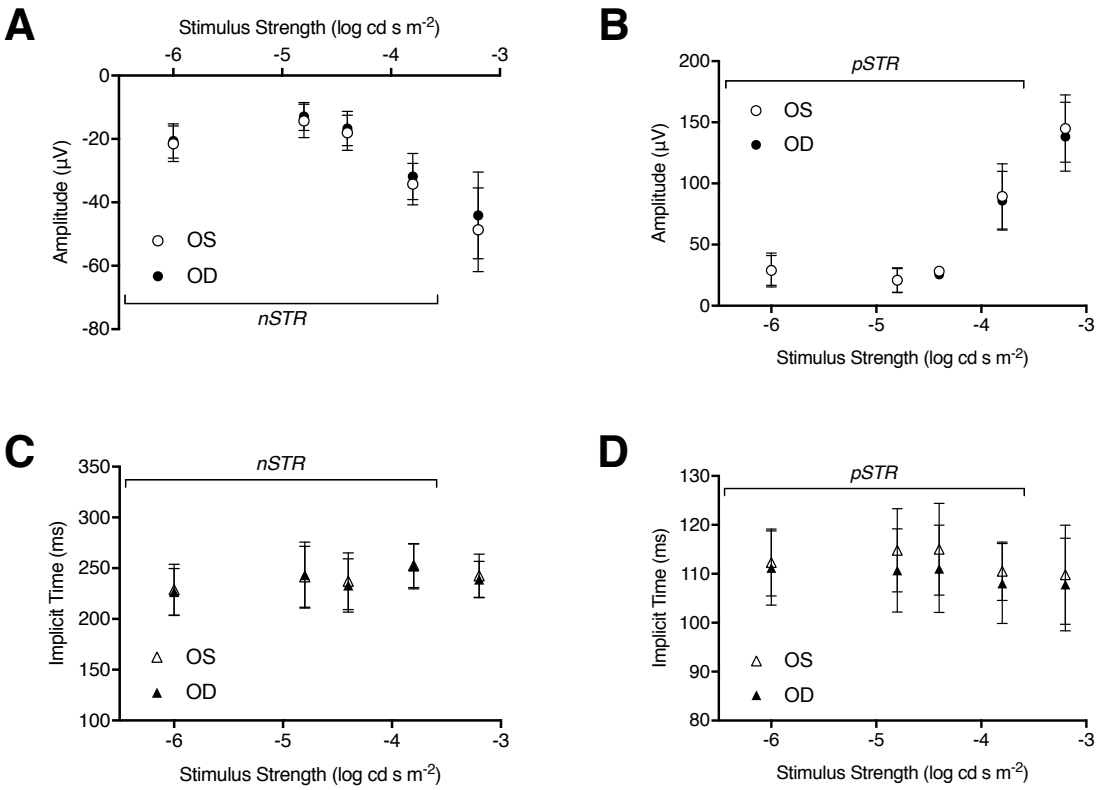

Figure 3.9 Baseline ERG measures prior to intravitreal injection. Averaged group data for right, OD (*filled circle or triangle*) and left, OS (*unfilled circle or triangle*) eyes of **A)** negative STR amplitudes, **B)** positive STR amplitudes, **C)** negative STR implicit times, and **D)** positive STR implicit times. No significant differences were found between the left and right eyes. Error bars represent 95% confidence interval; n = 6.

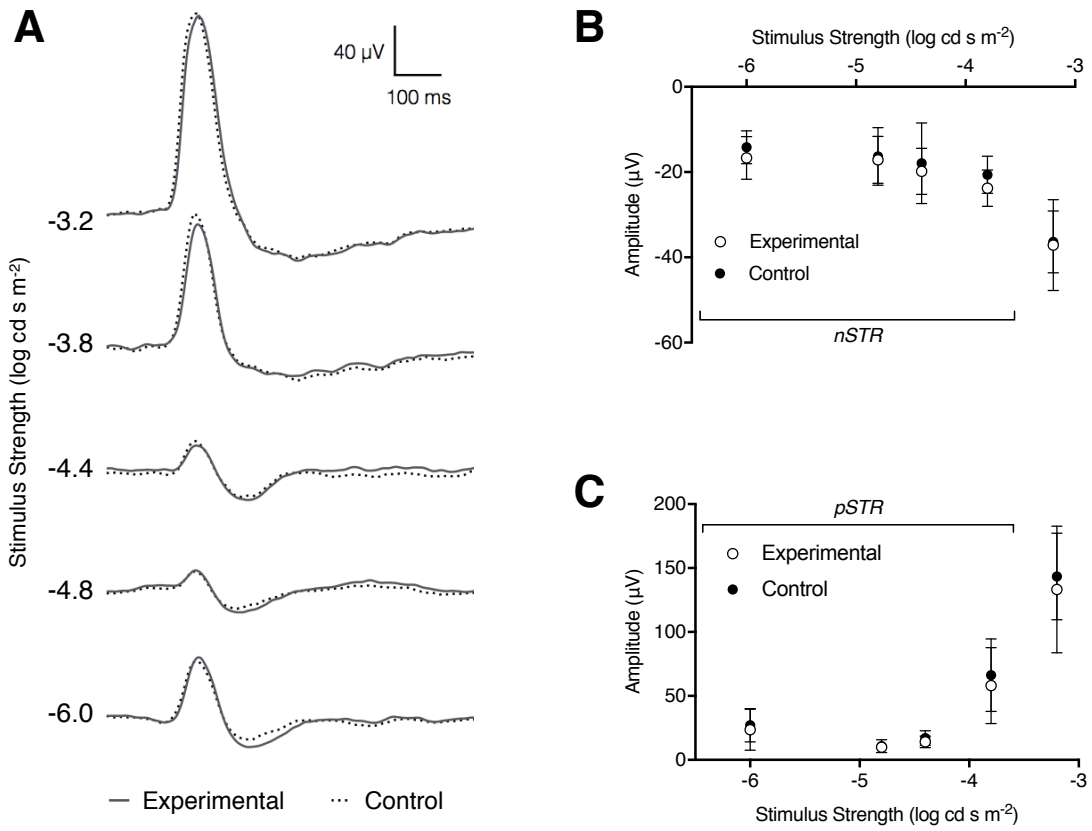

Figure 3.10 Effects of AAV2-DCX-GFP injection on the dark-adapted ERG amplitude 5-weeks post-injection. A) Example waveforms of ERG recordings obtained from AAV injected (*solid*) and control fellow (*dashed*) eyes over a range of low stimulus strengths. Averaged group data for control (*filled circles*) and experimental (*unfilled circles*) of **B)** negative STR and **C)** positive STR amplitudes. No significant differences were found between the experimental and control eyes. Error bars represent 95% confidence interval; n = 6.

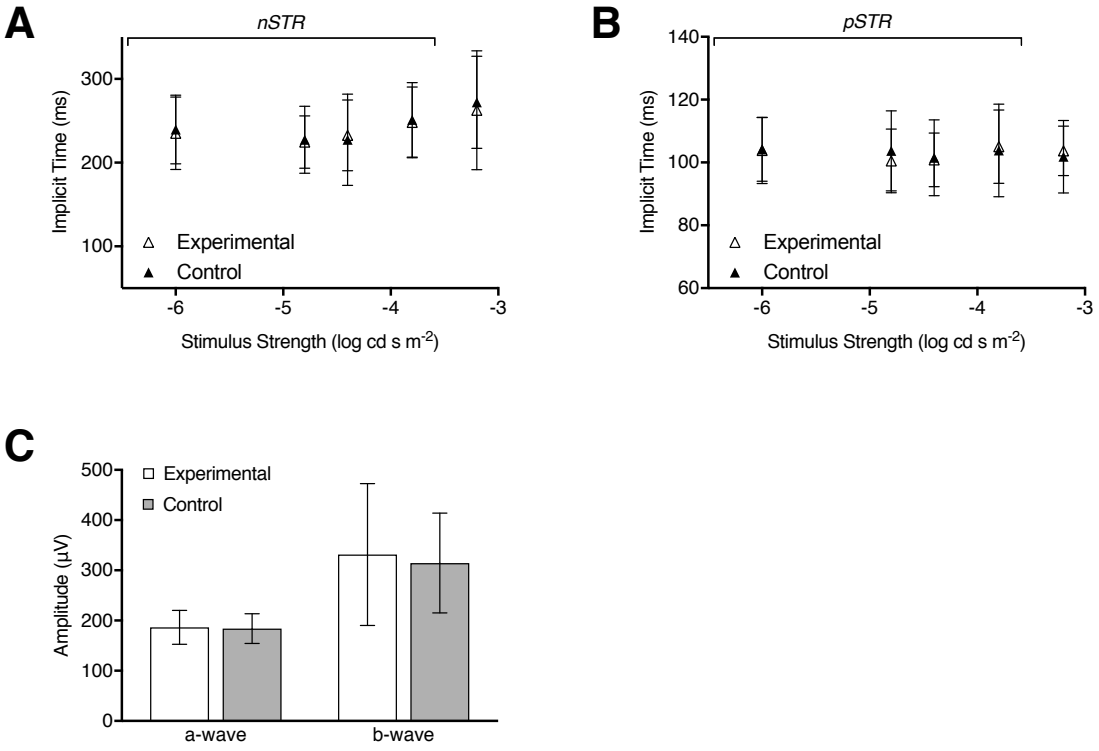

Figure 3.11 Effects of AAV2-DCX-GFP injection on the dark-adapted ERG implicit time and a- and b- waves. Averaged group data for control (*filled triangles*) and experimental (*unfilled triangles*) eyes of **A)** negative STR implicit times, and **B)** positive STR implicit times. **C)** Amplitudes of the a-wave and b-wave were measured in each eye for outer retina function. No significant differences were found between the left and right eyes. Error bars represent 95% confidence interval; n = 6.

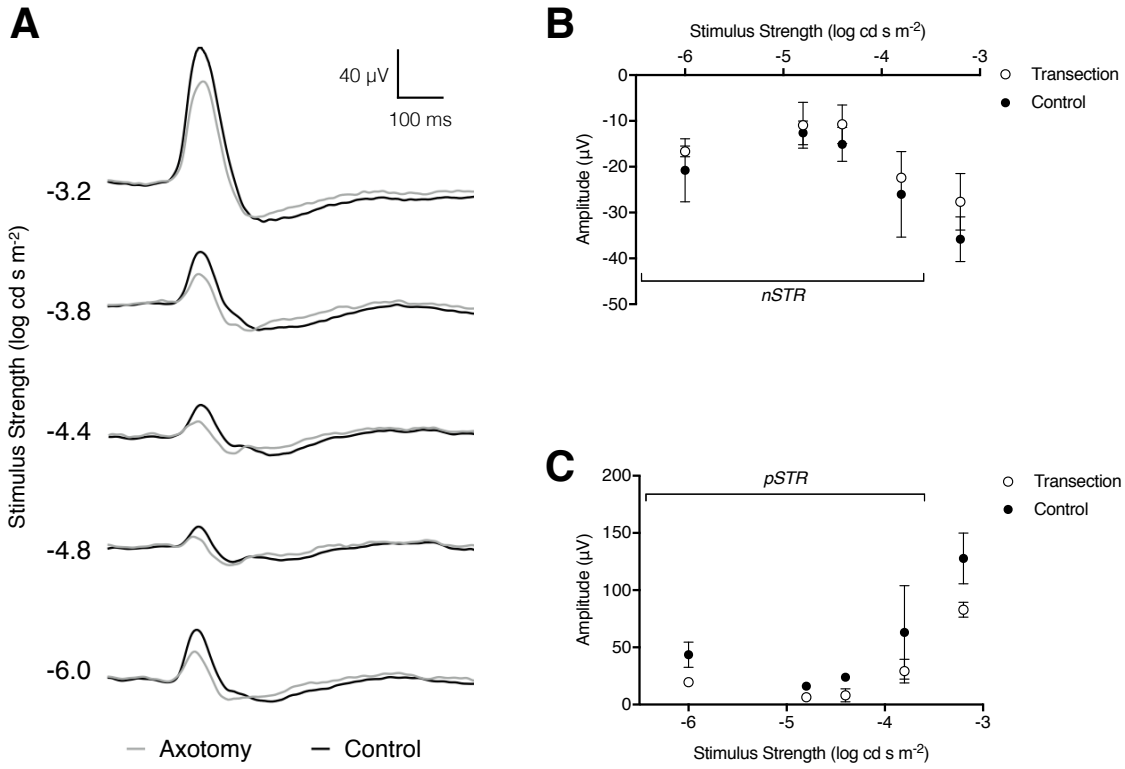

Figure 3.12 Effects of optic nerve transection on dark-adapted ERG. A) Example waveforms of ERG recordings obtained from control (*black*) and transected optic nerve (*gray*) eyes over a range of low stimulus strengths. Averaged group data for control (*filled circles*) and transection (*unfilled circles*) of **B)** negative STR and **C)** positive STR amplitudes. Error bars represent 95% confidence interval; n = 2

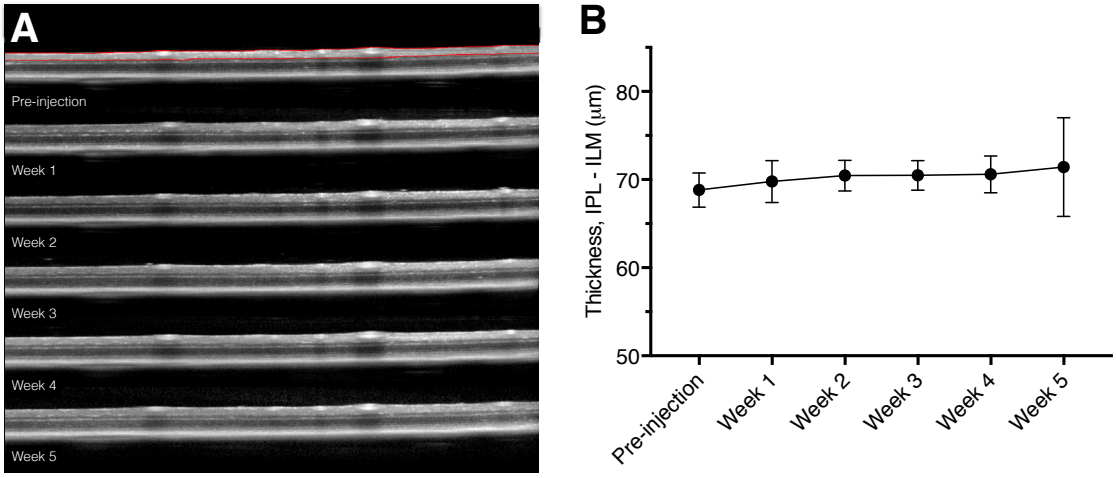

Figure 3.13 Longitudinal spectral domain optical coherence tomography (SD-OCT) scans of the left eye. A) Example scans in one animal obtained from raster scanning pattern at pre-injection and week 1, 2, 3, 4 and 5 after intravitreal injection. Red lines in pre-injection scan demonstrate segmentation. **B)** Mean thickness, inner plexiform layer to inner limiting membrane. No statistically significant difference was found between any of the time points. Error bars represent 95% confidence interval; n = 10.

Longitudinal fluorescence images corresponding to the same region of the retina before and after optic nerve transection are shown in Figure 3.14. The *in vivo* AAV2-DCX-GFP labelling is clearly visible, but at 14 days post-transection there were fewer GFP labelled cells with some cells losing all labelling, while others had diminished labelling, red and yellow arrows indicate examples in Figure 3.14, respectively.

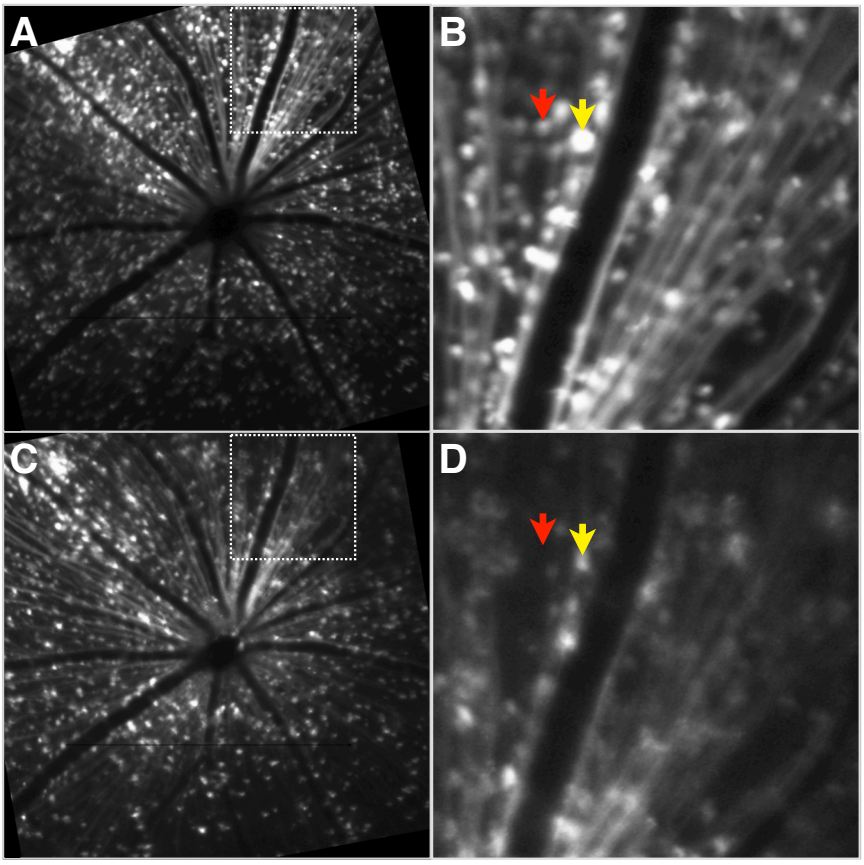

Figure 3.14 GFP labelling before and after optic nerve transection. *In vivo* CLSO fluorescence images from the same animal and retinal region, but different time points, following an intravitreal injection of AAV2-DCX-GFP vector **A-B)** 5 weeks post-injection and **C-D)** 14 days post-optic nerve transection (7 weeks post-injection) to demonstrate the effects of RGC death on GFP labelling. Panels B and D are higher magnification of the region marked by box in panels A and C, respectively. Arrows indicate examples of a cell that has lost all GFP labelling (*red*) and a cell with diminished GFP labelling (*yellow*).

3.4. Discussion and Conclusions

In this study we demonstrated that intravitreal injection administration of AAV vectors with a fluorescent reporter gene provides robust and sustained *in vivo* RGC labelling in mice. The GFP labelling was sufficiently strong to be detectable by non-invasive CSLO imaging with laser sources approved and used routinely in clinical practice. Between week 2 and week 4 there was a 69% increase in labelling for AAV2-CAG and 80% for AAV2-DCX. Furthermore, the GFP signal was persistent in individual RGCs for at least five weeks (Figures 3.4 and 3.5). There are two conclusions from the fluorescence trend important for the planning of longitudinal RGC survival experiments. Firstly, since the transduction of AAV vector requires approximately four weeks for maximal labelling (Figure 3.6), it was notable that GFP labelling was cumulative during this time and that the fluorescence signal was not transient. Secondly, we demonstrated a progressive decrease in RGC density following optic nerve transection (Figure 3.14). Furthermore, the *in vivo* electrophysiological assay of RGC health showed the AAV intravitreal injection did not cause measureable damage. These findings demonstrate that our technique of RGC labelling is a viable method to monitor real-time RGC survival in experimental disease models and interventions for neuroprotection and neuroregeneration.

AAV vector serotypes and capsids show preferential transduction to differing retinal cell types, even with ubiquitous promoters (Lebherz et al., 2008; Petrs-Silva et al., 2009; Surace and Auricchio, 2008), and is dependent on the injection site. Serotype 2 was chosen for this study because it most often shows the best transduction efficiency in RGCs when administered by intravitreal injection (Dinculescu et al., 2005; Hellstrom et al., 2009). Serotypes and engineered capsids (Petrs-Silva et al., 2009) can be used for improving transduction efficiency of

cells, while promoters can be used for improving transduction specificity. Ubiquitous promoters are commonly used, even when targeting specific cells, but could drive protein synthesis and cause side effects in other tissues and cells (Chandler et al., 2017; Russell, 2007). Therefore, use of specific promoters such as *DCX*, helps provide improved cell specific targeting and reduce the possible side effects induced by ubiquitous promoters. The specificity of RGC labelling with AAV vectors or comparing promoters has not been previously quantified with RGC-specific immunohistochemistry or markers. Transduction efficiency in the retina was either measured by total density of labelled cells across the retina (Martin et al., 2002) or fluorescence intensity within the retinal layers (Giove et al., 2010). We demonstrated a 19% increase in specificity to RGCs by utilizing a specific promoter compared to a ubiquitous promoter while labelling approximately the same proportion of total RGCs (Figure 3.8B). Choline acetyltransferase antibody labelling was used to show the presence of amacrine cells in the ganglion cell layer and did not co-localize with GFP positive cells. These results in processed retinal tissues demonstrated that the method of delivering fluorescent proteins via AAV2 and the specific *DCX* promoter yields high specificity for RGC labelling. A higher density of labelling was detected *ex vivo* than *in vivo* using the imaging methods we chose, though due to the small sample size in this study we cannot conclude there is no correlation between *in vivo* and *ex vivo* cell densities. *Ex vivo* tissue microscopy allowed for higher resolution imaging than the CSLO system and could have resulted in a larger number of detectable cells. Alternatively, further work could determine if AAV transduction/labelling is representative of the entire RGC population or is preferential to a specific RGC type. However, the ability to quantify cell densities from *in vivo* images could be a useful technique to calculate an estimate of total RGCs present in each animal.

We previously showed that intravitreal injection of the neuronal tracer, cholera toxin subunit B (CTB), resulted in fluorescence labelling of cells in the ganglion cell layer for *in vivo* imaging for at least 100 days post-injection. However, the CTB labelling was not specific to RGCs, with only 53% of CTB labelled cells being RGCs (Smith and Chauhan, 2015). Other researchers have described AAV-mediated GFP gene transfer for cross-sectional (Geng et al., 2009; Martin et al., 2002) or longitudinal (Lee et al., 2016) fluorescence imaging of the retina, but there is no previously published work that has quantified RGC density from *in vivo* images or reported the specificity of GFP labelling to RGCs. Martin *et al.* estimated a 75-85% transduction of RGCs in rats, approximately 2.5 times higher compared to our findings in mice, with AAV vectors containing GFP under the control of the ubiquitous CBA promoter and modified to include the woodchuck hepatitis post-transcriptional regulatory element (WPRE) (Martin et al., 2002). However, the high rate of transduction was achieved within 2 weeks after intravitreal injection and was attributed to the use of WPRE. The strengths of the RGC labelling studies described above, AAV vector labelling and specificity quantification, were combined to develop the protocol described in this study. The results imply that *in vivo* imaging of labelled RGCs from AAV vectors can provide a reliable method to quantify RGCs repeatedly and longitudinally without using transgenic animals or invasive labelling techniques such as retrograde labelling via the superior colliculus.

While the technique of RGC labelling described in this study does not label the entire RGC population, it does adequate labelling for sampling the total RGC population. The reported *in vivo* density measures provide an estimate of labelling across the retina with signal intensity that was at least twice that of the

background. This is an indication that the labelled cells are dispersed such that the resolution of the imaging system is able to adequately resolve individual cells. If all RGCs were transduced, it would be challenging to differentiate and quantify RGCs *in vivo* due to the high density labelling. In some applications of RGC targeting, such as high-resolution imaging and neuroprotective applications, it could be beneficial to have widespread transduction. The inner limiting membrane (ILM) has been reported to be a barrier to viral transduction via intravitreal delivery (Dalkara et al., 2009). This is likely the explanation for the observed cases of uneven labelling across the retina and a higher degree of GFP in the area closest to the injection site (Figure 3.5). A higher density of RGC labelling could have been achieved with improved transduction by compromising the ILM. To avoid possible disruption or integrity of the retina, we chose not use strategies such as enzymatic degradation of extracellular matrix of the ILM (Cehajic-Kapetanovic et al., 2011; Dalkara et al., 2009), vitreous aspiration prior to intravitreal injection (Da Costa et al., 2016; Tshilenge et al., 2016), formation of a bleb below the ILM to create a space for vector bolus (Boye et al., 2016), or ILM peeling (Takahashi et al., 2017), to reduce the resistance of the ILM to AAV transduction.

In summary, this work provides a novel method for quantifying RGCs in experimental studies and monitoring RGC loss in animal models. The results show a minimally invasive intravitreal injection of AAV vectors reliably label RGCs in mice for longitudinal *in vivo* visualization (Figure 3.4 and 3.5), *in vivo* quantification (Figure 3.6), *ex vivo* labelling (Figure 3.7), and *ex vivo* quantification (Figure 3.8). We show that the measures of RGC structure (retinal thickness) and function (ERG measures) are not affected by the administration of the AAV vectors. The high specificity of these AAV vectors to RGCs indicates there is

potential for diagnostic and therapeutic applications in diseases that cause RGC loss, such as glaucoma. Specifically, it would reduce the challenges presented by a heterogeneous population of cell types in the ganglion cell layer and the large amount of variability in the number of RGCs between individuals. Future work is required to investigate if AAV vectors can efficiently, reliably and specifically transduce human RGCs and the effects of introducing exogenous reporters into human neurons. Virus-based strategies are used for therapeutics, but their use for diagnostics would require a paradigm shift.

CHAPTER 4 General Discussion

4.1. Summary

The work enclosed in this thesis describes the development of a minimally invasive method for labelling RGCs from initial concept, to experimental design and implementation, and finally structural and functional evaluation. The intravitreal injection method constitutes one of the first attempts to quantify RGCs by bridging minimally invasive labelling in wild-type animals with longitudinal non-invasive monitoring of RGC density over time. This approach is directed by the motivation that RGCs cannot be directly imaged and quantified in a living organism unless genetic manipulation or an invasive procedure is used. The most commonly used methods of *in vivo* RGC quantification are transgenic animals and retrograde labelling; however, these can be costly or technically challenging, and have limited translation potential.

The ability to specifically and reproducibly label RGC somas was the first objective of this work and is essential for obtaining *in vivo* quantification or to be considered a viable biomarker of RGCs. An intravitreal injection of CTB provided clear labelling of individual cells at 10-15 days post-injection with 53% specificity to RGCs. To enhance this technique, the combination of intravitreal injection administration and non-invasive and *in vivo* CSLO imaging was used that permitted *in vivo* visualization of RGCs for at least 100 days post-injection. Moreover, the use of AAV vectors augments this technique with highly specific labelling of RGCs, 72-86%, for an extended period of time. Registration of images at each follow-up examination to the baseline image ensures that the same region of the retina is imaged and the same sample of RGCs measured. The technique

enables visualization of RGCs without extensive interventions and with commercially available imaging instruments.

The next research objective was to compare the rate of AAV transduction, *in vivo* image and signal quality, and specificity to RGCs between vectors with differing promoters. The experiments presented in Chapter 3 were designed around the objective to test if a tissue specific promoter would lead to improved efficacy of RGC labelling while maintaining a consistent and strong fluorescence signal for *in vivo* detection. Fluorescence images at weekly time points were obtained and used as a measure of changes in labelling over time. Our experimental results demonstrated that the AAV vectors resulted in an increased number of labelled cells until week 4, at which time labelling plateaued. A comparison study between vectors with the *CAG* and *DCX* promoters revealed that both groups had comparable image quality despite the engineered variants of GFP used between the vectors. To summarize, the AAV2-CAG vector provided a higher proportion of labelling across the retina, a higher density of detectable cells *in vivo*, and stronger fluorescence signal, whereas the AAV2-DCX vector showed a significantly higher specificity to RGCs. The studies demonstrated that each vector provides unique advantages compared to the other and each can be used to identify RGCs.

While the sustained and specific *in vivo* labelling of RGCs is critical for longitudinal studies, this labelling needs to accurately reflect the presence of RGCs without affecting the retinal structure or RGC function. The *in vivo* and longitudinal methodology to this work provides a powerful approach for monitoring the structural and functional effects of the labelling on the retina. Retinal thickness measures, which sampled precisely the same region at each

time point, showed the inner retinal thickness was unchanged as a result of the AAV vector injection. RGC function was assessed based on previous studies looking at the RGC component of ERG waveforms in mice generated from a light response (Smith et al., 2014). The RGC contribution to the mouse ERG is small and therefore difficult to isolate from a composite whole-retina recording. However, it is a quantifiable and objective measure of *in vivo* visual function. These *in vivo* measures showed that the AAV vector injection and labelling we used did not negatively impact the structural or functional properties of the retina as measured. Work completed to this point indicates that AAV vectors have applications as monitoring biomarkers for measuring "as an indicator of normal biological processes, pathogenic processes, or response to an exposure or intervention, including therapeutic interventions" (Group, 2016; Villani and Vujosevic, 2017).

This work would be incomplete without exploring if *in vivo* labelling decreases with RGC damage. After optic nerve transection, cells that had been previously labelled either ceased or significantly decreased expression of GFP. It is desirable to have an *in vivo* RGC marker that provides a longitudinal assessment of glaucomatous optic neuropathies, or models of such diseases (e.g., optic nerve transection). Similarly, it would be a useful for determining changes in the presence of RGCs for the development of neuroprotective strategies. We have established there are changes in GFP labelling following transection, but establishing the time course of labelling changes with cell viability would be useful. It is also important to determine that GFP signal is not transferred to other cell types such as glia. The need for this investigation is based on the premise that the application of *in vivo* labelling will be to directly assess RGCs by quantification.

4.2. Clinical Implications and Translation to Humans

The approximately 1000-fold difference in vitreous volume of a mouse compared to a human (Oyster, 1999; Remtulla and Hallett, 1985) has important implications in the concentration and rate at which the administered solution reaches the retina. It has been estimated that intravitreal drug transport in humans is composed of 30% convective flow, with the remainder being diffusive flow (Xu et al., 2000). Therefore, a sufficient volume and concentration must be administered to successfully transduce RGCs without initiating dangerous levels of immunogenicity.

Our results have demonstrated that an intravitreally injected AAV vector in mice transduces cells in the inner retina with specificity to RGCs of 72% with the AAV2-CAG vector and 86% with the AAV2-DCX vector. The transduction specificity in more representative animals, such as non-human primates, is not known. In addition to the vitreous volume, the inner limiting membrane acts as a barrier and is much thicker in primates compared to rodents (Dalkara et al., 2009; Matsumoto et al., 1984). Intravitreal injections of AAV vectors in non-human primates have demonstrated concentrated labelling in the GCL around the fovea, where the NFL and ILM is the thinnest (Yin et al., 2011; Yin et al., 2014). Procedures to reduce the impact of the ILM include enzyme degradation, vitrectomy or surgical peeling. All of these procedures have potential risks that compromise ILM integrity and lead to damage of the inner retina. An alternate method to circumvent the ILM is with the development of engineered AAV vectors that more efficiently cross the ILM and therefore have improved transduction of RGCs (Koilkonda et al., 2014; Petrs-Silva et al., 2009) or other retinal neurons (Boyd et al., 2016; Kay et al., 2013; Wassmer et al., 2017) when

administered intravitreally. An advantage of incorporating a reporter gene into AAV vectors is for rapid assessment of transduction efficiency.

The effect on visual function after administration or synthesis of exogenous fluorescent proteins in retinal neurons is not known. The excitation and emission spectra of GFP are comparable to fluorescein and are only modestly shifted – maximum excitation and maximum emission for fluorescein is 494 / 512 nm, respectively, and for enhanced GFP is 488 / 509 nm. Fluorescein is commonly used to visualize and image the retinal blood vessels by intravenous administration (Keane and Sadda, 2014; Novotny and Alvis, 1961; Roberts et al., 2015). However, fluorescein is very transient unless pathology is present, being only detectable in the retinal vessels for 10-20 minutes and systemic clearance is complete by 48 to 72 hours after administration. The presence of fluorescent proteins in the retina as a result of AAV vectors would persist for much longer durations and be present intracellularly rather than the vasculature. Fluorescein is the best example of fluorescence in the eye, though very different from the cellular labelling proposed here. A phase I clinical trial would be required to assess if the presence of GFP in retinal neurons alters visual acuity and colour vision.

4.2.1. Safety of Intravitreal Injections

The eye has conventionally been described as an immune privileged organ (Streilein, 2003; Zamiri et al., 2007), but recent evidence suggests that the eye does entirely suppress immune responses; rather it highly regulates or adapts them for tissue preservation (Benhar et al., 2012; Niederkorn and Stein-Streilein, 2010). An important consideration of administering any agent into the eye is the potential of a localised and/or systemic immune reaction. For example, cell

culture studies have shown that there can be immunomodulatory characteristics, specifically the suppression of T cell responses, with CTB application (Burkart et al., 1999; Burkart et al., 2002; Francis et al., 1992), however, there is no published research on the immune response of CTB administration in the intact living eye. It is possible that the immune system can adopt memory, specifically neutralizing antibodies. For the purpose of diagnostics, such as the work presented in this thesis, multiple and bilateral injections may be necessary to increase the number of labelled cells or follow disease progression in both eyes. With a repeated AAV vector injection or injection into the contralateral eye; the immune system is primed to respond, resulting in diminished transduction of subsequent AAV administration (Kotterman et al., 2015; Li et al., 2008). Interestingly, this finding has been shown to be largely unique to intravitreal injections and not reproduced in subretinal injections (Amado et al., 2010; Annear et al., 2011). Willett and Bennett have suggested a strategy to circumvent the adaptation of the immune system by injecting both eyes either simultaneously or within 14 days, before immunological memory has been established (Willett and Bennett, 2013).

Direct visualization of gene delivery is desirable to assess efficiency and localization of transduction. The exogenous gene for GFP as a reporter in AAV vectors is one strategy (Bennett et al., 1997; Flannery et al., 1997) and the approach we used in this work. However, of concern is the potential toxicity and immunogenicity of GFP, especially with it being processed and present in the host cell. Possible mechanisms of cellular damage resulting from the presence of GFP include reactive oxygen species generation, initiation of apoptosis and immunogenic response (Ansari et al., 2016; Liu et al., 1999). Studies that have been performed emphasize caution when using GFP for *in vivo* studies,

especially when considering its translational potential to humans (Stripecke et al., 1999; Yang et al., 2016). Specifically, it has been shown that when GFP is introduced intravenously there are different immune responses between animal strains and species (Skelton et al., 2001). Skelton *et al.* showed that C57BL/6 mice exhibit mild or lack of immunogenicity compared to BALB/c mice that develop high cytotoxic T lymphocyte responses following the intravenous GFP administration. It was also noted that the route of administration (intravenous vs. subcutaneous) was important and affected the survival outcome. However, there is a lack of research on the immune response to GFP when administered into the eye, specifically via intravitreal injection. We did not observe any gross anatomical changes of an immune response in our mice with OCT imaging (Figure 3.9). Similarly, Boye *et al.* labelled retinal neurons with AAV2-GFP vectors in primates and observed that OCT scans of the retina appeared normal (Boye et al., 2016). Further work is required to fully understand if AAV2 vectors or labelling via GFP gene transfer could affect labelling efficiency, cell health, or be a safety issue. The major implication of cellular GFP toxicity and immunogenicity in cell labelling studies is the underestimation of cells transduced by the vector.

4.3. Limitations

Animal studies in vision research provide valuable knowledge on the mechanisms of eye diseases, and the safety and efficacy of potential treatments. However, there are inherent limitations to using animals for studying human conditions. The major differences in the ocular anatomy between mice and humans have been described in Figure 1.2. It is likely that neuronal tracers and AAV vectors demonstrate higher transduction in mice due to the smaller vitreous volume, closer proximity of the injection site to the retina, and thinner

inner limiting membrane. Conversely, the flow dynamics of injected solution could be impeded by the high curvature of the mouse eye and retina compared to species with larger globes. Secondly, our experiments utilized young adult (2 – 6 month old) mice as they are readily available and able to undergo multiple procedures with minimal attrition. The use of young animals is a limitation as it is generally of interest to quantify RGCs, and subsequently RGC loss, in older human populations since age has been shown to be an increased risk factor for the incidence and progression of glaucoma (Chauhan et al., 2008; Klein et al., 1992; Leske et al., 2007).

Functional activity of individually labelled RGCs was not investigated. A functional assay of the whole retina with a proportion of RGCs labelled was completed and no difference was observed between the labelled and control eyes in the STR response (Figures 3.10 and 3.11). If there were reduced functional activity as a result of labelling cells, one would expect to see at least a modest decrease in STR amplitudes when approximately 25% of RGCs are labelled by GFP. To assess adverse functional changes in individual RGCs resulting from intracellular labelling, single-cell electrophysiology (e.g., whole-cell patch-clamp recordings) or large-scale multielectrode array (MEA) recordings could be used. Alternatively, the use of a genetically encoded calcium indicator (e.g., GCaMP) instead of GFP in a vector would allow for an *in vivo* functional test of RGC responses to light (Yin et al., 2014). The effect of light on intracellular calcium concentration of neurons, and specifically RGC calcium transients, can be quantified (Borghuis et al., 2011). The challenge is that fluorescence imaging uses visible light that adapts the retina and an alternate wavelength of light must be used to stimulate the rods and/or cones, subsequently activating RGCs. This is a

promising technique as it has the potential to provide longitudinal *in vivo* structural and functional assessment of RGCs.

4.4. Future Directions

Key results have been produced from this work that provide a strong foundation to use this labelling technique for proof-of-concept animal studies of glaucomatous damage and pre-clinical human evaluation. The methodology described in this thesis has been developed with the long-term objective to provide researchers and clinicians with the necessary labelling and longitudinal non-invasive visualization information to determine if there is a loss of RGCs in experimental disease models, aging or after therapeutic interventions. This methodology can also be adapted for use in studies currently underway in our laboratory: integration of AAV vector labelling with a model of chronic ocular hypertension and the applicability of AAV vectors for labelling RGCs in the human retina.

At the time this work was initiated there was no established animal model of glaucomatous damage that caused a chronic loss of RGCs, could be non-invasively imaged longitudinally, and was clinically relevant. Optic nerve transection or crush and retinal ischemia are methods that allow for non-invasive imaging, but are surrogate models of glaucoma. One of the most established and accepted experimental rodent models of glaucoma is injection of microbeads into the anterior chamber that cause an obstruction of aqueous through the trabecular meshwork, thereby inducing RGC degeneration via increased intraocular pressure (Sappington et al., 2010; Urcola et al., 2006; Weber and Zelenak, 2001). However, over the past few years there have been improvements to this method, specifically the use of magnetic microbeads (Samsel et al., 2011) that allow

manipulation of microbeads away from the pupil and into the anterior chamber angle to reduce the potential of impeding the visual axis for imaging. Provided the microbead model can be further developed so that non-invasive imaging is maintained when there is RGC loss, the labelling method described in this work could be incorporated to provide a non-invasive approach for measuring progressive RGC loss in the same animal as a result of chronically increased intraocular pressure.

The *in vivo* studies provide strong evidence for the effectiveness of AAV vectors for labelling mice RGCs. The promoters we used are human DNA sequences, therefore we are interested in determining if these AAV vectors are effective in labelling human RGCs. Using retinal explants from post-mortem human eyes could allow for adequate conditions and time for AAV transduction and subsequently fluorescent cell labelling to occur. This would help determine if the promoters used have the ability to be translated into human application for targeting RGCs without the use of primates. While human explants are axotomized RGCs and do not replicate *in vivo* conditions; they do provide a more ethical and less expensive model for validation experiments.

4.5. Significance

The ability to reliably label RGCs with a minimally invasive method provides a unique approach to monitoring RGCs over time. By doing so permits non-invasive imaging of RGCs in a living animal and thereby a direct measure to visualize and quantify over time. *In vivo* imaging of the retina will determine precisely when RGC loss is occurring, without terminating the experiment, and provides a more accurate tool to quantify RGC degeneration and loss. This is valuable in experimental studies of disease models and has the potential for

clinical applications in gene therapy, neuroprotection and diagnostic imaging when monitoring RGCs is desirable.

References

1998. Comparison of glaucomatous progression between untreated patients with normal-tension glaucoma and patients with therapeutically reduced intraocular pressures. Collaborative Normal-Tension Glaucoma Study Group. Am. J. Ophthalmol. 126, 487-497.

Abbott, C.J., Choe, T.E., Lusardi, T.A., Burgoyne, C.F., Wang, L., Fortune, B., 2013. Imaging axonal transport in the rat visual pathway. Biomed. Opt. Express 4, 364-386.

Alarcon-Martinez, L., Aviles-Trigueros, M., Galindo-Romero, C., Valiente-Soriano, J., Agudo-Barriuso, M., Villa Pde, L., Villegas-Perez, M.P., Vidal-Sanz, M., 2010. ERG changes in albino and pigmented mice after optic nerve transection. Vision Res. 50, 2176-2187.

Amado, D., Mingozzi, F., Hui, D., Bennicelli, J.L., Wei, Z., Chen, Y., Bote, E., Grant, R.L., Golden, J.A., Narfstrom, K., Syed, N.A., Orlin, S.E., High, K.A., Maguire, A.M., Bennett, J., 2010. Safety and efficacy of subretinal readministration of a viral vector in large animals to treat congenital blindness. Sci. Transl. Med. 2, 21ra16.

Aman, A.T., Fraser, S., Merritt, E.A., Rodigherio, C., Kenny, M., Ahn, M., Hol, W.G., Williams, N.A., Lencer, W.I., Hirst, T.R., 2001. A mutant cholera toxin B subunit that binds GM1- ganglioside but lacks immunomodulatory or toxic activity. Proc. Natl. Acad. Sci. U. S. A. 98, 8536-8541.

Angelucci, A., Clascá, F., Sur, M., 1996. Anterograde axonal tracing with the subunit B of cholera toxin: a highly sensitive immunohistochemical protocol for revealing fine axonal morphology in adult and neonatal brains. J. Neurosci. Methods 65, 101-112.

Annear, M.J., Bartoe, J.T., Barker, S.E., Smith, A.J., Curran, P.G., Bainbridge, J.W., Ali, R.R., Petersen-Jones, S.M., 2011. Gene therapy in the second eye of RPE65-deficient dogs improves retinal function. Gene Ther. 18, 53-61.

Ansari, A.M., Ahmed, A.K., Matsangos, A.E., Lay, F., Born, L.J., Marti, G., Harmon, J.W., Sun, Z., 2016. Cellular GFP toxicity and immunogenicity: potential confounders in in vivo cell tracking experiments. Stem Cell Rev 12, 553-559.

Bainbridge, J.W.B., Smith, A.J., Barker, S.S., Robbie, S., Henderson, R., Balaggan, K., Viswanathan, A., Holder, G.E., Stockman, A., Tyler, N., Petersen-Jones, S., Bhattacharya, S.S., Thrasher, A.J., Fitzke, F.W., Carter, B.J., Rubin, G.S., Moore, A.T., Ali, R.R., 2008. Effect of gene therapy on visual function in Leber's Congenital Amaurosis. N. Engl. J. Med. 358, 2231-2239.

Balendra, S.I., Normando, E.M., Bloom, P.A., Cordeiro, M.F., 2015. Advances in retinal ganglion cell imaging. Eye (Lond) 29, 1260-1269.

Barnett, E.M., Elangovan, B., Bullok, K.E., Piwnica-Worms, D., 2006. Selective cell uptake of modified Tat peptide–fluorophore conjugates in rat retina in ex vivo and in vivo models. Invest. Ophthalmol. Vis. Sci. 47, 2589-2595.

Barnett, E.M., Zhang, X., Maxwell, D., Chang, Q., Piwnica-Worms, D., 2009. Single-cell imaging of retinal ganglion cell apoptosis with a cell-penetrating, activatable peptide probe in an in vivo glaucoma model. Proc. Natl. Acad. Sci. U. S. A. 106, 9391-9396.

Benhar, I., London, A., Schwartz, M., 2012. The privileged immunity of immune privileged organs: the case of the eye. Front Immunol 3, 296.

Bennett, J., Duan, D., Engelhardt, J.F., Maguire, A.M., 1997. Real-time, noninvasive in vivo assessment of adeno-associated virus-mediated retinal transduction. Invest. Ophthalmol. Vis. Sci. 38, 2857-2863.

Bodeutsch, N., Thanos, S., 2000. Migration of phagocytotic cells and development of the murine intraretinal microglial network: an in vivo study using fluorescent dyes. Glia 32, 91-101.

Borghuis, B.G., Tian, L., Xu, Y., Nikonov, S.S., Vardi, N., Zemelman, B.V., Looger, L.L., 2011. Imaging light responses of targeted neuron populations in the rodent retina. J. Neurosci. 31, 2855-2867.

Boyd, R.F., Sledge, D.G., Boye, S.L., Boye, S.E., Hauswirth, W.W., Komaromy, A.M., Petersen-Jones, S.M., Bartoe, J.T., 2016. Photoreceptor-targeted gene delivery using intravitreally administered AAV vectors in dogs. Gene Ther. 23, 223-230.

Boye, S.E., Alexander, J.J., Witherspoon, C.D., Boye, S.L., Peterson, J.J., Clark, M.E., Sandefer, K.J., Girkin, C.A., Hauswirth, W.W., Gamlin, P.D., 2016. Highly efficient delivery of adeno-associated viral vectors to the primate retina. Hum. Gene Ther. 27, 580-597.

Burgoyne, C.F., Downs, J.C., Bellezza, A.J., Suh, J.K., Hart, R.T., 2005. The optic nerve head as a biomechanical structure: a new paradigm for understanding the role of IOP-related stress and strain in the pathophysiology of glaucomatous optic nerve head damage. Prog. Retin. Eye Res. 24, 39-73.

Burkart, V., Kim, Y., Kauer, M., Kolb, H., 1999. Induction of tolerance in macrophages by cholera toxin B chain. Pathobiology 67, 314-317.

Burkart, V., Kim, Y.E., Hartmann, B., Ghiea, I., Syldath, U., Kauer, M., Fingberg, W., Hanifi-Moghaddam, P., Muller, S., Kolb, H., 2002. Cholera toxin B pretreatment of macrophages and monocytes diminishes their proinflammatory responsiveness to lipopolysaccharide. J. Immunol. 168, 1730-1737.

Bussel, I.I., Wollstein, G., Schuman, J.S., 2013. OCT for glaucoma diagnosis, screening and detection of glaucoma progression. Br. J. Ophthalmol. 98, ii15-ii19.

Calkins, D.J., 2012. Critical pathogenic events underlying progression of neurodegeneration in glaucoma. Prog. Retin. Eye Res. 31, 702-719.

Campbell, R.J., Bronskill, S.E., Bell, C.M., Paterson, J.M., Whitehead, M., Gill, S.S., 2010. Rapid expansion of intravitreal drug injection procedures, 2000 to 2008: a population-based analysis. Arch. Ophthalmol. 128, 359-362.

Cehajic-Kapetanovic, J., Le Goff, M.M., Allen, A., Lucas, R.J., Bishop, P.N., 2011. Glycosidic enzymes enhance retinal transduction following intravitreal delivery of AAV2. Mol. Vis. 17, 1771-1783.

Chandler, R.J., Sands, M.S., Venditti, C.P., 2017. Recombinant adeno-associated viral integration and genotoxicity: insights from animal models. Hum. Gene Ther. 28, 314-322.

Charbel Issa, P., Singh, M.S., Lipinski, D.M., Chong, N.V., Delori, F.C., Barnard, A.R., MacLaren, R.E., 2012. Optimization of in vivo confocal autofluorescence imaging of the ocular fundus in mice and its application to models of human retinal degeneration. Invest. Ophthalmol. Vis. Sci. 53, 1066-1075.

Chauhan, B.C., 1996. Confocal scanning laser tomography. Can. J. Ophthalmol. 31, 152-156.

Chauhan, B.C., Mikelberg, F.S., Balaszi, A.G., LeBlanc, R.P., Lesk, M.R., Trope, G.E., Canadian Glaucoma Study, G., 2008. Canadian Glaucoma Study: 2. risk factors for the progression of open-angle glaucoma. Arch. Ophthalmol. 126, 1030-1036.

Chauhan, B.C., Stevens, K.T., Levesque, J.M., Nuschke, A.C., Sharpe, G.P., O'Leary, N., Archibald, M.L., Wang, X., 2012. Longitudinal in vivo imaging of retinal ganglion cells and retinal thickness changes following optic nerve injury in mice. PLoS ONE 7, e40352.

Chong, G.T., Lee, R.K., 2012. Glaucoma versus red disease: imaging and glaucoma diagnosis. Curr. Opin. Ophthalmol. 23, 79-88.

Cong, L., Ren, L., Danias, J., Mittag, T., 2005. Quantitation of mouse RGCs by direct labeling with antibodies to neurofilament, PGP 9.5, Osteopontin, and Brn3 compared to retrograde labeling with Aminostilbamidine. Invest. Ophthalmol. Vis. Sci. 46.

Cook, P.B., Werblin, F.S., 1994. Spike initiation and propagation in wide field transient amacrine cells of the salamander retina. J. Neurosci. 14, 3852-3861.

Cordeiro, M.F., Guo, L., Luong, V., Harding, G., Wang, W., Jones, H.E., Moss, S.E., Sillito, A.M., Fitzke, F.W., 2004. Real-time imaging of single nerve cell apoptosis in retinal neurodegeneration. Proc. Natl. Acad. Sci. U. S. A. 101, 13352-13356.

Cordeiro, M.F., Migdal, C., Bloom, P., Fitzke, F.W., Moss, S.E., 2011. Imaging apoptosis in the eye. Eye 25, 545-553.

Cordeiro, M.F., Normando, E.M., Cardoso, M.J., Miodragovic, S., Jeylani, S., Davis, B.M., Guo, L., Ourselin, S., A'Hern, R., Bloom, P.A., 2017. Real-time imaging of single neuronal cell apoptosis in patients with glaucoma. Brain 140, 1757-1767.

Curcio, C.A., Allen, K.A., 1990. Topography of ganglion cells in human retina. J. Comp. Neurol. 300, 5-25.

Da Costa, R., Roger, C., Segelken, J., Barben, M., Grimm, C., Neidhardt, J., 2016. A novel method combining vitreous aspiration and intravitreal AAV2/8 injection results in retina-wide transduction in adult mice. Invest. Ophthalmol. Vis. Sci. 57, 5326-5334.

Dalkara, D., Kolstad, K.D., Caporale, N., Visel, M., Klimczak, R.R., Schaffer, D.V., Flannery, J.G., 2009. Inner limiting membrane barriers to AAV-mediated retinal transduction from the vitreous. Mol. Ther. 17, 2096-2102.

de Leeuw, C.N., Dyka, F.M., Boye, S.L., Laprise, S., Zhou, M., Chou, A.Y., Borretta, L., McInerny, S.C., Banks, K.G., Portales-Casamar, E., Swanson, M.I., D'Souza, C.A., Boye, S.E., Jones, S.J., Holt, R.A., Goldowitz, D., Hauswirth, W.W., Wasserman, W.W., Simpson, E.M., 2014. Targeted CNS delivery using human MiniPromoters and demonstrated compatibility with adeno-associated viral vectors. Molecular therapy. Methods & clinical development 1, 5.

Dezawa, M., Takano, M., Negishi, H., Mo, X., Oshitari, T., Sawada, H., 2002. Gene transfer into retinal ganglion cells by in vivo electroporation: a new approach. Micron 33, 1-6.

Dinculescu, A., Glushakova, L., Min, S.H., Hauswirth, W.W., 2005. Adeno-associated virus-vectored gene therapy for retinal disease. Hum. Gene Ther. 16, 649-663.

Donaldson, P.J., Grey, A.C., Maceo Heilman, B., Lim, J.C., Vaghefi, E., 2017. The physiological optics of the lens. Prog. Retin. Eye Res. 56, e1-e24.

Drager, U.C., Olsen, J.F., 1981. Ganglion cell distribution in the retina of the mouse. Invest. Ophthalmol. Vis. Sci. 20, 285-293.

Eljarrat-Binstock, E., Pe'er, J., Domb, A.J., 2010. New techniques for drug delivery to the posterior eye segment. Pharm. Res. 27, 530-543.

Ernest, P.J., Schouten, J.S., Beckers, H.J., Hendrikse, F., Prins, M.H., Webers, C.A., 2013. An evidence-based review of prognostic factors for glaucomatous visual field progression. Ophthalmology 120, 512-519.

Farah, M.H., Easter, S.S., 2005. Cell birth and death in the mouse retinal ganglion cell layer. J. Comp. Neurol. 489, 120-134.

Feng, G., Mellor, R.H., Bernstein, M., Keller-Peck, C., Nguyen, Q.T., Wallace, M., Nerbonne, J.M., Lichtman, J.W., Sanes, J.R., 2000. Imaging neuronal subsets in transgenic mice expressing multiple spectral variants of GFP. Neuron 28, 41-51.

Fite, K.V., Janusonis, S., 2002. Optic afferents to the parabrachial nucleus. Brain Res. 943, 9-14.

Flannery, J.G., Zolotukhin, S., Vaquero, M.I., LaVail, M.M., Muzyczka, N., Hauswirth, W.W., 1997. Efficient photoreceptor-targeted gene expression in vivo by recombinant adeno-associated virus. Proc. Natl. Acad. Sci. U. S. A. 94, 6916-6921.

Folliot, S., Briot, D., Conrath, H., Provost, N., Cherel, Y., Moullier, P., Rolling, F., 2003. Sustained tetracycline-regulated transgene expression in vivo in rat retinal ganglion cells using a single type 2 adeno-associated viral vector. J. Gene Med. 5, 493-501.

Francis, M.L., Ryan, J., Jobling, M.G., Holmes, R.K., Moss, J., Mond, J.J., 1992. Cyclic AMP-independent effects of cholera toxin on B cell activation. II. Binding of ganglioside GM1 induces B cell activation. J. Immunol. 148, 1999-2005.

Galindo-Romero, C., Avilés-Trigueros, M., Jiménez-López, M., Valiente-Soriano, F.J., Salinas-Navarro, M., Nadal-Nicolás, F., Villegas-Pérez, M.P., Vidal-Sanz, M., Agudo-Barriuso, M., 2011. Axotomy-induced retinal ganglion cell death in adult mice: quantitative and topographic time course analyses. Exp. Eye Res. 92, 377-387.

Galvao, J., Davis, B.M., Cordeiro, M.F., 2013. In vivo imaging of retinal ganglion cell apoptosis. Curr. Opin. Pharmacol. 13, 123-127.

Garcia-Frigola, C., Carreres, M.I., Vegar, C., Herrera, E., 2007. Gene delivery into mouse retinal ganglion cells by in utero electroporation. BMC Dev. Biol. 7.

Geng, Y., Greenberg, K.P., Wolfe, R., Gray, D.C., Hunter, J.J., Dubra, A., Flannery, J.G., Williams, D.R., Porter, J., 2009. In vivo imaging of microscopic structures in the rat retina. Invest. Ophthalmol. Vis. Sci. 50, 5872-5879.

Germain, F., Istillarte, M., Gómez-Vicente, V., Pérez-Rico, C., de la Villa, P., 2013. Electroretinographical and histological study of mouse retina after optic nerve section: a comparison between wild-type and retinal degeneration 1 mice. Clin. Experiment. Ophthalmol. 41, 593-602.

Giove, T.J., Sena-Esteves, M., Eldred, W.D., 2010. Transduction of the inner mouse retina using AAVrh8 and AAVrh10 via intravitreal injection. Exp. Eye Res. 91, 652-659.

Gonatas, N.K., Stieber, A., Gonatas, J., Mommoi, T., Fishman, P.H., 1983. Endocytosis of exogenous GM1 ganglioside and cholera toxin by neuroblastoma cells. Mol. Cell. Biol. 3, 91-101.

Gordon, M.O., Beiser, J.A., Brandt, J.D., Heuer, D.K., Higginbotham, E.J., Johnson, C.A., Keltner, J.L., Miller, J.P., Parrish, R.K., 2nd, Wilson, M.R., Kass, M.A., 2002. The Ocular Hypertension Treatment Study: baseline factors that predict the onset of primary open-angle glaucoma. Arch. Ophthalmol. 120, 714-720; discussion 829-730.

Gossman, M.V.M.D., 2004. Systematic evaluation of the mouse eye: anatomy, pathology, and biomethods. J. Neuroophthalmol. 24, 84-85.

Gray, D.C., Merigan, W., Wolfing, J.I., Gee, B.P., Porter, J., Dubra, A., Twietmeyer, T.H., Ahamd, K., Tumbar, R., Reinholz, F., Williams, D.R., 2006. In vivo fluorescence imaging of primate retinal ganglion cells and retinal pigment epithelial cells. Opt. Express 14, 7144-7158.

Gross, S.P., Vershinin, M., Shubeita, G.T., 2007. Cargo transport: two motors are sometimes better than one. Curr. Biol. 17, R478-486.

Group, F.-N.B.W., 2016. BEST (Biomarkers, EndpointS, and other Tools) Resource. Silver Spring (MD): Food and Drug Administration (US).

Guo, L., Normando, E.M., Nizari, S., Lara, D., Cordeiro, M.F., 2010. Tracking longitudinal retinal changes in experimental ocular hypertensionusing the cSLO and spectral domain-OCT. Invest. Ophthalmol. Vis. Sci. 51, 6504-6513.

Harwerth, R.S., Quigley, H.A., 2006. Visual field defects and retinal ganglion cell losses in patients with glaucoma. Arch. Ophthalmol. 124, 853-859.

Hattar, S., Kumar, M., Park, A., Tong, P., Tung, J., Yau, K.W., Berson, D.M., 2006. Central projections of melanopsin-expressing retinal ganglion cells in the mouse. J. Comp. Neurol. 497, 326-349.

Hellstrom, M., Ruitenberg, M.J., Pollett, M.A., Ehlert, E.M., Twisk, J., Verhaagen, J., Harvey, A.R., 2009. Cellular tropism and transduction properties of seven adeno-associated viral vector serotypes in adult retina after intravitreal injection. Gene Ther. 16, 521-532.

Hernandez, M.R., 2000. The optic nerve head in glaucoma: role of astrocytes in tissue remodeling. Prog. Retin. Eye Res. 19, 297-321.

Higashide, T., Kawaguchi, I., Ohkubo, S., Takeda, H., Sugiyama, K., 2006. In vivo imaging and counting of rat retinal ganglion cells using a scanning laser ophthalmoscope. Invest. Ophthalmol. Vis. Sci. 47, 2943-2950.

Hirokawa, N., Takemura, R., 2005. Molecular motors and mechanisms of directional transport in neurons. Nat. Rev. Neurosci. 6, 201-214.

Humayun, M.S., Prince, M., de Juan, E., Barron, Y., Moskowitz, M., Klock, I.B., Milam, A.H., 1999. Morphometric analysis of the extramacular retina from postmortem eyes with retinitis pigmentosa. Invest. Ophthalmol. Vis. Sci. 40, 143-148.

IEC, 2014. Safety of laser products - Part 1: Equipment classification and requirements. IEC (International Electrotechnical Commission), Geneva, Switzerland.

Illing, R.B., Wässle, H., 1981. The retinal projection to the thalamus in the cat: a quantitative investigation and a comparison with the retinotectal pathway. J. Comp. Neurol. 202, 265-285.

Jacobson, S.G., Cideciyan, A.V., Ratnakaram, R., Heon, E., Schwartz, S.B., Roman, A.J., Peden, M.C., Aleman, T.S., Boye, S.L., Sumaroka, A., Conlon, T.J., Calcedo, R., Pang, J.J., Erger, K.E., Olivares, M.B., Mullins, C.L., Swider, M., Kaushal, S., Feuer, W.J., Iannaccone, A., Fishman, G.A., Stone, E.M., Byrne, B.J., Hauswirth, W.W., 2012. Gene therapy for leber congenital amaurosis caused by RPE65 mutations: safety and efficacy in 15 children and adults followed up to 3 years. Arch. Ophthalmol. 130, 9-24.

Jager, R.D., Aiello, L.P., Patel, S.C., Cunningham, E.T.J., 2004. Risks of intravitreous injection: a comprehensive review. Retina 24, 676-698.

Jeon, C.-J., Strettoi, E., Masland, R.H., 1998. The major cell populations of the mouse retina. J. Neurosci. 18, 8936-8946.

Jeun, M., Jeoung, J.W., Moon, S., Kim, Y.J., Lee, S., Paek, S.H., Chung, K.W., Park, K.H., Bae, S., 2011. Engineered superparamagnetic $Mn_{0.5}Zn_{0.5}Fe_2O_4$ nanoparticles as a heat shock protein induction agent for ocular neuroprotection in glaucoma. Biomaterials 32, 387-394.

Johnson, L.N., Cashman, S.M., Kumar-Singh, R., 2007. Cell-penetrating peptide for enhanced delivery of nucleic acids and drugs to ocular tissues including retina and cornea. Mol. Ther. 16, 107-114.

Jonas, J.B., Spandau, U.H., Schlichtenbrede, F., 2008. Short-term complications of intravitreal injections of triamcinolone and bevacizumab. Eye 22, 590-591.

Kalesnykas, G., Oglesby, E.N., Zack, D.J., Cone, F.E., Steinhart, M.R., Tian, J., Pease, M.E., Quigley, H.A., 2012. Retinal ganglion cell morphology after optic nerve crush and experimental glaucoma. Invest. Ophthalmol. Vis. Sci. 53, 3847-3857.

Kass, M.A., Heuer, D.K., Higginbotham, E.J., Johnson, C.A., Keltner, J.L., Miller, J.P., Parrish, R.K., 2nd, Wilson, M.R., Gordon, M.O., 2002. The Ocular Hypertension Treatment Study: a randomized trial determines that topical ocular hypotensive medication delays or prevents the onset of primary open-angle glaucoma. Arch. Ophthalmol. 120, 701-713.

Kay, C.N., Ryals, R.C., Aslanidi, G.V., Min, S.H., Ruan, Q., Sun, J., Dyka, F.M., Kasuga, D., Ayala, A.E., Van Vliet, K., Agbandje-McKenna, M., Hauswirth, W.W., Boye, S.L., Boye, S.E., 2013. Targeting photoreceptors via intravitreal delivery using novel, capsid-mutated AAV vectors. PLoS ONE 8, e62097.

Keane, P.A., Sadda, S.R., 2014. Retinal imaging in the twenty-first century: state of the art and future directions. Ophthalmology 121, 2489-2500.

Keenan, T.D.L., Wotton, C.J., Goldacre, M.J., 2012. Trends over time and geographical variation in rates of intravitreal injections in England. Br. J. Ophthalmol. 96, 413-418.

Kerrigan-Baumrind, L.A., Quigley, H.A., Pease, M.E., Kerrigan, D.F., Mitchell, R.S., 2000. Number of ganglion cells in glaucoma eyes compared with threshold visual field tests in the same persons. Invest. Ophthalmol. Vis. Sci. 41, 741-748.

Kielczewski, J.L., Pease, M.E., Quigley, H.A., 2005. The effect of experimental glaucoma and optic nerve transection on amacrine cells in the rat retina. Invest. Ophthalmol. Vis. Sci. 46, 3188-3196.

Klein, B.E., Klein, R., Sponsel, W.E., Franke, T., Cantor, L.B., Martone, J., Menage, M.J., 1992. Prevalence of glaucoma. The Beaver Dam Eye Study. Ophthalmology 99, 1499-1504.

Köbbert, C., Apps, R., Bechmann, I., Lanciego, J.L., Mey, J., Thanos, S., 2000. Current concepts in neuroanatomical tracing. Prog. Neurobiol. 62, 327-351.

Koilkonda, R.D., Yu, H., Chou, T.H., Feuer, W.J., Ruggeri, M., Porciatti, V., Tse, D., Hauswirth, W.W., Chiodo, V., Boye, S.L., Lewin, A.S., Neuringer, M., Renner, L., Guy, J., 2014. Safety and effects of the vector for the Leber hereditary optic neuropathy gene therapy clinical trial. JAMA Ophthalmol 132, 409-420.

Kolb, H., Linberg, K.A., Fisher, S.K., 1992. Neurons of the human retina: a Golgi study. J. Comp. Neurol. 318, 147-187.

Kotterman, M.A., Yin, L., Strazzeri, J.M., Flannery, J.G., Merigan, W.H., Schaffer, D.V., 2015. Antibody neutralization poses a barrier to intravitreal adeno-associated viral vector gene delivery to non-human primates. Gene Ther. 22, 116-126.

Kuno, N., Fujii, S., 2010. Biodegradable intraocular therapies for retinal disorders: progress to date. Drugs Aging 27, 117-134.

Kwak, H.W., D'Amico, D.J., 1992. Evaluation of the retinal toxicity and pharmacokinetics of dexamethasone after intravitreal injection. Arch. Ophthalmol. 110, 259-266.

Kwong, J.M.K., Caprioli, J., Piri, N., 2010. RNA binding protein with multiple splicing: a new marker for retinal ganglion cells. Invest. Ophthalmol. Vis. Sci. 51, 1052-1058.

Kwong, J.M.K., Quan, A., Kyung, H., Piri, N., Caprioli, J., 2011. Quantitative analysis of retinal ganglion cell survival with Rbpms Immunolabeling in animal models of optic neuropathies. Invest. Ophthalmol. Vis. Sci.

Lambert, W., Ruiz, L., Crish, S., Wheeler, L., Calkins, D., 2011. Brimonidine prevents axonal and somatic degeneration of retinal ganglion cell neurons. Mol. Neurodegener. 6.

Lebel, K., Gonder, J., Davies, B., Zaour, N., 2013. Real-world utilization data over 4 years of ranibizumab injections for the treatment of wet age-related macular degeneration in Canada. Value Health 16, A510.

Lebherz, C., Maguire, A., Tang, W., Bennett, J., Wilson, J.M., 2008. Novel AAV serotypes for improved ocular gene transfer. The Journal of Gene Medicine 10, 375-382.

Lee, J.Y., Hwang, Y., Kim, J.H., Kim, Y.S., Jung, B.K., Kim, P., Lee, H., 2016. In vivo fluorescence retinal imaging following AAV2-mediated gene delivery in the rat retina. Invest. Ophthalmol. Vis. Sci. 57, 3390-3396.

Lei, Y., Garrahan, N., Hermann, B., Fautsch, M.P., Johnson, D.H., Hernandez, M.R., Boulton, M., Morgan, J.E., 2011. Transretinal degeneration in ageing human retina: a multiphoton microscopy analysis. Br. J. Ophthalmol. 95, 727-730.

Leite, M.T., Zangwill, L.M., Weinreb, R.N., Rao, H.L., Alencar, L.M., Sample, P.A., Medeiros, F.A., 2010. Effect of disease severity on the performance of Cirrus spectral-domain OCT for glaucoma diagnosis. Invest. Ophthalmol. Vis. Sci. 51, 4104-4109.

Leske, M.C., Connell, A.M., Schachat, A.P., Hyman, L., 1994. The Barbados Eye Study. Prevalence of open angle glaucoma. Arch. Ophthalmol. 112, 821-829.

Leske, M.C., Heijl, A., Hussein, M., Bengtsson, B., Hyman, L., Komaroff, E., Early Manifest Glaucoma Trial, G., 2003. Factors for glaucoma progression and the effect of treatment: the early manifest glaucoma trial. Arch. Ophthalmol. 121, 48-56.

Leske, M.C., Wu, S.Y., Honkanen, R., Nemesure, B., Schachat, A., Hyman, L., Hennis, A., Barbados Eye Studies, G., 2007. Nine-year incidence of open-angle glaucoma in the Barbados Eye Studies. Ophthalmology 114, 1058-1064.

Leung, C.K., Lindsey, J.D., Crowston, J.G., Lijia, C., Chiang, S., Weinreb, R.N., 2008a. Longitudinal profile of retinal ganglion cell damage after optic nerve crush with blue-light confocal scanning laser ophthalmoscopy. Invest. Ophthalmol. Vis. Sci. 49, 4898-4902.

Leung, C.K.-S., Weinreb, R.N., Li, Z.W., Liu, S., Lindsey, J.D., Choi, N., Liu, L., Cheung, C.Y.-l., Ye, C., Qiu, K., Chen, L.J., Yung, W.H., Crowston, J.G., Pu, M., So, K.F., Pang, C.P., Lam, D.S.C., 2011. Long-term in vivo imaging and measurement of dendritic shrinkage of retinal ganglion cells. Invest. Ophthalmol. Vis. Sci. 52, 1539-1547.

Leung, C.K.S., Lindsey, J.D., Chen, L., Liu, Q., Weinreb, R.N., 2009. Longitudinal profile of retinal ganglion cell damage assessed with blue-light confocal scanning laser ophthalmoscopy after ischaemic reperfusion injury. Br. J. Ophthalmol. 93, 964-968.

Leung, C.K.S., Lindsey, J.D., Crowston, J.G., Ju, W.-K., Liu, Q., Bartsch, D.-U., Weinreb, R.N., 2008b. In vivo imaging of murine retinal ganglion cells. J. Neurosci. Methods 168, 475-478.

Levin, L.A., Nilsson, S.F.E., Hoeve, J.V., Wu, S., Kaufman, P.L., Alm, A., 2011. Adler's Physiology of the Eye, 11 ed. Elsevier Health Sciences.

Li, Q., Miller, R., Han, P.Y., Pang, J., Dinculescu, A., Chiodo, V., Hauswirth, W.W., 2008. Intraocular route of AAV2 vector administration defines humoral immune response and therapeutic potential. Mol. Vis. 14, 1760-1769.

Liang, J., Williams, D.R., Miller, D.T., 1997. Supernormal vision and high-resolution retinal imaging through adaptive optics. J. Opt. Soc. Am. A Opt. Image Sci. Vis. 14, 2884-2892.

Liu, H.S., Jan, M.S., Chou, C.K., Chen, P.H., Ke, N.J., 1999. Is green fluorescent protein toxic to the living cells? Biochem. Biophys. Res. Commun. 260, 712-717.

Lund, R.D., 1965. Uncrossed visual pathways of hooded and albino rats. Science 149, 1506-1507.

Maguire, A.M., Simonelli, F., Pierce, E.A., Pugh, E.N., Mingozzi, F., Bennicelli, J., Banfi, S., Marshall, K.A., Testa, F., Surace, E.M., Rossi, S., Lyubarsky, A., Arruda, V.R., Konkle, B., Stone, E., Sun, J., Jacobs, J., Dell'Osso, L., Hertle, R., Ma, J.-x., Redmond, T.M., Zhu, X., Hauck, B., Zelenaia, O., Shindler, K.S., Maguire, M.G., Wright, J.F., Volpe, N.J., McDonnell, J.W., Auricchio, A., High, K.A., Bennett, J., 2008. Safety and efficacy of gene transfer for Leber's congenital amaurosis. N. Engl. J. Med. 358, 2240-2248.

Marschall, S., Sander, B., Mogensen, M., Jørgensen, T., Andersen, P., 2011. Optical coherence tomography—current technology and applications in clinical and biomedical research. Anal. Bioanal. Chem. 400, 2699-2720.

Martin, K.R.G., Klein, R.L., Quigley, H.A., 2002. Gene delivery to the eye using adeno-associated viral vectors. Methods 28, 267-275.

Massey, S.C., 2006. Functional anatomy of the mammalian retina, in: Ryan, S.J. (Ed.), Retina: Basic Science, Inherited Retinal Disease, and Tumors, 4 ed. Elsevier/Mosby, Philadelphia, pp. 43-82.

Matsuda, T., Cepko, C.L., 2004. Electroporation and RNA interference in the rodent retina in vivo and in vitro. Proc. Natl. Acad. Sci. U. S. A. 101, 16-22.

Matsumoto, B., Blanks, J.C., Ryan, S.J., 1984. Topographic variations in the rabbit and primate internal limiting membrane. Invest. Ophthalmol. Vis. Sci. 25, 71-82.

Medeiros, N.E., Curcio, C.A., 2001. Preservation of ganglion cell layer neurons in age-related macular degeneration. Invest. Ophthalmol. Vis. Sci. 42, 795-803.

Mikkelsen, J.D., 1992. Visualization of efferent retinal projections by immunohistochemical identification of cholera toxin subunit B. Brain Res. Bull. 28, 619-623.

Miller, D.T., Kocaoglu, O.P., Wang, Q., Lee, S., 2011. Adaptive optics and the eye (super resolution OCT). Eye (Lond) 25, 321-330.

Mitchell, P., Smith, W., Attebo, K., Healey, P.R., 1996. Prevalence of open-angle glaucoma in Australia. The Blue Mountains Eye Study. Ophthalmology 103, 1661-1669.

Mitrofanis, J., Provis, J.M., 1990. A distinctive soma size gradient among catecholaminergic neurones of human retinae. Brain Res. 527, 69-75.

Murphy, J.A., Nickerson, P.E.B., Clarke, D.B., 2007. Injury to retinal ganglion cell axons increases polysialylated neural cell adhesion molecule (PSA-NCAM) in the adult rodent superior colliculus. Brain Res. 1163, 21-32.

Myles, M.E., Neumann, D.M., Hill, J.M., 2005. Recent progress in ocular drug delivery for posterior segment disease: emphasis on transscleral iontophoresis. Adv. Drug Deliv. Rev. 57, 2063-2079.

Nadal-Nicolas, F.M., Jimenez-Lopez, M., Salinas-Navarro, M., Sobrado-Calvo, P., Alburquerque-Bejar, J.J., Vidal-Sanz, M., Agudo-Barriuso, M., 2012. Whole number, distribution and co-expression of Brn3 transcription factors in retinal ganglion cells of adult albino and pigmented rats. PLoS ONE 7, e49830.

Nema, H.V., Nema, N., 2013. Recent Advances in Ophthalmology. Jaypee Brothers Medical Publishers, New Delhi, India.

Nickerson, J.M., Goodman, P., Chrenek, M.A., Bernal, C.J., Berglin, L., Redmond, T.M., Boatright, J.H., 2012. Subretinal delivery and electroporation in

pigmented and nonpigmented adult mouse eyes. Methods Mol. Biol. 884, 53-69.

Niederkorn, J.Y., Stein-Streilein, J., 2010. History and physiology of immune privilege. Ocul. Immunol. Inflamm. 18, 19-23.

Novotny, H.R., Alvis, D.L., 1961. A method of photographing fluorescence in circulating blood in the human retina. Circulation 24, 82-86.

Oglesby, E., Quigley, H.A., Zack, D.J., Cone, F.E., Steinhart, M.R., Tian, J., Pease, M.E., Kalesnykas, G., 2012. Semi-automated, quantitative analysis of retinal ganglion cell morphology in mice selectively expressing yellow fluorescent protein. Exp. Eye Res. 96, 107-115.

Osborne, N.N., Melena, J., Chidlow, G., Wood, J.P., 2001. A hypothesis to explain ganglion cell death caused by vascular insults at the optic nerve head: possible implication for the treatment of glaucoma. Br. J. Ophthalmol. 85, 1252-1259.

Oyster, C.W., 1999. The Human Eye: Structure and Function. Sinauer Associates.

Pang, J.-J., Wu, S.M., 2011. Morphology and immunoreactivity of retrogradely double-labeled ganglion cells in the mouse retina. Invest. Ophthalmol. Vis. Sci. 52, 4886-4896.

Pang, J.J., Gao, F., Wu, S.M., 2002a. Relative contributions of bipolar cell and amacrine cell inputs to light responses of ON, OFF and ON-OFF retinal ganglion cells. Vision Res. 42, 19-27.

Pang, J.J., Gao, F., Wu, S.M., 2002b. Segregation and integration of visual channels: layer-by-layer computation of ON-OFF signals by amacrine cell dendrites. J. Neurosci. 22, 4693-4701.

Perry, V.H., 1981. Evidence for an amacrine cell system in the ganglion cell layer of the rat retina. Neuroscience 6, 931-944.

Petrs-Silva, H., Dinculescu, A., Li, Q., Deng, W.T., Pang, J.J., Min, S.H., Chiodo, V., Neeley, A.W., Govindasamy, L., Bennett, A., Agbandje-McKenna, M., Zhong, L., Li, B., Jayandharan, G.R., Srivastava, A., Lewin, A.S., Hauswirth, W.W., 2011. Novel properties of tyrosine-mutant AAV2 vectors in the mouse retina. Mol. Ther. 19, 293-301.

Petrs-Silva, H., Dinculescu, A., Li, Q., Min, S.H., Chiodo, V., Pang, J.J., Zhong, L., Zolotukhin, S., Srivastava, A., Lewin, A.S., Hauswirth, W.W., 2009. High-efficiency transduction of the mouse retina by tyrosine-mutant AAV serotype vectors. Mol. Ther. 17, 463-471.

Pierce, E.A., Bennett, J., 2015. The status of RPE65 gene therapy trials: safety and efficacy. Cold Spring Harb Perspect Med 5.

Piri, N., Kwong, J.M.K., Song, M., Caprioli, J., 2006. Expression of hermes gene is restricted to the ganglion cells in the retina. Neurosci. Lett. 405, 40-45.

Portales-Casamar, E., Swanson, D.J., Liu, L., de Leeuw, C.N., Banks, K.G., Ho Sui, S.J., Fulton, D.L., Ali, J., Amirabbasi, M., Arenillas, D.J., Babyak, N., Black, S.F., Bonaguro, R.J., Brauer, E., Candido, T.R., Castellarin, M., Chen, J., Chen, Y., Cheng, J.C., Chopra, V., Docking, T.R., Dreolini, L., D'Souza, C.A., Flynn, E.K., Glenn, R., Hatakka, K., Hearty, T.G., Imanian, B., Jiang, S., Khorasan-zadeh, S., Komljenovic, I., Laprise, S., Liao, N.Y., Lim, J.S., Lithwick, S., Liu, F., Liu, J., Lu, M., McConechy, M., McLeod, A.J., Milisavljevic, M., Mis, J., O'Connor, K., Palma, B., Palmquist, D.L., Schmouth, J.F., Swanson, M.I., Tam, B., Ticoll, A., Turner, J.L., Varhol, R., Vermeulen, J., Watkins, R.F., Wilson, G., Wong, B.K., Wong, S.H., Wong, T.Y., Yang, G.S., Ypsilanti, A.R., Jones, S.J., Holt, R.A., Goldowitz, D., Wasserman, W.W., Simpson, E.M., 2010. A regulatory toolbox of MiniPromoters to drive selective expression in the brain. Proc. Natl. Acad. Sci. U. S. A. 107, 16589-16594.

Purves, D., Augustine, G.J., Fitzpatrick, D., (Eds.), 2001. The Retina, Neuroscience, 2nd edition ed. Sinauer Associates, Sunderland, MA.

Qiu, X., Johnson, J.R., Wilson, B.S., Gammon, S.T., Piwnica-Worms, D., Barnett, E.M., 2014. Single-cell resolution imaging of retinal ganglion cell apoptosis in vivo using a cell-penetrating caspase-activatable peptide probe. PLoS ONE 9, e88855.

Quigley, H.A., 1996. Number of people with glaucoma worldwide. Br. J. Ophthalmol. 80, 389-393.

Quigley, H.A., 1999. Neuronal death in glaucoma. Prog. Retin. Eye Res. 18, 39-57.

Quigley, H.A., 2004. New paradigms in the mechanisms and management of glaucoma. Eye 19, 1241-1248.

Quigley, H.A., Green, W.R., 1979. The histology of human glaucoma cupping and optic nerve damage: clinicopathologic correlation in 21 eyes. Ophthalmology 86, 1803-1830.

Ramón y Cajal, S., 1911. Histologie du système nerveux de l'homme & des vertébrés. Maloine, Paris.

Raza, A.S., Hood, D.C., 2015. Evaluation of a method for estimating retinal ganglion cell counts using visual fields and optical coherence tomography. Invest. Ophthalmol. Vis. Sci. 56, 2254-2268.

Remington, L.A., 2012. Retina, Clinical Anatomy and Physiology of the Visual System (Third Edition). Butterworth-Heinemann, Saint Louis, pp. 61-92.

Remtulla, S., Hallett, P.E., 1985. A schematic eye for the mouse, and comparisons with the rat. Vision Res. 25, 21-31.

Resnikoff, S., Pascolini, D., Etya'ale, D., Kocur, I., Pararajasegaram, R., Pokharel, G.P., Mariotti, S.P., 2004. Global data on visual impairment in the year 2002. Bull. World Health Organ. 82, 844-851.

Rifkin, L., Schaal, S., 2012. Factors affecting patients' pain intensity during in office intravitreal injection procedure. Retina 32, 696-700.

Roberts, P., Waldstein, S.M., Schmidt-Erfurth, U., 2015. A focus on the imaging of the retina. Expert Review of Ophthalmology, 1-17.

Rodieck, R.W., 1979. Visual pathways. Annu. Rev. Neurosci. 2, 193-225.

Rodrigues, E.B., Grumann, A., Jr., Penha, F.M., Shiroma, H., Rossi, E., Meyer, C.H., Stefano, V., Maia, M., Magalhaes, O., Jr., Farah, M.E., 2011. Effect of needle type and injection technique on pain level and vitreal reflux in intravitreal injection. J. Ocul. Pharmacol. Ther. 27, 197-203.

Rodriguez, A.R., de Sevilla Müller, L.P., Brecha, N.C., 2014. The RNA binding protein RBPMS is a selective marker of ganglion cells in the mammalian retina. J. Comp. Neurol. 522, 1411-1443.

Rosenfeld, P.J., Schwartz, S.D., Blumenkranz, M.S., Miller, J.W., Haller, J.A., Reimann, J.D., Greene, W.L., Shams, N., 2005. Maximum tolerated dose of a humanized anti-vascular endothelial growth factor antibody fragment for

treating neovascular age-related macular degeneration. Ophthalmology 112, 1048-1053.

Rossi, E.A., Chung, M., Dubra, A., Hunter, J.J., Merigan, W.H., Williams, D.R., 2011. Imaging retinal mosaics in the living eye. Eye (Lond) 25, 301-308.

Rossi, E.A., Granger, C.E., Sharma, R., Yang, Q., Saito, K., Schwarz, C., Walters, S., Nozato, K., Zhang, J., Kawakami, T., Fischer, W., Latchney, L.R., Hunter, J.J., Chung, M.M., Williams, D.R., 2017. Imaging individual neurons in the retinal ganglion cell layer of the living eye. Proc. Natl. Acad. Sci. U. S. A. 114, 586-591.

Russell, D.W., 2007. AAV vectors, insertional mutagenesis, and cancer. Mol. Ther. 15, 1740-1743.

Ryu, M., Nakazawa, T., Akagi, T., Tanaka, T., Watanabe, R., Yasuda, M., Himori, N., Maruyama, K., Yamashita, T., Abe, T., Akashi, M., Nishida, K., 2011. Suppression of phagocytic cells in retinal disorders using amphiphilic poly(gamma-glutamic acid) nanoparticles containing dexamethasone. J. Control. Release 151, 65-73.

Saati, S., Lo, R., Li, P.Y., Meng, E., Varma, R., Humayun, M.S., 2010. Mini drug pump for ophthalmic use. Curr. Eye Res. 35, 192-201.

Sabel, B.A., Engelmann, R., Humphrey, M.F., 1997. In vivo confocal neuroimaging (ICON) of CNS neurons. Nat. Med. 3, 244-247.

Salinas-Navarro, M., Jimenez-Lopez, M., Valiente-Soriano, F.J., Alarcon-Martinez, L., Aviles-Trigueros, M., Mayor, S., Holmes, T., Lund, R.D., Villegas-Perez, M.P., Vidal-Sanz, M., 2009a. Retinal ganglion cell population in adult albino and pigmented mice: a computerized analysis of the entire population and its spatial distribution. Vision Res. 49, 637-647.

Salinas-Navarro, M., Mayor-Torroglosa, S., Jimenez-Lopez, M., Aviles-Trigueros, M., Holmes, T.M., Lund, R.D., Villegas-Perez, M.P., Vidal-Sanz, M., 2009b. A computerized analysis of the entire retinal ganglion cell population and its spatial distribution in adult rats. Vision Res. 49, 115-126.

Sample, P.A., 2000. Short-wavelength automated perimetry: it's role in the clinic and for understanding ganglion cell function. Prog. Retin. Eye Res. 19, 369-383.

Samsel, P.A., Kisiswa, L., Erichsen, J.T., Cross, S.D., Morgan, J.E., 2011. A novel method for the induction of experimental glaucoma using magnetic microspheres. Invest. Ophthalmol. Vis. Sci. 52, 1671-1675.

Sanchez, J., Holmgren, J., 2011. Cholera toxin - a foe & a friend. Indian J. Med. Res. 133, 153-163.

Sanchez-Farias, N., Candal, E., 2015. Doublecortin is widely expressed in the developing and adult retina of sharks. Exp. Eye Res. 134, 90-100.

Sappington, R.M., Carlson, B.J., Crish, S.D., Calkins, D.J., 2010. The microbead occlusion model: a paradigm for induced ocular hypertension in rats and mice. Invest. Ophthalmol. Vis. Sci. 51, 207-216.

Schlamp, C.L., Montgomery, A.D., Mac Nair, C.E., Schuart, C., Willmer, D.J., Nickells, R.W., 2013. Evaluation of the percentage of ganglion cells in the ganglion cell layer of the rodent retina. Mol. Vis. 19, 1387-1396.

Schuman, J.S., 2008. Spectral domain optical coherence tomography for glaucoma (an AOS thesis). Trans. Am. Ophthalmol. Soc. 106, 426-458.

Schwarz, A., Futerman, A.H., 1996. The localization of gangliosides in neurons of the central nervous system: the use of anti-ganglioside antibodies. Biochimica et Biophysica Acta (BBA) - Reviews on Biomembranes 1286, 247-267.

Simon, P., Thanos, S., 1998. Combined methods of retrograde staining, layer-separation and viscoelastic cell stabilization to isolate retinal ganglion cells in adult rats. J. Neurosci. Methods 83, 113-124.

Skeie, J.M., Tsang, S.H., Mahajan, V.B., 2011. Evisceration of mouse vitreous and retina for proteomic analyses. J. Vis. Exp.

Skelton, D., Satake, N., Kohn, D.B., 2001. The enhanced green fluorescent protein (eGFP) is minimally immunogenic in C57BL/6 mice. Gene Ther. 8, 1813-1814.

Smith, B.J., Wang, X., Chauhan, B.C., Cote, P.D., Tremblay, F., 2014. Contribution of retinal ganglion cells to the mouse electroretinogram. Doc. Ophthalmol. 128, 155-168.

Smith, C.A., Chauhan, B.C., 2015. Imaging retinal ganglion cells: Enabling experimental technology for clinical application. Prog. Retin. Eye Res. 44, 1-14.

Somfai, G.M., Salinas, H.M., Puliafito, C.A., Fernandez, D.C., 2007. Evaluation of potential image acquisition pitfalls during optical coherence tomography and their influence on retinal image segmentation. J. Biomed. Opt. 12, 041209-041213.

Spear, P.D., Kim, C.B.Y., Ahmad, A., Tom, B.W., 1996. Relationship between numbers of retinal ganglion cells and lateral geniculate neurons in the rhesus monkey. Vis. Neurosci. 13, 199-203.

Streilein, J.W., 2003. Ocular immune privilege: therapeutic opportunities from an experiment of nature. Nat. Rev. Immunol. 3, 879-889.

Stripecke, R., Carmen Villacres, M., Skelton, D., Satake, N., Halene, S., Kohn, D., 1999. Immune response to green fluorescent protein: implications for gene therapy. Gene Ther. 6, 1305-1312.

Sung, N.S., Crowley, Jr, W.F., Genel, M., et al., 2003. Central challenges facing the national clinical research enterprise. JAMA 289, 1278-1287.

Surace, E.M., Auricchio, A., 2008. Versatility of AAV vectors for retinal gene transfer. Vision Res. 48, 353-359.

Surgucheva, I., Weisman, A.D., Goldberg, J.L., Shnyra, A., Surguchov, A., 2008. γ-Synuclein as a marker of retinal ganglion cells. Mol. Vis. 14, 1540-1548.

Takahashi, K., Igarashi, T., Miyake, K., Kobayashi, M., Yaguchi, C., Iijima, O., Yamazaki, Y., Katakai, Y., Miyake, N., Kameya, S., Shimada, T., Takahashi, H., Okada, T., 2017. Improved intravitreal AAV-mediated inner retinal gene transduction after surgical internal limiting membrane peeling in Cynomolgus monkeys. Mol. Ther. 25, 296-302.

Tatham, A.J., Weinreb, R.N., Zangwill, L.M., Liebmann, J.M., Girkin, C.A., Medeiros, F.A., 2013. Estimated retinal ganglion cell counts in glaucomatous eyes with localized retinal nerve fiber layer defects. Am. J. Ophthalmol. 156, 578-587 e571.

Taylor, W.R., 1996. Response properties of long-range axon-bearing amacrine cells in the dark-adapted rabbit retina. Vis. Neurosci. 13, 599-604.

Tezel, G., 2008. TNF-alpha signaling in glaucomatous neurodegeneration. Prog. Brain Res. 173, 409-421.

Thanos, S., Indorf, L., Naskar, R., 2002. In vivo FM: using conventional fluorescence microscopy to monitor retinal neuronal death in vivo. Trends Neurosci. 25, 441-444.

Tielsch, J.M., Sommer, A., Katz, J., Royall, R.M., Quigley, H.A., Javitt, J., 1991. Racial variations in the prevalence of primary open-angle glaucoma. The Baltimore Eye Survey. JAMA 266, 369-374.

Tshilenge, K.-T., Ameline, B., Weber, M., Mendes-Madeira, A., Nedellec, S., Biget, M., Provost, N., Libeau, L., Blouin, V., Deschamps, J.Y., Le Meur, G., Colle, M.-A., Moullier, P., Pichard, V., Rolling, F., 2016. Vitrectomy prior to intravitreal injection of AAV2/2 vector promotes efficient transduction of retinal ganglion cells in dogs and non-human primates. Human Gene Therapy Methods.

Urcola, J.H., Hernandez, M., Vecino, E., 2006. Three experimental glaucoma models in rats: comparison of the effects of intraocular pressure elevation on retinal ganglion cell size and death. Exp. Eye Res. 83, 429-437.

van Oterendorp, C., Diaz-Santana, L., Bull, N., Biermann, J., Jordan, J.F., Lagreze, W.A., Martin, K.R., 2011. Light scattering and wavefront aberrations in in vivo imaging of the rat eye: a comparison study. Invest. Ophthalmol. Vis. Sci. 52, 4551-4559.

Vanderah, T.W., Gould, D.J., Nolte, J., 2015. Nolte's The human brain : an introduction to its functional anatomy, Seventh edition. ed.

Vianna, J.R., Danthurebandara, V.M., Sharpe, G.P., Hutchison, D.M., Belliveau, A.C., Shuba, L.M., Nicolela, M.T., Chauhan, B.C., 2015. Importance of normal aging in estimating the rate of glaucomatous neuroretinal rim and retinal nerve fiber layer loss. Ophthalmology 122, 2392-2398.

Vidal-Sanz, M., Bray, G.M., Villegas-Perez, M.P., Thanos, S., Aguayo, A.J., 1987. Axonal regeneration and synapse formation in the superior colliculus by retinal ganglion cells in the adult rat. J. Neurosci. 7, 2894-2909.

Vidal-Sanz, M., Salinas-Navarro, M., Nadal-Nicolás, F.M., Alarcón-Martínez, L., Valiente-Soriano, F.J., Miralles de Imperial, J., Avilés-Trigueros, M., Agudo-Barriuso, M., Villegas-Pérez, M.P., 2011. Understanding glaucomatous damage: anatomical and functional data from ocular hypertensive rodent retinas. Prog. Retin. Eye Res. 31, 1-27.

Villani, E., Vujosevic, S., 2017. Foreword: Biomarkers and surrogate endpoints in ophthalmic clinical research. Invest. Ophthalmol. Vis. Sci. 58, BIOi-BIOii.

Wakabayashi, T., Kosaka, J., Mori, T., Takamori, Y., Yamada, H., 2008. Doublecortin expression continues into adulthood in horizontal cells in the rat retina. Neurosci. Lett. 442, 249-252.

Wang, X., Archibald, M.L., Stevens, K., Baldridge, W.H., Chauhan, B.C., 2010. Cyan fluorescent protein (CFP) expressing cells in the retina of Thy1-CFP transgenic mice before and after optic nerve injury. Neurosci. Lett. 468, 110-114.

Wassmer, S.J., Carvalho, L.S., Gyorgy, B., Vandenberghe, L.H., Maguire, C.A., 2017. Exosome-associated AAV2 vector mediates robust gene delivery into the murine retina upon intravitreal injection. Sci Rep 7, 45329.

Weale, R.A., 2004. Toward a future for aging eyes, in: Werner, J.S., Chalupa, L.M. (Eds.), The visual neurosciences. MIT Press, Cambridge, Mass., pp. 205-212.

Webb, R.H., Hughes, G.W., Delori, F.C., 1987. Confocal scanning laser ophthalmoscope. Appl. Opt. 26, 1492-1499.

Weber, A.J., Zelenak, D., 2001. Experimental glaucoma in the primate induced by latex microspheres. J. Neurosci. Methods 111, 39-48.

Weinreb, R.N., Khaw, P.T., 2004. Primary open-angle glaucoma. Lancet 363, 1711-1720.

Wells, L.A., Furukawa, S., Sheardown, H., 2011. Photoresponsive PEG-anthracene grafted hyaluronan as a controlled-delivery biomaterial. Biomacromolecules 12, 923-932.

Wensor, M.D., McCarty, C.A., Stanislavsky, Y.L., Livingston, P.M., Taylor, H.R., 1998. The prevalence of glaucoma in the Melbourne Visual Impairment Project. Ophthalmology 105, 733-739.

Willett, K., Bennett, J., 2013. Immunology of AAV-mediated gene transfer in the eye. Front Immunol 4, 261.

Williams, D.R., 2011. Imaging single cells in the living retina. Vision Res. 51, 1379-1396.

Williams, R.W., Strom, R.C., Rice, D.S., Goldowitz, D., 1996. Genetic and environmental control of variation in retinal ganglion cell number in mice. J. Neurosci. 16, 7193-7205.

Wojtkowski, M., Srinivasan, V., Fujimoto, J.G., Ko, T., Schuman, J.S., Kowalczyk, A., Duker, J.S., 2005. Three-dimensional retinal imaging with high-speed ultrahigh-resolution optical coherence tomography. Ophthalmology 112, 1734-1746.

Xiang, M., Zhou, L., Macke, J., Yoshioka, T., Hendry, S., Eddy, R., Shows, T., Nathans, J., 1995. The Brn-3 family of POU-domain factors: primary structure, binding specificity, and expression in subsets of retinal ganglion cells and somatosensory neurons. J. Neurosci. 15, 4762-4785.

Xu, J., Heys, J., Barocas, V., Randolph, T., 2000. Permeability and diffusion in vitreous humor: implications for drug delivery. Pharm. Res. 17, 664-669.

Yang, C., Hao, F., He, J., Lu, T., Klein, R.L., Zhao, L.R., Duan, W.M., 2016. Sequential adeno-associated viral vector serotype 9-green fluorescent protein gene transfer causes massive inflammation and intense immune response in rat striatum. Hum. Gene Ther. 27, 528-543.

Yin, L., Greenberg, K., Hunter, J.J., Dalkara, D., Kolstad, K.D., Masella, B.D., Wolfe, R., Visel, M., Stone, D., Libby, R.T., DiLoreto, D., Schaffer, D., Flannery, J., Williams, D.R., Merigan, W.H., 2011. Intravitreal injection of AAV2 transduces macaque inner retina. Invest. Ophthalmol. Vis. Sci. 52, 2775-2783.

Yin, L., Masella, B., Dalkara, D., Flannery, J.G., Schaffer, D.V., Williams, D.R., Merigan, W.H., 2012. In vivo imaging of ganglion cell physiology in macaque fovea using a calcium indicator. J. Vis. 12, 55.

Yin, L., Masella, B., Dalkara, D., Zhang, J., Flannery, J.G., Schaffer, D.V., Williams, D.R., Merigan, W.H., 2014. Imaging light responses of foveal ganglion cells in the living macaque eye. J. Neurosci. 34, 6596-6605.

Yu, J., Daniels, B.A., Baldridge, W.H., 2009. Slow excitation of cultured rat retinal ganglion cells by activating group I metabotropic glutamate receptors. J. Neurophysiol. 102, 3728-3739.

Zamiri, P., Sugita, S., Streilein, J.W., 2007. Immunosuppressive properties of the pigmented epithelial cells and the subretinal space. Chem. Immunol. Allergy 92, 86-93.

Zhong, L., Li, B., Mah, C.S., Govindasamy, L., Agbandje-McKenna, M., Cooper, M., Herzog, R.W., Zolotukhin, I., Warrington, K.H., Jr., Weigel-Van Aken, K.A., Hobbs, J.A., Zolotukhin, S., Muzyczka, N., Srivastava, A., 2008. Next generation of adeno-associated virus 2 vectors: point mutations in tyrosines lead to high-efficiency transduction at lower doses. Proc. Natl. Acad. Sci. U. S. A. 105, 7827-7832.

Zinser, G., Wijnaendts-van-Resandt, R.V., Dreher, A.W., Weinreb, R.N., Harbarth, U., Schroder, H., Burk, R.O., 1989. Confocal laser tomographic scanning of the eye. Proc. SPIE 1161, 337-344.

APPENDIX A: Methods

A.1 Intravitreal Injections

The retina is located in an optically accessible part of the central nervous system permitting imaging and access to the retinal ganglion cells. Because the vitreous abuts the retinal ganglion cell axons in the retinal nerve fibre layer, a vitreal injection allows drugs and other compounds to be delivered in close proximity to the RGCs.

This method of administration was used in mice for this work. Pupils were dilated with topical mydriatics, one drop of 1% tropicamide (Alcon Canada Inc., Mississauga, ON, Canada) and 2.5% phenylephrine hydrochloride (Alcon Cnaada) prior to injection. For CTB injections, mice were then anaesthetized with isoflurane (Baxter Corporation, Mississauga, ON, Canada) with 3-4% volume for induction with 1.5 L/min oxygen flow and maintained at 1.5-3% volume for 0.8 L/min oxygen flow. For AAV injections, intraperitoneal injection of ketamine (100 mg/kg) and xylazine (10 mg/kg) was. Injections of AAV vector were performed inside a Biological Safety Cabinet, therefore injectable anaesthesia was preferred to reduce workspace clutter during injections. An operating microscope was used to visualize the eye and injection.

A.2 Confocal Scanning Laser Ophthalmoscope

A simplified schematic of the light path of the CSLO system and human eye is shown in Figure A.1. This demonstrates how a confocal system uses a pinhole to eliminate scattered light. Briefly, the laser emits parallel beams of light to scan the retina point-by-point. Light rays backscattered from the retina are deviated by the beam splitter to the detector. Out of focus rays that originate in front of or

behind the focal plane result in a smeared image. The presence of a pinhole, which is optically conjugate to the laser focal plane, suppresses or eliminates rays outside of the focal plane, resulting in a sharper image.

The CSLO system is equipped with a laser for 820 nm excitation (infrared) for baseline fundus imaging at the level of the nerve fiber layer. For cellular fluorescence imaging, a 488 nm excitation laser was used with a bandpass filter between 505-545 nm for emission detection. The excitation and emission spectra for GFP and Alexa Fluor® 488 are show in Figure A.2.

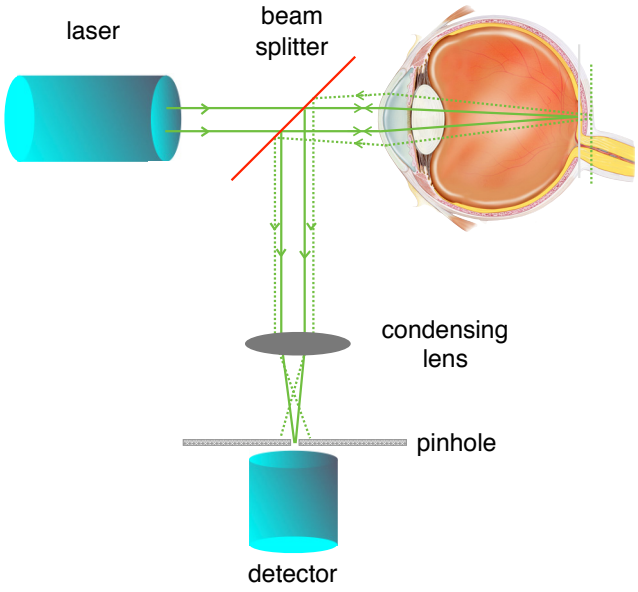

Figure A.1 Confocal scanning laser ophthalmoscope diagram. Schematic diagram with the principal components and optical light path of a confocal scanning laser ophthalmoscope.

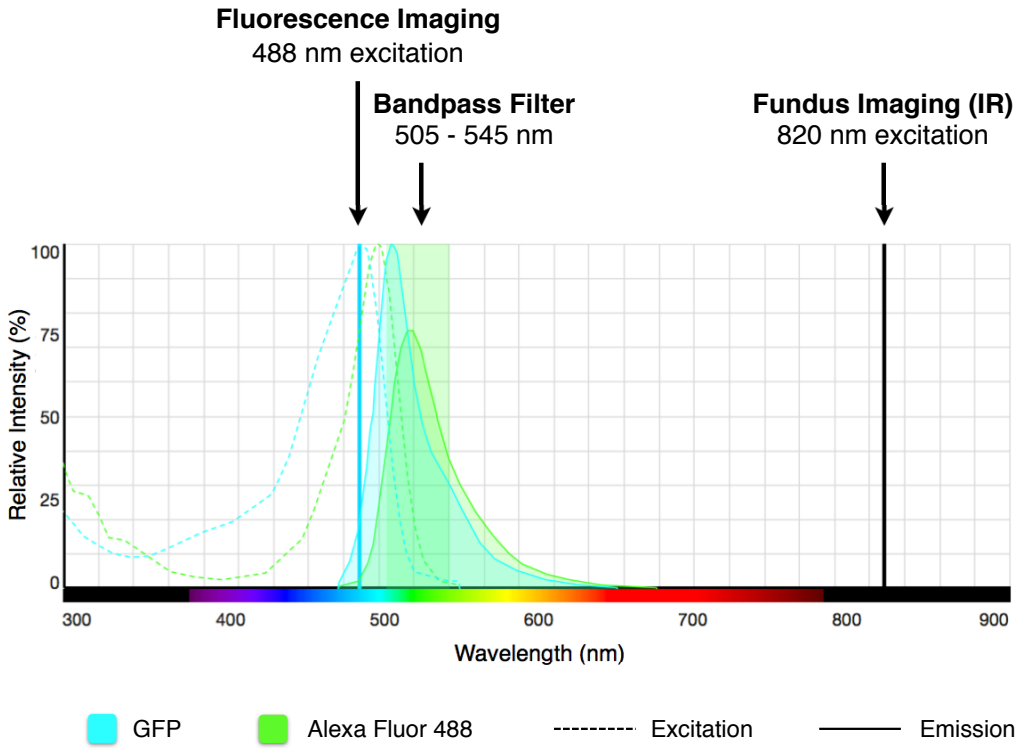

Figure A.2 Fluorescence spectra of GFP and Alexa Fluor® 488. The graph shows excitation (dashed line) and emission (solid line) spectra of the fluorophores (GFP, cyan and Alexa Fluor® 488, green) used in the experiments, in addition to the laser and filter wavelengths of the CSLO system.

The CSLO camera (Spectralis Multiline, Heidelberg Engineering, Heidelberg, Germany) is mounted on a custom-made manipulator with an animal table (Figure A.3). This set-up allows the operator to manipulate the camera or animal such that the optics are centred on the entrance pupil. In the correct position, the camera can be rotated about its axis without introducing off-axis errors. A heating pad is placed on the animal table to maintain body temperature for the duration of the procedure.

Modifications to the optics were made to accommodate imaging the mouse retina. Firstly, an auxiliary +25 diopter lens (Heidelberg Engineering) was attached to the camera objective for all imaging sessions. Secondly, custom settings for OCT imaging were used: ReferenceArmOffset = -23500 and EyeLengthStepSize = 1250.

Software features include real-time eye tracking, for intra-session motion and image alignment, for inter-session image registration. Eye tracking improves image quality and reduces image artefacts due to eye movement and respiration during image acquisition. Image registration ensures that precisely the same region of the retina is imaged in the longitudinal study; therefore, allowing the same cell population to be followed *in vivo* over time.

The axial resolution of the CSLO in mouse is between 50-80 μm and the lateral resolution approximately 5 μm. To demonstrate that the axial resolution is sufficient to differentiate labelling in the ganglion cell layer (GCL) from that in the inner nuclear layer (INL), an image focused on each layer was acquired and then superimposed to determine if there was overlap (Figure A.4).

Figure A.3 CLSO setup for imaging of mice. The camera (yellow arrow) is mounted on a customized frame with knobs (red arrows) that allow for rotation in any direction around the animal platform, which can also be moved horizontally and vertically.

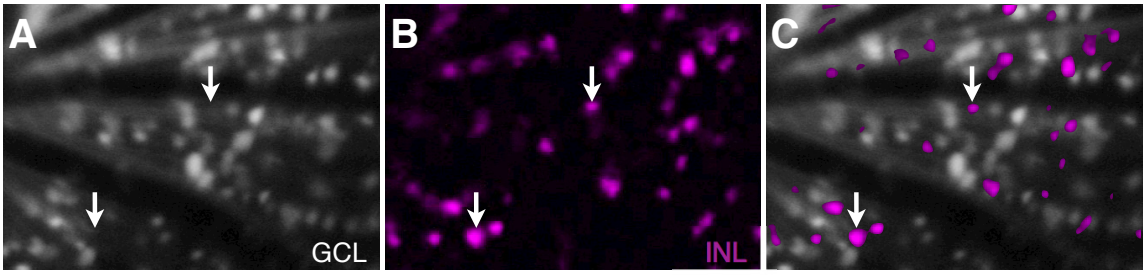

Figure A.4 Fluorescence images of living mouse retina to demonstrate axial resolution capabilities of the CSLO system. Differentiation of the A) ganglion cell layer (GCL) from the B) inner nuclear layer (INL) is shown. Pseudocolouring was applied to the INL image for clear distinction from the GCL. C) When the two layers are superimposed there is minimal overlap of cellular labelling between the two images. This provides evidence that when focussed on the GCL the fluorescence detection is primarily of cells that reside in the GCL.

APPENDIX B: Custom Made Image Processing and Analysis Tools

B.1 Semi-Automated Image Analysis and Quantification of In Vivo Fluorescence Images

Custom MATLAB code was written for calculating the density of labelled cells from CSLO fluorescence images.

```
%Image processing and cell counting for in vivo cSLO images (from
%Heidelberg Spectralis) of mouse retinas.
%
%Written 03 April 2013 by Corey A. Smith
%Modified from original (CSLOCount.m)

close all;
clear all;

%INPUT AND OUTPUT DIRECTIORY FOR IMAGES
input_dir = [pwd '/Input Images/AAV/'];
output_dir = [pwd '/Output Images/AAV/'];

% SEARCH FOR IMAGE FILES
files = dir( [input_dir '*.tif']);
filenames = {files.name};
DateStamp = {files.date};

%NUMBER OF FILES
num_files = length(files);

%CREATE THE OUTPUT FILE
fid = fopen('output.txt','a');

%WRITE THE VARIABLES IN THE FIRST ROW
fprintf(fid,'Filename\t Date Modified\t Width\t Height\t Black Pixels\t
ONH Area\t Total Image Area\t Count\t Density\n');

 for file_index = 1:num_files

    file_string = char(filenames(file_index));
    date_stamp = char(DateStamp(file_index));

    %READ IN IMAGES
    IMG = imread([input_dir file_string]);

    %REMOVE GREEN OCT REFERENCE BAR
    diff_im = imsubtract(IMG(:,:,3), rgb2gray(IMG));
    greenMap = diff_im > (double(IMG(:,:,3))-double(rgb2gray(IMG)));
    IMG = rgb2gray(IMG);
    IMG = imsubtract(IMG,im2uint8(greenMap));

    %CROP IMAGES (REMOVE BOTTOM TITLE BAR)
```

```
    IMG = IMG(1:1536, 1:1536);

    %REMOVE AREA WHERE SCALE BAR RESIDES
    IMG(1486:1536,1:60) = false;

    %SCALING FACTOR (um/pixel)
    IMG_Scale = 1.77/2;  %Divided by 2 because scaling factors provided
were for HS mode (not HR)
    [M,N] = size(IMG);
    IMG_Area_um = (M * IMG_Scale) * (N * IMG_Scale);
    IMG_Area_mm = (M * (IMG_Scale/1000)) * (N * (IMG_Scale/1000));
    IMG_Area = IMG_Area_mm;

    %REMOVE BLACK BACKGROUND AREA FROM IMAGE ORIENTATION
    black_pixel_count = length(find(IMG==0));

    %REMOVE AREA OF ONH
    imshow(IMG);
    disp('Interactively place a polygon around the ONH by clicking to
specify vertex locations.');
    disp('Double-click or right-click to finish positioning the
polygon.');
    H = impoly;
    position = wait(H);
    pos = getPosition(H);
    close;
    X = pos(:,1);
    Y = pos(:,2);
    ONH_Area = polyarea(X,Y);

    %SUBTRACT BACKGROUND AREA AND ONH AREA ELEMENTS FROM TOTAL IMAGE
AREA
    IMG_Area = IMG_Area - (ONH_Area * (IMG_Scale/1000)^2) -
(black_pixel_count * (IMG_Scale/1000)^2);

    IMG2=adapthisteq(IMG,'NumTiles',[20 20]);

    %MEDIAN ENHANCEMENT FILTER AND GAUSSIAN BLUR
    sigma = 3;
    cutoff = ceil(3*sigma);
    G = fspecial('gaussian',2*cutoff+1,sigma);
    IMG2 = imfilter(IMG2,G,'same');

    %INVERT IMAGE
    IMG2=imcomplement(IMG2);

    f=IMG2;
    g=f;

    %disp('Indicate pixel area to be analyzed.');
    P=200;

    %FIND ALL REGIONAL MINIMA
    rm=imhmin(g,10);

    %OBTAIN INTERNAL MARKERS
```

```
    im=imextendedmin(rm,10,4);      %Originally H was set at 10

    %%IMPORTANT CONSIDERATION%%
    se = strel('disk',2);
    im = imclose(im,se);

    lg = bwareaopen(im,P);
    se2 = strel('disk',5);
    lg_erode = imerode(lg,se2);

    sm = im & ~bwareaopen(im,P);
    sm_erode = imdilate(sm,se2);

    %REMOVE SMALL AND LARGE OBJECTS IN IMAGE (AREA BASED)
    im = (im & ~bwareaopen(im,P)) + lg_erode;
      %Originally was set at 385 then 300

    h=im;
    h=im2bw(h);

    %CALCULATE NUMBER OF REGIONS AND DENSITY
    [L,NUM] = bwlabeln(h);
    numstr = num2str(NUM);
    density_mm = NUM/IMG_Area;

    %OVERLAY FIGURE WITH COUNTED POINTS
    cc = bwconncomp(h, 4);
    positionArray = regionprops(cc, {'Centroid'});
    positionArray = struct2cell(positionArray);
    positionArray = cellfun(@transpose, positionArray,
'UniformOutput',false);
    positionArray = cell2mat(positionArray);

    %DISPLAY RESULTS
    subplot(1,2,1), imshow(IMG)
    subplot(1,2,2), imshow(IMG);
    hold on;
    scatter(positionArray(1, :), positionArray(2, :), 2, 'r','filled');

    %CHANGE DEFAULT DISPLAY FIGURE PROPERTIES AND INCLUDE CELL COUNT
VALUE
    set(gcf,'position',[235 267 980 427])
    title(['Cell Count = ' numstr ],'FontSize',14)

        %WIRTE THE RESULTS FOR EACH IMAGE TO OUTPUT FILE
fprintf(fid,'%s\t%s\t%f\t%f\t%f\t%f\t%f\t%f\t%f\n',file_string,date_sta
mp,M,N,black_pixel_count,ONH_Area,IMG_Area,NUM,density_mm);

    %SAVE FIGURE
    print( [ output_dir  file_string( 1 : end - 4 ) '.png' ] , '-dpng'
, '-r600' )
    close;

    w = warning('query','last');
    id = w.identifier;
    warning('off',id);
```

```
end

 %CLOSE OUTPUT FILE
fclose(fid);

 %CLOSE FIGURE
close
```

B.2 Image Quality and Signal-to-Noise Analysis of In Vivo Fluorescence Images

Custom MATLAB code was written for separating the signal from the background and calculating the mean signal (S) and background (B) values in each image. Measures of image quality and signal-to-noise ratio were calculated post-processing in a spreadsheet using the following formulas:

Signal-to-background ratio: $SBR = \frac{\bar{S}}{\bar{B}}$

Signal-to-noise ratio: $SNR = \frac{\bar{S}}{\sigma_B}$

Contrast-to-noise ratio: $CNR = \frac{\bar{S}-\bar{B}}{\sigma_B}$

```
%SIGNAL TO NOISE ANALYSIS OF CSLO IMAGES
%
%Written 29 June 2016 by Corey A. Smith
%Modified from original (threshold_mask.m)

close all; clear all

%INPUT AND OUTPUT DIRECTIORY FOR IMAGES
input_dir = [pwd '/'];
output_dir = [pwd '/Output Images/'];
mkdir( output_dir )

% SEARCH FOR IMAGE FILES
files = dir( [input_dir '*.tif']);
filenames = {files.name};
DateStamp = {files.date};

%NUMBER OF FILES
num_files = length(files);

%CREATE THE OUTPUT FILE
fid = fopen('output_snr.txt','a');

%WRITE THE VARIABLES IN THE FIRST ROW
fprintf(fid,'Filename\t Threshold\t Mean Signal\t SDGL1\t Mean
Background\t SDGL2\t Background Area\t Signal Area\t Ratio(GL2/GL1)\t
Difference\n');


for file_index = 1:num_files

  file_string = char(filenames(file_index));
  date_stamp = char(DateStamp(file_index));
```

```
%READ IN IMAGES
IMG = imread([input_dir file_string]);

    %REMOVE GREEN OCT REFERENCE BAR
    diff_im = imsubtract(IMG(:,:,3), rgb2gray(IMG));
    greenMap = diff_im > (double(IMG(:,:,3))-double(rgb2gray(IMG)));
    IMG = rgb2gray(IMG);
%Converts white line to black
    IMG = imsubtract(IMG,im2uint8(greenMap));

    %CROP IMAGES (REMOVE BOTTOM TITLE BAR)
    IMG = IMG(1:1536, 1:1536);

    %REMOVE AREA WHERE SCALE BAR RESIDES
    IMG(1486:1536,1:60) = false;

    sigma = 3;
    cutoff = ceil(3*sigma);
    G = fspecial('gaussian',2*cutoff+1,sigma);
    IMG2 = imfilter(IMG,G,'same');

    %INVERT IMAGE
    %IMG2=imcomplement(IMG2);

    f=IMG2;
    g=f;

    %FIND ALL REGIONAL MINIMA
    rm=imhmin(g,10);

    rm = adapthisteq(rm,'NumTiles',[20 20]);

% 1)Select an initial estimate for T -- Threshold is determined by the
% FILTERED IMAGE
grayImage = rm;

level = graythresh(f(f>0));
T = 255*level;

% 2)Segment the image using T. This will produce two
% groups of pixels. G1 consisting of all pixels with gray
% level values >T and G2 consisting of pixels with values <=T.
G1 = grayImage > T;
G2 = grayImage <= T;

SIGNAL = IMG;
BACK = IMG;

SIGNAL(G1==0)=0;
BACK(G2==0)=0;

imshowpair(SIGNAL,BACK,'montage')

%SAVE FIGURE
print( [ output_dir  file_string( 1 : end - 4 ) 'filtered.png' ] , '-
```

```
dpng' , '-r600' );

pause;
close;
% 3)Compute the average gray level values mean1 and
% mean2 for the pixels in regions G1 and G2.
    [ii,~,v] = find(IMG(G1));        %CALCUATE AVERAGE EXCLUDING ZEROS
    meanSignal = mean2(v);
    sdGL1 = std2(v);
%   semGL1 = std(v)/sqrt(length(v));

    [kk,~,x] = find(IMG(G2));
    meanBackground = mean2(x);
    sdGL2 = std2(x);
%   semGL2 = std(x)/sqrt(length(x));

ratio = meanBackground/meanSignal;
difference = meanSignal - meanBackground;
areaBackground = bwarea(G1);
areaSignal = bwarea(G2);

    %WIRTE THE RESULTS FOR EACH IMAGE TO OUTPUT FILE
    fprintf(fid,'%s\t %f\t %f\t %f\t %f\t %f\t %f\t %f\t %f\t %f\n',...

file_string,T,meanSignal,sdGL1,meanBackground,sdGL2,areaBackground,area
Signal,ratio,difference);

end

%CLOSE OUTPUT FILE
fclose(fid);
```

B.3 Measurement of Retinal Thickness in Mice from Optical Coherence Tomography Raster Scans

Custom made MATLAB code was written for calculating the total retinal thickness and ILM-IPL thickness from OCT images acquired using the raster scanning pattern of 19 B-scans.

```
%OCT processing to calculate retinal thickness using Excel files
exported from HEYEX.

close all;
clear all;

%%
%INPUT DIRECTORY FOR IMAGES
input_dir = [ pwd '/' ];
output_dir = [ pwd '/' ];

%SEARCH FOR IMAGE FILES
files = dir( [ input_dir '*.xls' ] );
filenames = { files.name };

%NUMBER OF FILES
num_files = length(files);

%CREATE THE OUTPUT FILE
%NOTE: Output file must not be open for this to work
fid = fopen('output.txt','a');

%WRITE THE VARIABLES IN THE FIRST ROW
fprintf(fid,'Filename\t Number of Scans\t Total Average\t Total SD\t
Total SEM\t Inner Average\t Inner SD\t Inner SEM\n');

%%
for file_index = 1:num_files

file_string = char(filenames(file_index));
[num,txt,raw] = xlsread([file_string]);
[nrows,ncols] = size(num);
num_scans = (nrows + 1) / 34;

ILM1 = 4;
NFL1 = 7;
GCL1 = 10;
IPL1 = 13;
INL1 = 16;
OPL1 = 19;
ELM1 = 22;
RPE1 = 31;
BM1 = 34;
```

```
num = [zeros(1,ncols);num];

%CONVERT NAN VALUES TO ZERO
num(isnan(num)) = 0;
num = mat2cell(num,repmat(34,num_scans,1),ncols);

results_final = zeros(num_scans,2);
results = zeros(num_scans,1);

for scan_index = 1 : num_scans

    temp = num{scan_index,1};
    ILM = temp(ILM1,:);
    INL = temp(INL1,:);
    IPL = temp(IPL1,:);
    BM = temp(BM1,:);

    inner = (IPL - ILM)/1000;
    retina = (BM - ILM)/1000;

    m = inner;
    m2 = retina;

    m(m>mean(m)+3*std(m))=0;   %REMOVES OUTLIERS MORE THAN 3 SD FROM
MEAN (PURPOSE IS TO REMOVE THOSE THAT ARE SUBTRACTED BY ZERO)
    m2(m2>mean(m2)+3*std(m2))=0;

    m(m<0) = 0;
    m2(m2<0) = 0;

    [ii,~,v] = find(m);        %CALCUATE AVERAGE EXCLUDING ZEROS
    avg = mean(v);
    sd = std(v);
    sem = std(v)/sqrt(length(v));

    [kk,~,x] = find(m2);
    avg2 = mean(x);
    sd2 = std(x);
    sem2 = std(x)/sqrt(length(x));

  diff = 256 - length(inner);
  if diff > 0
      inner = [inner, nan(1, diff)];
  end

  diff2 = 256 - length(m);
  if diff2 > 0
      m = [m, nan(1,diff2)];
  end

  diff3 = 256 - length(m2);
  if diff3 > 0
      m2 = [m2, nan(1,diff3)];
  end
```

```
  results_after(scan_index,:) = m;
  results_after2(scan_index,:) = m2;

  results_final(scan_index,1) = avg;
  results_final(scan_index,2) = sem;

end

%%
%SELECT FIRST N B-SCANS AND N FOUR B-SCANS
N = 6;          %CAN BE CHANGED TO DESIRED NUMBER OF B-SCANS TO ANALYZE
ABOVE AND BELOW ONH
results_top = results_after(1:N,:);
results_bottom = results_after((num_scans - (N - 1)):num_scans,:);
results_subset = [results_top;results_bottom];

results_top2 = results_after2(1:N,:);
results_bottom2 = results_after2((num_scans - (N - 1)):num_scans,:);
results_subset2 = [results_top2;results_bottom2];

%%
%CALCULATE MEAN ALONG B-SCAN (FROM SUBSET)
bscan_avg = mean(results_subset);       %!!!!NOTE DOES NOT EXCLUDE
ZEROS!!!!
bscan_sd = std(results_subset);

%%
%CALCULATE TOTAL MEAN
[jj,~,w] = find(results_subset);
inner_avg = nanmean(w);
inner_sd = nanstd(w);
inner_sem = nanstd(w)/sqrt(length(w));

[ll,~,y] = find (results_subset2);
retina_avg = nanmean(y);
retina_sd = nanstd(y);
retina_sem = nanstd(y)/sqrt(length(y));



%%
%WIRTE THE RESULTS FOR EACH IMAGE TO OUTPUT FILE
    fprintf(fid,'%s\t %f\t %f\t %f\t %f\t %f\t %f\t %f\n',...

file_string,num_scans,retina_avg,retina_sd,retina_sem,inner_avg,inner_s
d,inner_sem);

end

%CLOSE OUTPUT FILE
fclose(fid);
```

APPENDIX C: Prototype Intravitreal Injection Device for Mice

Performing intravitreal injections in mice is a challenging procedure that requires precision and is inherently subject to variability. The challenge is primarily due to the small size of the globe and large lens, creating a situation where needle depth and angle are vitally important for a successful injection. The best available methods to date are manual injection or with injection with micro-manipulators. Manual injection is relatively quick and only requires a microscope, but is not reproducible and has greater potential for adverse effects such as retinal tear/detachment or cataract from inadvertently impacting the lens. Micro-manipulators allow for precise delivery, but are expensive and require a large amount of space and setup time. A prototype device was developed, based on the InVitria® (FCI Ophthalmics Inc., Pembroke, MA, USA) injection assistant for human intravitreal injections designed by Dr. Arnaldo Gonçalves. The design uses a guide cylinder for the syringe and needle, consequently ensuring for a fixed angle and depth. The presented prototype was adapted to the dimensions and anatomy of the mouse eye (Figures C.1 and C.2).

The device was manufactured with 3D printing and tested on C57BL/6 mice. We found that the base of the device often abutted on the bone structures surrounding the eye, resulting in inadequate pressure to fix the eye position or puncture the sclera. This was particularly a problem in young mice with smaller eye diameter. Further design and testing was required, however, it could not be completed within the timeframe of the presented experiments. Nonetheless, the prototype has the potential to provide an efficient, reproducible, and cost-effective alternative for intravitreal injections in experimental animals.

Figure C.1 Drawings of intravitreal injection device for mice. These drawings were created with computer-aided design (CAD) software and used as the template for 3D printing. Yellow sphere depicts approximate size and location of the mouse eye in relation to the device. Dimensions are in millimetres.

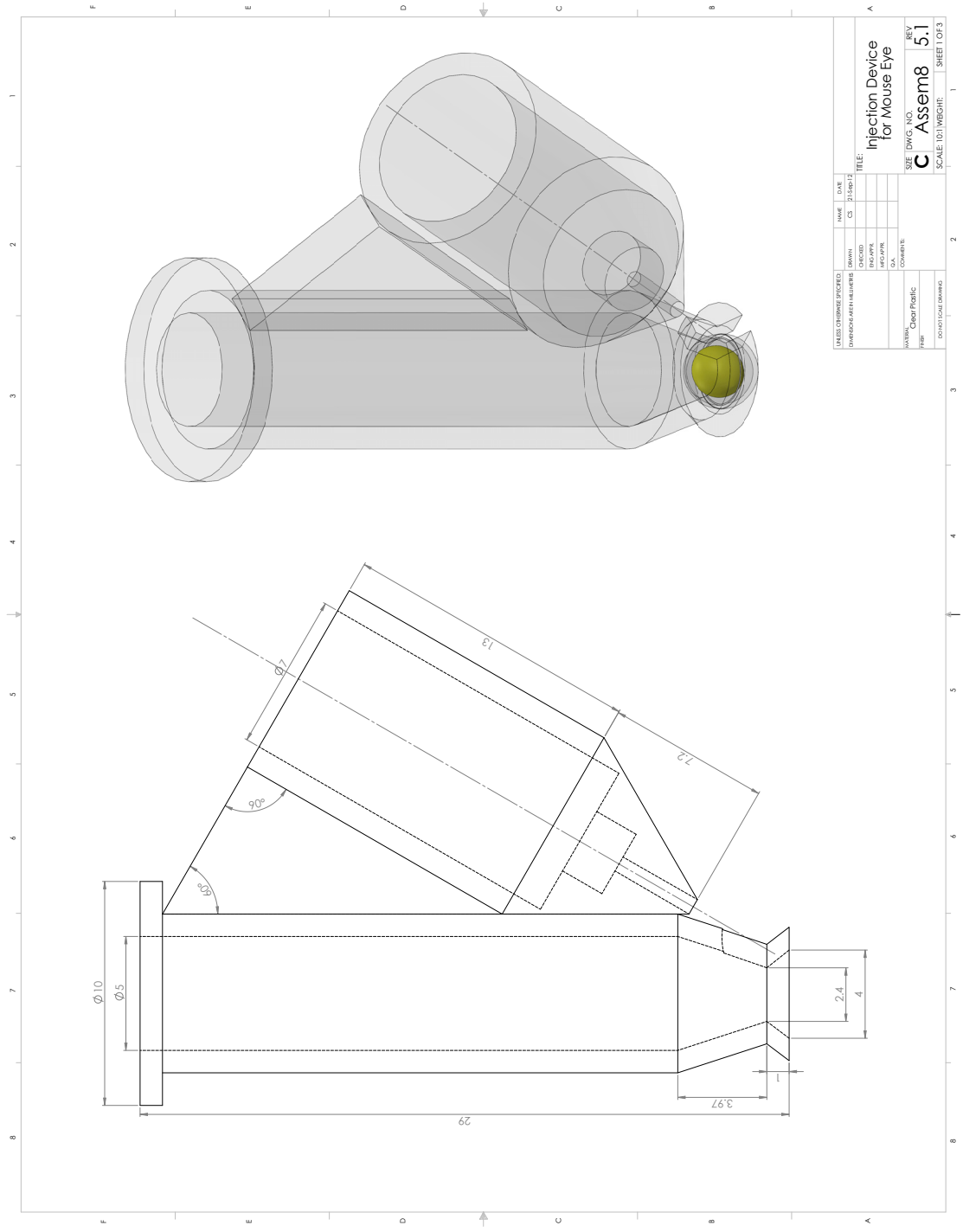
Injection Device
for Mouse Eye
Assem8
5.1
SHEET 1 OF 3
Clear Plastic
13
7.2
Ø7
90°
30°
Ø10
Ø5
2.4
4
1
3.97
29

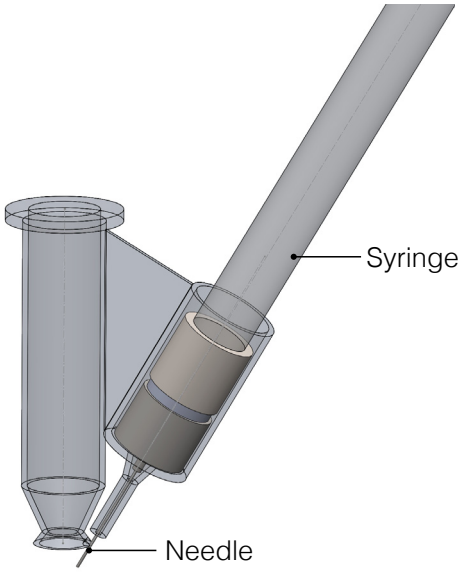

Figure C.2 3D rendering of an intravitreal injection device for mice. The protype device is shown with a drawing of a Hamilton Syringe in the syringe guide with a needle in the position that is expected to allow for a mid-vitreous injection of a mouse eye.

APPENDIX D: Copyright Permissions

Chapter 1: Introduction

ELSEVIER LICENSE
TERMS AND CONDITIONS

Aug 21, 2017

This Agreement between Corey A Smith ("You") and Elsevier ("Elsevier") consists of your license details and the terms and conditions provided by Elsevier and Copyright Clearance Center.

License Number	4173610141467
License date	Aug 21, 2017
Licensed Content Publisher	Elsevier
Licensed Content Publication	Elsevier Books
Licensed Content Title	Nolte's the Human Brain
Licensed Content Author	Todd W. Vanderah,Douglas J. Gould
Licensed Content Date	Jan 1, 2016
Licensed Content Volume	n/a
Licensed Content Issue	n/a
Licensed Content Pages	40
Start Page	419
End Page	458
Type of Use	reuse in a thesis/dissertation
Intended publisher of new work	other
Portion	figures/tables/illustrations
Number of figures/tables/illustrations	1
Format	both print and electronic
Are you the author of this Elsevier chapter?	No
Will you be translating?	No
Original figure numbers	Figure 17-4
Title of your thesis/dissertation	Labelling and Longitudinal In Vivo Imaging of Retinal Ganglion Cells
Expected completion date	Aug 2017
Estimated size (number of pages)	150
Requestor Location	Corey A Smith Physiology & Biophysics Dalhousie University 5850 College Street, PO Box 15000 Halifax, NS B3H4R2 Canada Attn: Corey A Smith
Billing Type	Invoice

Billing Address	Corey A Smith Physiology & Biophysics Dalhousie University 5850 College Street, PO Box 15000 Halifax, NS B3H4R2 Canada Attn: Corey A Smith
Total	0.00 USD

Terms and Conditions

INTRODUCTION

1. The publisher for this copyrighted material is Elsevier. By clicking "accept" in connection with completing this licensing transaction, you agree that the following terms and conditions apply to this transaction (along with the Billing and Payment terms and conditions established by Copyright Clearance Center, Inc. ("CCC"), at the time that you opened your Rightslink account and that are available at any time at http://myaccount.copyright.com).

GENERAL TERMS

2. Elsevier hereby grants you permission to reproduce the aforementioned material subject to the terms and conditions indicated.
3. Acknowledgement: If any part of the material to be used (for example, figures) has appeared in our publication with credit or acknowledgement to another source, permission must also be sought from that source. If such permission is not obtained then that material may not be included in your publication/copies. Suitable acknowledgement to the source must be made, either as a footnote or in a reference list at the end of your publication, as follows:
"Reprinted from Publication title, Vol /edition number, Author(s), Title of article / title of chapter, Pages No., Copyright (Year), with permission from Elsevier [OR APPLICABLE SOCIETY COPYRIGHT OWNER]." Also Lancet special credit - "Reprinted from The Lancet, Vol. number, Author(s), Title of article, Pages No., Copyright (Year), with permission from Elsevier."
4. Reproduction of this material is confined to the purpose and/or media for which permission is hereby given.
5. Altering/Modifying Material: Not Permitted. However figures and illustrations may be altered/adapted minimally to serve your work. Any other abbreviations, additions, deletions and/or any other alterations shall be made only with prior written authorization of Elsevier Ltd. (Please contact Elsevier at permissions@elsevier.com). No modifications can be made to any Lancet figures/tables and they must be reproduced in full.
6. If the permission fee for the requested use of our material is waived in this instance, please be advised that your future requests for Elsevier materials may attract a fee.
7. Reservation of Rights: Publisher reserves all rights not specifically granted in the combination of (i) the license details provided by you and accepted in the course of this licensing transaction, (ii) these terms and conditions and (iii) CCC's Billing and Payment terms and conditions.
8. License Contingent Upon Payment: While you may exercise the rights licensed immediately upon issuance of the license at the end of the licensing process for the transaction, provided that you have disclosed complete and accurate details of your proposed use, no license is finally effective unless and until full payment is received from you (either by publisher or by CCC) as provided in CCC's Billing and Payment terms and conditions. If full payment is not received on a timely basis, then any license preliminarily granted shall be deemed automatically revoked and shall be void as if never granted. Further, in the event that you breach any of these terms and conditions or any of CCC's Billing and Payment terms and conditions, the license is automatically revoked and shall be void as if never granted. Use of materials as described in a revoked license, as well as any use of the

materials beyond the scope of an unrevoked license, may constitute copyright infringement and publisher reserves the right to take any and all action to protect its copyright in the materials.
9. Warranties: Publisher makes no representations or warranties with respect to the licensed material.
10. Indemnity: You hereby indemnify and agree to hold harmless publisher and CCC, and their respective officers, directors, employees and agents, from and against any and all claims arising out of your use of the licensed material other than as specifically authorized pursuant to this license.
11. No Transfer of License: This license is personal to you and may not be sublicensed, assigned, or transferred by you to any other person without publisher's written permission.
12. No Amendment Except in Writing: This license may not be amended except in a writing signed by both parties (or, in the case of publisher, by CCC on publisher's behalf).
13. Objection to Contrary Terms: Publisher hereby objects to any terms contained in any purchase order, acknowledgment, check endorsement or other writing prepared by you, which terms are inconsistent with these terms and conditions or CCC's Billing and Payment terms and conditions. These terms and conditions, together with CCC's Billing and Payment terms and conditions (which are incorporated herein), comprise the entire agreement between you and publisher (and CCC) concerning this licensing transaction. In the event of any conflict between your obligations established by these terms and conditions and those established by CCC's Billing and Payment terms and conditions, these terms and conditions shall control.
14. Revocation: Elsevier or Copyright Clearance Center may deny the permissions described in this License at their sole discretion, for any reason or no reason, with a full refund payable to you. Notice of such denial will be made using the contact information provided by you. Failure to receive such notice will not alter or invalidate the denial. In no event will Elsevier or Copyright Clearance Center be responsible or liable for any costs, expenses or damage incurred by you as a result of a denial of your permission request, other than a refund of the amount(s) paid by you to Elsevier and/or Copyright Clearance Center for denied permissions.

LIMITED LICENSE

The following terms and conditions apply only to specific license types:
15. **Translation**: This permission is granted for non-exclusive world **English** rights only unless your license was granted for translation rights. If you licensed translation rights you may only translate this content into the languages you requested. A professional translator must perform all translations and reproduce the content word for word preserving the integrity of the article.
16. **Posting licensed content on any Website**: The following terms and conditions apply as follows: Licensing material from an Elsevier journal: All content posted to the web site must maintain the copyright information line on the bottom of each image; A hyper-text must be included to the Homepage of the journal from which you are licensing at http://www.sciencedirect.com/science/journal/xxxxx or the Elsevier homepage for books at http://www.elsevier.com; Central Storage: This license does not include permission for a scanned version of the material to be stored in a central repository such as that provided by Heron/XanEdu.
Licensing material from an Elsevier book: A hyper-text link must be included to the Elsevier homepage at http://www.elsevier.com . All content posted to the web site must maintain the copyright information line on the bottom of each image.

Posting licensed content on Electronic reserve: In addition to the above the following clauses are applicable: The web site must be password-protected and made available only to bona fide students registered on a relevant course. This permission is granted for 1 year only. You may obtain a new license for future website posting.

17. **For journal authors:** the following clauses are applicable in addition to the above:
Preprints:
A preprint is an author's own write-up of research results and analysis, it has not been peer-reviewed, nor has it had any other value added to it by a publisher (such as formatting, copyright, technical enhancement etc.).
Authors can share their preprints anywhere at any time. Preprints should not be added to or enhanced in any way in order to appear more like, or to substitute for, the final versions of articles however authors can update their preprints on arXiv or RePEc with their Accepted Author Manuscript (see below).
If accepted for publication, we encourage authors to link from the preprint to their formal publication via its DOI. Millions of researchers have access to the formal publications on ScienceDirect, and so links will help users to find, access, cite and use the best available version. Please note that Cell Press, The Lancet and some society-owned have different preprint policies. Information on these policies is available on the journal homepage.
Accepted Author Manuscripts: An accepted author manuscript is the manuscript of an article that has been accepted for publication and which typically includes author-incorporated changes suggested during submission, peer review and editor-author communications.
Authors can share their accepted author manuscript:

- immediately
    - via their non-commercial person homepage or blog
    - by updating a preprint in arXiv or RePEc with the accepted manuscript
    - via their research institute or institutional repository for internal institutional uses or as part of an invitation-only research collaboration work-group
    - directly by providing copies to their students or to research collaborators for their personal use
    - for private scholarly sharing as part of an invitation-only work group on commercial sites with which Elsevier has an agreement
- After the embargo period
    - via non-commercial hosting platforms such as their institutional repository
    - via commercial sites with which Elsevier has an agreement

In all cases accepted manuscripts should:

- link to the formal publication via its DOI
- bear a CC-BY-NC-ND license - this is easy to do
- if aggregated with other manuscripts, for example in a repository or other site, be shared in alignment with our hosting policy not be added to or enhanced in any way to appear more like, or to substitute for, the published journal article.

Published journal article (JPA): A published journal article (PJA) is the definitive final record of published research that appears or will appear in the journal and embodies all value-adding publishing activities including peer review co-ordination, copy-editing, formatting, (if relevant) pagination and online enrichment.
Policies for sharing publishing journal articles differ for subscription and gold open access articles:
Subscription Articles: If you are an author, please share a link to your article rather than the full-text. Millions of researchers have access to the formal publications on ScienceDirect, and so links will help your users to find, access, cite, and use the best available version.
Theses and dissertations which contain embedded PJAs as part of the formal submission can be posted publicly by the awarding institution with DOI links back to the formal publications on ScienceDirect.

If you are affiliated with a library that subscribes to ScienceDirect you have additional private sharing rights for others' research accessed under that agreement. This includes use for classroom teaching and internal training at the institution (including use in course packs and courseware programs), and inclusion of the article for grant funding purposes.
Gold Open Access Articles: May be shared according to the author-selected end-user license and should contain a CrossMark logo, the end user license, and a DOI link to the formal publication on ScienceDirect.
Please refer to Elsevier's posting policy for further information.
18. **For book authors** the following clauses are applicable in addition to the above: Authors are permitted to place a brief summary of their work online only. You are not allowed to download and post the published electronic version of your chapter, nor may you scan the printed edition to create an electronic version. **Posting to a repository:** Authors are permitted to post a summary of their chapter only in their institution's repository.
19. **Thesis/Dissertation**: If your license is for use in a thesis/dissertation your thesis may be submitted to your institution in either print or electronic form. Should your thesis be published commercially, please reapply for permission. These requirements include permission for the Library and Archives of Canada to supply single copies, on demand, of the complete thesis and include permission for Proquest/UMI to supply single copies, on demand, of the complete thesis. Should your thesis be published commercially, please reapply for permission. Theses and dissertations which contain embedded PJAs as part of the formal submission can be posted publicly by the awarding institution with DOI links back to the formal publications on ScienceDirect.

Elsevier Open Access Terms and Conditions
You can publish open access with Elsevier in hundreds of open access journals or in nearly 2000 established subscription journals that support open access publishing. Permitted third party re-use of these open access articles is defined by the author's choice of Creative Commons user license. See our open access license policy for more information.
Terms & Conditions applicable to all Open Access articles published with Elsevier:
Any reuse of the article must not represent the author as endorsing the adaptation of the article nor should the article be modified in such a way as to damage the author's honour or reputation. If any changes have been made, such changes must be clearly indicated.
The author(s) must be appropriately credited and we ask that you include the end user license and a DOI link to the formal publication on ScienceDirect.
If any part of the material to be used (for example, figures) has appeared in our publication with credit or acknowledgement to another source it is the responsibility of the user to ensure their reuse complies with the terms and conditions determined by the rights holder.
Additional Terms & Conditions applicable to each Creative Commons user license:
CC BY: The CC-BY license allows users to copy, to create extracts, abstracts and new works from the Article, to alter and revise the Article and to make commercial use of the Article (including reuse and/or resale of the Article by commercial entities), provided the user gives appropriate credit (with a link to the formal publication through the relevant DOI), provides a link to the license, indicates if changes were made and the licensor is not represented as endorsing the use made of the work. The full details of the license are available at http://creativecommons.org/licenses/by/4.0.
CC BY NC SA: The CC BY-NC-SA license allows users to copy, to create extracts, abstracts and new works from the Article, to alter and revise the Article, provided this is not done for commercial purposes, and that the user gives appropriate credit (with a link to the formal publication through the relevant DOI), provides a link to the license, indicates if changes were made and the licensor is not represented as endorsing the use made of the work. Further, any new works must be made available on the same conditions. The full details of the license are available at http://creativecommons.org/licenses/by-nc-sa/4.0.
CC BY NC ND: The CC BY-NC-ND license allows users to copy and distribute the Article,

Chapter 2: Imaging retinal ganglion cells: Enabling experimental technology for clinical application.

Smith CA, Chauhan BC. Imaging retinal ganglion cells: Enabling experimental technology for clinical application. *Prog Retin Eye Res* 2015;44:1-14.

ELSEVIER LICENSE
TERMS AND CONDITIONS

Jun 14, 2017

This Agreement between Corey A Smith ("You") and Elsevier ("Elsevier") consists of your license details and the terms and conditions provided by Elsevier and Copyright Clearance Center.

License Number	4127721027595
License date	Jun 14, 2017
Licensed Content Publisher	Elsevier
Licensed Content Publication	Progress in Retinal and Eye Research
Licensed Content Title	Imaging retinal ganglion cells: Enabling experimental technology for clinical application
Licensed Content Author	Corey A. Smith,Balwantray C. Chauhan
Licensed Content Date	Jan 1, 2015
Licensed Content Volume	44
Licensed Content Issue	n/a
Licensed Content Pages	14
Start Page	1
End Page	14
Type of Use	reuse in a thesis/dissertation
Portion	full article
Format	both print and electronic
Are you the author of this Elsevier article?	Yes
Will you be translating?	No
Order reference number	
Title of your thesis/dissertation	Labelling and Longitudinal In Vivo Imaging of Retinal Ganglion Cells
Expected completion date	Aug 2017
Estimated size (number of pages)	150
Elsevier VAT number	GB 494 6272 12
Requestor Location	Corey A Smith Physiology & Biophysics Dalhousie University 5850 College Street, PO Box 15000 Halifax, NS B3H4R2 Canada Attn: Corey A Smith
Total	0.00 CAD

10. Indemnity: You hereby indemnify and agree to hold harmless publisher and CCC, and their respective officers, directors, employees and agents, from and against any and all claims arising out of your use of the licensed material other than as specifically authorized pursuant to this license.
11. No Transfer of License: This license is personal to you and may not be sublicensed, assigned, or transferred by you to any other person without publisher's written permission.
12. No Amendment Except in Writing: This license may not be amended except in a writing signed by both parties (or, in the case of publisher, by CCC on publisher's behalf).
13. Objection to Contrary Terms: Publisher hereby objects to any terms contained in any purchase order, acknowledgment, check endorsement or other writing prepared by you, which terms are inconsistent with these terms and conditions or CCC's Billing and Payment terms and conditions. These terms and conditions, together with CCC's Billing and Payment terms and conditions (which are incorporated herein), comprise the entire agreement between you and publisher (and CCC) concerning this licensing transaction. In the event of any conflict between your obligations established by these terms and conditions and those established by CCC's Billing and Payment terms and conditions, these terms and conditions shall control.
14. Revocation: Elsevier or Copyright Clearance Center may deny the permissions described in this License at their sole discretion, for any reason or no reason, with a full refund payable to you. Notice of such denial will be made using the contact information provided by you. Failure to receive such notice will not alter or invalidate the denial. In no event will Elsevier or Copyright Clearance Center be responsible or liable for any costs, expenses or damage incurred by you as a result of a denial of your permission request, other than a refund of the amount(s) paid by you to Elsevier and/or Copyright Clearance Center for denied permissions.

LIMITED LICENSE

The following terms and conditions apply only to specific license types:
15. **Translation**: This permission is granted for non-exclusive world **English** rights only unless your license was granted for translation rights. If you licensed translation rights you may only translate this content into the languages you requested. A professional translator must perform all translations and reproduce the content word for word preserving the integrity of the article.
16. **Posting licensed content on any Website**: The following terms and conditions apply as follows: Licensing material from an Elsevier journal: All content posted to the web site must maintain the copyright information line on the bottom of each image; A hyper-text must be included to the Homepage of the journal from which you are licensing at http://www.sciencedirect.com/science/journal/xxxxx or the Elsevier homepage for books at http://www.elsevier.com; Central Storage: This license does not include permission for a scanned version of the material to be stored in a central repository such as that provided by Heron/XanEdu.
Licensing material from an Elsevier book: A hyper-text link must be included to the Elsevier homepage at http://www.elsevier.com . All content posted to the web site must maintain the copyright information line on the bottom of each image.

Posting licensed content on Electronic reserve: In addition to the above the following clauses are applicable: The web site must be password-protected and made available only to bona fide students registered on a relevant course. This permission is granted for 1 year only. You may obtain a new license for future website posting.
17. **For journal authors:** the following clauses are applicable in addition to the above:
Preprints:

A preprint is an author's own write-up of research results and analysis, it has not been peer-reviewed, nor has it had any other value added to it by a publisher (such as formatting, copyright, technical enhancement etc.).
Authors can share their preprints anywhere at any time. Preprints should not be added to or enhanced in any way in order to appear more like, or to substitute for, the final versions of articles however authors can update their preprints on arXiv or RePEc with their Accepted Author Manuscript (see below).
If accepted for publication, we encourage authors to link from the preprint to their formal publication via its DOI. Millions of researchers have access to the formal publications on ScienceDirect, and so links will help users to find, access, cite and use the best available version. Please note that Cell Press, The Lancet and some society-owned have different preprint policies. Information on these policies is available on the journal homepage.
Accepted Author Manuscripts: An accepted author manuscript is the manuscript of an article that has been accepted for publication and which typically includes author-incorporated changes suggested during submission, peer review and editor-author communications.
Authors can share their accepted author manuscript:

- immediately
    - via their non-commercial person homepage or blog
    - by updating a preprint in arXiv or RePEc with the accepted manuscript
    - via their research institute or institutional repository for internal institutional uses or as part of an invitation-only research collaboration work-group
    - directly by providing copies to their students or to research collaborators for their personal use
    - for private scholarly sharing as part of an invitation-only work group on commercial sites with which Elsevier has an agreement
- After the embargo period
    - via non-commercial hosting platforms such as their institutional repository
    - via commercial sites with which Elsevier has an agreement

In all cases accepted manuscripts should:

- link to the formal publication via its DOI
- bear a CC-BY-NC-ND license - this is easy to do
- if aggregated with other manuscripts, for example in a repository or other site, be shared in alignment with our hosting policy not be added to or enhanced in any way to appear more like, or to substitute for, the published journal article.

Published journal article (JPA): A published journal article (PJA) is the definitive final record of published research that appears or will appear in the journal and embodies all value-adding publishing activities including peer review co-ordination, copy-editing, formatting, (if relevant) pagination and online enrichment.
Policies for sharing publishing journal articles differ for subscription and gold open access articles:
Subscription Articles: If you are an author, please share a link to your article rather than the full-text. Millions of researchers have access to the formal publications on ScienceDirect, and so links will help your users to find, access, cite, and use the best available version.
Theses and dissertations which contain embedded PJAs as part of the formal submission can be posted publicly by the awarding institution with DOI links back to the formal publications on ScienceDirect.

SPRINGER LICENSE
TERMS AND CONDITIONS

Jun 20, 2017

This Agreement between Corey A Smith ("You") and Springer ("Springer") consists of your license details and the terms and conditions provided by Springer and Copyright Clearance Center.

License Number	4133180912062
License date	Jun 20, 2017
Licensed Content Publisher	Springer
Licensed Content Publication	Analytical and Bioanalytical Chemistry
Licensed Content Title	Optical coherence tomography—current technology and applications in clinical and biomedical research
Licensed Content Author	Sebastian Marschall
Licensed Content Date	Jan 1, 2011
Licensed Content Volume	400
Licensed Content Issue	9
Type of Use	Thesis/Dissertation
Portion	Figures/tables/illustrations
Number of figures/tables/illustrations	1
Author of this Springer article	No
Order reference number	
Original figure numbers	Figure 4
Title of your thesis / dissertation	Labelling and Longitudinal In Vivo Imaging of Retinal Ganglion Cells
Expected completion date	Aug 2017
Estimated size(pages)	150
Requestor Location	Corey A Smith Physiology & Biophysics Dalhousie University 5850 College Street, PO Box 15000 Halifax, NS B3H4R2 Canada Attn: Corey A Smith
Billing Type	Invoice
Billing Address	Corey A Smith Physiology & Biophysics Dalhousie University 5850 College Street, PO Box 15000 Halifax, NS B3H4R2 Canada Attn: Corey A Smith

Total 0.00 CAD

Terms and Conditions

Introduction
The publisher for this copyrighted material is Springer. By clicking "accept" in connection with completing this licensing transaction, you agree that the following terms and conditions apply to this transaction (along with the Billing and Payment terms and conditions established by Copyright Clearance Center, Inc. ("CCC"), at the time that you opened your Rightslink account and that are available at any time at http://myaccount.copyright.com).
Limited License
With reference to your request to reuse material on which Springer controls the copyright, permission is granted for the use indicated in your enquiry under the following conditions:
- Licenses are for one-time use only with a maximum distribution equal to the number stated in your request.
- Springer material represents original material which does not carry references to other sources. If the material in question appears with a credit to another source, this permission is not valid and authorization has to be obtained from the original copyright holder.
- This permission
• is non-exclusive
• is only valid if no personal rights, trademarks, or competitive products are infringed.
• explicitly excludes the right for derivatives.
- Springer does not supply original artwork or content.
- According to the format which you have selected, the following conditions apply accordingly:
• **Print and Electronic:** This License include use in electronic form provided it is password protected, on intranet, or CD-Rom/DVD or E-book/E-journal. It may not be republished in electronic open access.
• **Print:** This License excludes use in electronic form.
• **Electronic:** This License only pertains to use in electronic form provided it is password protected, on intranet, or CD-Rom/DVD or E-book/E-journal. It may not be republished in electronic open access.
For any electronic use not mentioned, please contact Springer at permissions.springer@spi-global.com.
- Although Springer controls the copyright to the material and is entitled to negotiate on rights, this license is only valid subject to courtesy information to the author (address is given in the article/chapter).
- If you are an STM Signatory or your work will be published by an STM Signatory and you are requesting to reuse figures/tables/illustrations or single text extracts, permission is granted according to STM Permissions Guidelines: http://www.stm-assoc.org/permissions-guidelines/
For any electronic use not mentioned in the Guidelines, please contact Springer at permissions.springer@spi-global.com. If you request to reuse more content than stipulated in the STM Permissions Guidelines, you will be charged a permission fee for the excess content.
Permission is valid upon payment of the fee as indicated in the licensing process. If permission is granted free of charge on this occasion, that does not prejudice any rights we might have to charge for reproduction of our copyrighted material in the future.
-If your request is for reuse in a Thesis, permission is granted free of charge under the following conditions:

No Amendment Except in Writing
This license may not be amended except in a writing signed by both parties (or, in the case of Springer, by CCC on Springer's behalf).
Objection to Contrary Terms
Springer hereby objects to any terms contained in any purchase order, acknowledgment, check endorsement or other writing prepared by you, which terms are inconsistent with these terms and conditions or CCC's Billing and Payment terms and conditions. These terms and conditions, together with CCC's Billing and Payment terms and conditions (which are incorporated herein), comprise the entire agreement between you and Springer (and CCC) concerning this licensing transaction. In the event of any conflict between your obligations established by these terms and conditions and those established by CCC's Billing and Payment terms and conditions, these terms and conditions shall control.
Jurisdiction
All disputes that may arise in connection with this present License, or the breach thereof, shall be settled exclusively by arbitration, to be held in the Federal Republic of Germany, in accordance with German law.
Other conditions:
V 12AUG2015

Questions? customercare@copyright.com or +1-855-239-3415 (toll free in the US) or +1-978-646-2777.

AMERICAN MEDICAL ASSOCIATION LICENSE TERMS AND CONDITIONS

Aug 20, 2017

This Agreement between Corey A Smith ("You") and American Medical Association ("American Medical Association") consists of your license details and the terms and conditions provided by American Medical Association and Copyright Clearance Center.

All payments must be made in full to CCC. For payment instructions, please see information listed at the bottom of this form.

License Number	4173351024692
License date	Aug 20, 2017
Licensed Content Publisher	American Medical Association
Licensed Content Publication	JAMA
Licensed Content Title	Central Challenges Facing the National Clinical Research Enterprise
Licensed Content Author	Sung, Nancy S.; Crowley, Jr, William F.
Licensed Content Date	Mar 12, 2003
Licensed Content Volume	289
Licensed Content Issue	10
Volume number	289
Issue number	10
Type of Use	Dissertation/Thesis
Requestor type	student
Format	print and electronic
Portion	figures/tables/images
Number of figures/tables/images	1
List of figures/tables/images	Figure 1
Will you be translating?	no
Circulation/distribution	150
Distributing to	Worldwide
Order reference number	
Title of your thesis / dissertation	Labelling and Longitudinal In Vivo Imaging of Retinal Ganglion Cells
Expected completion date	Aug 2017
Requestor Location	Corey A Smith Physiology & Biophysics Dalhousie University 5850 College Street, PO Box 15000 Halifax, NS B3H4R2 Canada Attn: Corey A Smith
Publisher Tax ID	36-0727175

Billing Type	Invoice
Billing Address	Corey A Smith Physiology & Biophysics Dalhousie University 5850 College Street, PO Box 15000 Halifax, NS B3H4R2 Canada Attn: Corey A Smith
Total	50.33 CAD
Terms and Conditions	

American Medical Association's Terms and Conditions

1. The publisher for the copyrighted material you seek permission to license ("Licensed Material") is the American Medical Association ("Publisher"). By clicking "accept" in connection with completing this licensing transaction, you agree that the following terms and conditions apply to this transaction (along with the Billing and Payment terms and conditions established by Copyright Clearance Center, Inc. ["CCC"] at the time that you opened your Rightslink account and that are available at any time at http://myaccount.copyright.com).
2. Publisher hereby grants to you a non-exclusive license to use the Licensed Material subject to the limitations set forth herein. Licenses are for one-time use only and are limited to the use identified in your request with a maximum distribution equal to the number that you identified in the licensing process. Any form of republication must be completed within one year from the date hereof (although copies prepared before then may be distributed thereafter); and any electronic posting is limited to a period of one year.
3. **You may only obtain permission via this website to use material owned by the Publisher.** If you seek a license to use a figure, photograph, table, or illustration from an AMA publication, journal, or article, it is your responsibility to examine each such item as published to determine whether a credit to, or copyright notice of, a third-party owner was published adjacent to the item. Permission to use any material published in an AMA publication, journal, or article which is reprinted with permission of a third party must be obtained from the third-party owner. **The Publisher disclaims any responsibility for any use you make of items owned by third parties without their permission.**
4. Licenses may be exercised anywhere in the world.
5. You may not alter or modify the Licensed Material in any manner, except for the following:
    - The Licensed Material may be superficially modified within the scope of the license granted (color, layout, etc) to suit the style/format of the proposed republication provided that specific content or data are not altered, omitted, or selectively presented; modification must not alter the meaning of the material or in any way reflect negatively on the publisher, the journal, or author(s).
    - Within the scope of the license granted, the Licensed Material may be translated from the original English into another language where specifically covered in the grant of license.
6. Publisher reserves all rights not specifically granted in (i) the license details provided by you and accepted in the course of this licensing transaction, (ii) these terms and conditions, and (iii) CCC's Billing and Payment terms and conditions.
7. While you may exercise the rights licensed immediately upon issuance of the license at the end of the licensing process for the transaction, provided that you have disclosed complete and accurate details of your proposed use, no license is finally effective unless and until full payment is received from you (either by Publisher or by CCC) as provided in CCC's Billing and Payment terms and conditions. If full payment is not received on a timely basis, then any license preliminarily granted shall be deemed automatically revoked and shall be void as if never granted. Further, in the event that you breach any of these terms and conditions or any of CCC's Billing and Payment terms and conditions, the license is automatically revoked and shall be void as if never granted. Use of Licensed Materials as described in a revoked license, as well as any use of the Licensed Materials beyond the scope of an unrevoked license, may constitute copyright infringement and Publisher reserves the right to take any and all action to protect its copyright in the Licensed Materials.
8. You must include the following copyright and permission notice in connection with any

reproduction of the Licensed Material provide credit/attribution to the original publication - with full citation: "Reproduced with permission from [Journal Title. Year. Volume(Issue): page numbers or doi]. Copyright©(Year of Publication) American Medical Association. All rights reserved."

9. THE LICENSED MATERIAL IS PROVIDED ON AN "AS IS" BASIS. PUBLISHER MAKES NO REPRESENTATIONS WITH RESPECT TO, AND DISCLAIMS ALL WARRANTIES, EXPRESS OR IMPLIED, RELATING TO, THE LICENSED MATERIAL, INCLUDING WITHOUT LIMITATION, IMPLIED WARRANTIES OF MERCHANTABILITY OR FITNESS FOR A PARTICULAR PURPOSE
10. You hereby indemnify and agree to hold harmless Publisher and CCC, and their respective officers, directors, employees, and agents, from and against any and all claims, liability, damages, costs, and expenses, including reasonable attorneys' fees, arising out of your use of the Licensed Material other than as specifically authorized pursuant to this license, including claims for defamation or infringement of or damage to rights of copyright, publicity, privacy, or other tangible or intangible property.
11. This license is personal to you and may not be sublicensed, assigned, or transferred by you to any other person without Publisher's written permission.
12. This license may not be amended except in writing signed by both parties (or, in the case of Publisher, by CCC on Publisher's behalf).
13. Publisher hereby objects to any terms contained in any purchase order, acknowledgement, check endorsement, or other writing prepared by you in which terms are inconsistent with these terms and conditions or CCC's Billing and Payment terms and conditions. These terms and conditions, together with CCC's Billing and Payment terms and conditions (which are incorporated herein), comprise the entire agreement between you and Publisher (and CCC) concerning this licensing transaction. In the event of any conflict between your obligations established by these terms and conditions and those established by CCC's Billing and Payment terms and conditions, these terms and conditions shall prevail.
14. This license and the licensing transaction shall be governed by and construed in accordance with the laws of the State of Illinois. You hereby agree that any dispute that may arise in connection with this license or the licensing transaction shall be submitted to binding arbitration in Chicago, Illinois, in accordance with the American Arbitration Association's rules for resolution of commercial disputes, and any award resulting from such arbitration may be entered as a judgment in any court with jurisdiction thereof.
15. Other Terms and Conditions:

Terms and Conditions for Content Services

Subject to these terms of use, any terms set forth on the particular order, and payment of the applicable fee, you may make the following uses of the ordered materials:

- Content Rental: You may access and view a single electronic copy of the materials ordered for the time period designated at the time the order is placed. Access to the materials will be provided through a dedicated content viewer or other portal, and access will be discontinued upon expiration of the designated time period. An order for Content Rental does not include any rights to print, download, save, create additional copies, to distribute or to reuse in any way the full text or parts of the materials.

V-03162016; V3.0

You will be invoiced within 48 hours of this transaction date. You may pay your invoice by credit card upon receipt of the invoice for this transaction. Please follow instructions provided at that time.
To pay for this transaction now; please remit a copy of this document along with your payment. Payment should be in the form of a check or money order referencing your account number and this invoice number RLNK502421392.

Make payments to "COPYRIGHT CLEARANCE CENTER" and send to:

Copyright Clearance Center